KLINIK FÜR STRAHLENTHERAPIE UND RADIOONKOLOGIE
FACHBEREICH MEDIZIN
PHILIPPS-UNIVERSITÄT MARBURG
DIREKTORIN: PROF. DR. MED. RITA ENGENHART-CABILLIC

DOSIMETRISCHE UND PLANUNGSTECHNISCHE UNTERSUCHUNGEN DER TOMOTHERAPY (ACCURAY)

INAUGURAL-DISSERTATION

ZUR
ERLANGUNG DES DOKTORGRADES DER MEDIZINWISSENSCHAFTEN
(DR. RER. MED.)
DEM FACHBEREICH MEDIZIN DER PHILIPPS-UNIVERSITÄT MARBURG
VORGELEGT VON

SIMON HOWITZ AUS ZWICKAU

MARBURG, 2020

Angenommen vom Fachbereich Medizin der Philipps-Universität Marburg am:

28.10.2020

Gedruckt mit Genehmigung des Fachbereichs Medizin

Prodekan:	Prof. Dr. Rolf Müller
Referentin:	Prof. Dr. med. Dipl.-Phys. Hilke Vorwerk
Referent:	Prof. Dr. rer. nat. Klemens Zink
Korreferent:	Prof. Dr. med. Andreas H. Mahnken

ZUSAMMENFASSUNG

Die TomoTherapy bietet eine einzigartige Möglichkeit der intensitäts-modulierten Strahlentherapie. Ein schlitzartiger hochenergetischer, ionisierender Photonenstrahl wird durch einen binären Multi-Lamellen-Kollimator geformt und eine Vielzahl solcher Projektionen aus verschiedenen Einstrahlwinkeln auf ein Zielgebiet kumuliert. Durch diese Technik wird eine homogene Dosisverteilung im Zielgebiet, zumeist Tumorgewebe, mit steilen Gradienten zum Normalgewebe erreicht.

Die Vorzüge der einzigartigen Bestrahlungstechnik der TomoTherapy wurden kombiniert, um eine neue Methode der robusten Ganzkörperbestrahlung zu entwickeln und in die klinische Routine zu implementieren.

Von nationalen und internationalen Dosimetrieprotokollen vorgeschriebene Referenzbedingungen für die Absolutdosimetrie sind mit dem Bestrahlungsgerät TomoTherapyHD unter mehreren Aspekten nicht zu erreichen. Mittels Monte Carlo Simulationen werden Fragestellungen beantwortet, die Unsicherheiten der Absolutdosimetrie reduzieren.

Die Unsicherheiten der Dosimetrie kleiner Felder werden in vielen Publikationen untersucht. In dieser Arbeit wird erstmalig eine fluenzgewichtete Subfeldgröße eines helikalen TomoTherapy Planes definiert. Dieser Parameter bietet die Möglichkeit einer Beschreibung der Komplexität eines Bestrahlungsplanes und ist eine Größe, um Genauigkeiten von Messsystemen für die Patientenqualitätssicherungen in der klinischen Dosimetrie zu verifizieren.

In der vorliegenden kumulativen Dissertation werden Hintergründe zu den beschriebenen Sachverhalten beschrieben und die entsprechenden Ergebnisse vorgestellt. Mit dieser Arbeit wird ein Beitrag geleistet, die Qualitätssicherung der Strahlentherapie weiter zu verbessern und Ungenauigkeiten in der klinischen Dosimetrie zu minimieren.

SUMMARY

TomoTherapy offers a unique possibility of intensity-modulated radiation therapy. An high-energy, photon fan beam is formed by a binary multi-leaf collimator and a large number of such projections from different gantry angles are accumulated on a planning target volume. This technique achieves a homogeneous dose distribution in the target volume, mostly tumor tissue, with steep gradients to normal tissue.

The advantages of the unique radiation technology of TomoTherapy were combined to develop a new method of robust whole-body radiation and to implement it in clinical routine.

Reference conditions for absolute dosimetry prescribed by german and international dosimetry protocols cannot be achieved with the radiation therapy device TomoTherapyHD in several respects. Monte Carlo simulations answer questions that reduce uncertainties in absolute dosimetry.

The uncertainties of dosimetry in small fields are examined in many publications. In this work, a fluence-weighted subfield size of helical TomoTherapy plans is defined for the first time. This parameter offers the possibility of describing the complexity of a radiation treatment plan and is a parameter for verifying the accuracy of measurement systems for patient quality assurance in clinical dosimetry.

In this cumulative dissertation, background information on the described issues are described and the corresponding results are presented. This work contributes to further improving the quality assurance of radiation therapy and minimizing inaccuracies in clinical dosimetry.

INHALTSVERZEICHNIS

1. EINFÜHRUNG UND ÜBERSICHT

Die Beschreibung der Bestrahlungstechnik Helikale TomoTherapy wurde 1993 von Mackie et al [53, 54] erstmalig publiziert. Ähnlich zur Computertomographie rotiert hier die Strahlenquelle kontinuierlich um den Patienten, während der Bestrahlungstisch mit dem Patienten durch die Gantry bewegt wird. Der therapeutische Strahl ist ein ungefilterter 6-MV-Photonenstrahl, welcher in longitudinale Richtung durch Y-Blenden (1.0, 2.5 oder 5.0 cm) und in lateraler Richtung durch einen Multi-Lamellen-Kollimator (0.625 cm Lamellenbreite im Isozentrum) fokussiert wird [40, 55]. Die 10 cm dicken Lamellen, die sich innerhalb von 20 ms öffnen und schließen, können ausschließlich die Zustände geöffnet oder geschlossen annehmen. Man spricht daher von einem binären Multi-Lamellen-Kollimator [7, 48, 72].
Die TomoTherapy ist damit eine besondere Form der intensitätsmodulierten Strahlentherapie (IMRT) [87]. Die Dosisbeiträge werden dabei vornehmlich über optimierte Beamlets appliziert, d.h. bevorzugt geöffnete Lamellen bei geeigneten Projektionswinkeln [8].

Grundlage für die Bestrahlungsplanung ist eine kV-Bestrahlungsplanungs-Computertomographie (BPL-CT), bei der die Patienten unter Bestrahlungsbedingungen (Lagerung, Organfüllstände etc.) gescannt werden. Risikostrukturen und Zielgebiete werden in einem Structure Set (nach DICOM Standard [57]) segmentiert. Durch den inversen Planungsprozess der IMRT werden die optimalen Beamlets ermittelt, indem Dosisvorgaben mit entsprechenden Wichtungsfaktoren für Zielgebiete und alle relevanten, segmentierten Risikostrukturen in einer Zielfunktion beschrieben werden.

So werden selbst komplex geformte Planungszielgebiete hochkonformal mit einer besonders homogenen Dosisverteilung bestrahlt und umliegendes Normalgewebe bestmöglich geschont [16, 39, 60, 84, 88].
Die hochkonformale TomoTherapy-Bestrahlungstechnik stellt erhöhte Anforderungen an eine exakte Lagerungskontrolle. Eine bildgestützte Strahlentherapie (Image Guided Radio Therapy, IGRT [31]) wird an der TomoTherapyHD durch eine Megavolt-Computertomographie (MV-CT) realisiert. Mit dem therapeutischen Linearbeschleuniger kann dafür ein 3.5-MV-Photonenbeam erzeugt werden. Durch ein Xenon-Gas-Detektor-Array, welches sich gegenüber der Strahlenquelle befindet, kann vor jeder Bestrahlung ein 3D-MV-CT aufgenommen werden und mit dem BPL-CT fusioniert werden [56].
Des Weiteren ermöglicht es die TomoTherapy, die Dosisverteilung auf dem MV-CT zu berechnen, um die tatsächlich applizierte Dosis beurteilen zu können, und bietet damit durch die komplette Integration eine einfache Lösung für die adaptive Strahlentherapie [47].

Ein Vorteil, der sich aus der TomoTherapy gegenüber sonstigen IMRT-Bestrahlungstechniken ergibt, liegt darin, nicht durch die Feldgröße des Kollimators limitiert zu sein. Durch die kontinuierliche Bewegung des Tisches während der Bestrahlung können Zielgebiete mit einer Länge von bis zu 135 cm mit dem hochenergetischen 6-MV-Photonenstrahl behandelt werden [34, 38].
Bei herkömmlichen Bauformen klinischer Linearbeschleuniger beträgt die maximale Feldgröße 40x40 cm^2 im Isozentrum. Konzepte für die Ganzkörper-Bestrahlungen basieren daher auf einer Kombination angrenzender opponierender Strahlenfelder, auf geschwenkten Gegenfeldern in kurzem Quell-Patienten-Abstand, oder auf Bestrahlungen mit sehr großem Quell-Patienten-Abstand in unterschiedlichsten Patientenpositionen. Eine notwendige Dosisreduktion an dem Risikoorgan

Lunge erfolgt dabei durch Absorptionsblöcke, die sowohl die Dosis als auch die Dosisleistung reduzieren. Resultierende Unterdosierungen im Normalgewebe vor bzw. hinter der Lunge werden optional durch Elektronenfelder aufgesättigt [65, 66].

In dieser Arbeit wurde eine Methode entwickelt, die Ganzkörper-Bestrahlung mit dem TomoTherapyHD Bestrahlungsgerät durchzuführen [71]. Dabei sollten folgende Ziele erreicht werden:

a) homogene Dosisverteilung im Normalgewebe
b) reduzierte, homogene Dosisverteilung in den Lungen
c) reproduzierbare Dosisapplikation im Patienten, der Bestrahlungsplanung entsprechend
d) bequeme Lagerung des Patienten, ausschließlich in Rückenlage

Im Vordergrund stand hierfür eine neue Bestrahlungstechnik: TomoDirect. Zwei bis zwölf bestmögliche feste Einstrahlwinkel werden im Planungsprozess bestimmt. Während der Tisch durch die Gantry-Öffnung bewegt wird, bleibt die Gantry auf der geplanten Position stehen und die Dosis wird durch IMRT-optimierte Subfelder appliziert. Dieser Vorgang wird für alle Gantry-Winkel wiederholt, bis die optimierte Fluenz abgestrahlt wurde [27, 59].

1.1. TomoTherapy spezifische Planungsparameter

Die inverse IMRT-Optimierung der TomoTherapy unterscheidet sich nicht wesentlich von konventionellen IMRT-Techniken mit klinischen Linearbeschleunigern [87]. Dennoch gibt es ausgewählte Planungsparameter, die vornehmlich für die Optimierung von TomoTherapy-Plänen von Bedeutung sind. Diese werden im Folgenden für die Techniken TomoHelical und TomoDirect ausgeführt.

Die **Feldgröße (Field Width, FW)** beschreibt die Größe des Strahlenfeldes im Isozentrum in longitudinaler Ausdehnung und wird durch die Y-Blenden bestimmt. Im Planungsprozess kann zwischen drei möglichen Y-Blenden-Öffnungen gewählt werden: 1.0, 2.5 und 5.0 cm. Durch kleinere Feldgrößen können steilere Dosisgradienten in cranio-caudaler Richtung erzeugt werden. Allerdings steigt damit, aufgrund des kleineren Outputs, die Strahlzeit erheblich an.
TomoEdge ermöglicht ein dynamisches Öffnen und Schließen der Y-Blenden am Anfang und Ende der zu bestrahlenden Zielgebiete. So werden auch bei größeren Feldgrößen sehr steile Dosisgradienten in cranio-caudaler Richtung erreicht und gesundes Gewebe wird besser geschont [43, 81].

Der **Pitch** beschreibt den Vorschub des Tisches pro Gantryrotation, geteilt durch die Feldgröße [48].
Kissick et al [46] und Chen et al [17] beschreiben geeignete Pitches, um Dosisinhomogenitäten im Hochdosisgebiet, sogenannte *ripple effects*, zu minimieren. Bei zentral gelegenen Zielgebieten sind optimale Pitchwerte gegeben durch 0.86/n, wobei n ein beliebiger ganzzahliger Wert größer gleich eins ist.
Der Pitchfaktor wird limitiert durch die technischen Parameter der Gantryrotationszeit (12 … 60 s) und der Tischgeschwindigkeit (0.0125 … 40 mm/s) [12].

Eine Gantryrotation wird im Planungsprozess in 51 gleichverteilte Gantrywinkel, sogenannte Projektionen, unterteilt [80]. Die Fluenzmodulation innerhalb einer Projektion wird durch individuelle **Lamellen-Öffnungszeiten (leaf-opening time, LOT)** realisiert. Die LOT liegt zwischen 20 ms und der Projektionszeit (Gantrayrotationszeit/51) [51]. Die LOTs für den gesamten Plan werden in der DICOM-standardisierten RT-Plan-Datei in einem Sinogramm, also einer zweidimensionalen Matrix in Abhängigkeit vom Gantrywinkel und der Lamellennummer, zusammengefasst. Im Planungsprozess können die LOTs nicht unmittelbar beeinflusst werden.

Der **Modulationsfaktor (MF)** ist das Verhältnis der längsten LOT zum Mittelwert aller LOTs, die größer als Null sind [48]. Im Planungsprozess besteht die Möglichkeit, einen maximalen MF zu definieren. Je größer dieser ist, desto größer ist die Bandbreite der verwendeten LOTs aufgrund einer verlangsamten Gantryrotation [12, 77].

In **TomoDirect** ist der **Pitch** als Tischvorschub pro Projektion definiert. Das Maximum ist dabei ein Zehntel der Feldgröße.
Die Projektionsdauer wird limitiert durch die Tischgeschwindigkeit und die Höhe der Energiedosis.
Damit kann durch den Pitch in beiden Techniken TomoHelical und TomoDirect bestimmt werden, wie sehr sich einzelne Projektionen in longitudinaler Richtung überschneiden.

Eine Technik, die zur Robustheit von TomoDirect-Bestrahlungen beitragen kann, ist die **Erweiterung der Strahlausdehnung**. Dafür kann für jede X-Kante eines jeden Strahlwinkels die Feldgröße um bis zu fünf Lamellen, also bis zu 3.125 cm, erweitert werden. Die LOT der erweiterten Lamellen entspricht der durchschnittlichen LOT der zweit- und dritt-äußersten Lamellen der

Strahlkante. So werden Zielgebiete, die sich durch Lagerungsunsicherheiten oder Veratmungen bewegen, sicherer mit der verschriebenen Dosis bestrahlt [78].

1.2. Dosimetrische Problemstellungen bei der TomoTherapy

Die Dosimetrie ist die Lehre der Messung der Energiedosis, die durch ionisierende Strahlung und damit verbundene Wechselwirkung erzeugt wird.

1.2.1. Strahlenqualitätsindex

In der klinischen Dosimetrie sind mit Luft gefüllte Ionisationskammern für die Messung der Wasserenergiedosis (D_w) das Standardverfahren. D_w für hochenergetische Photonenstrahlung ist das Ergebnis einer Multiplikation des Anzeigewertes der Ionisationskammer (M), dem Kalibierfaktor (N), dem Korrektionsfaktor für die Strahlenqualität (k_q) und weiteren Korrektionsfaktoren (k_i), die aufgrund nie erreichter Idealbedingungen (Bragg-Gray Bedingungen [14, 32, 33]) systematische Messabweichungen korrigieren:

$$D_w = M\ N\ k_q \prod_i k_i$$

Ionisationskammern werden in Deutschland mit ^{60}Co-Gammastrahlung kalibriert. Weicht das Energiespektrum ionisierender hochenergetischer Strahlung von den Kalibrierbedingungen ab, weisen Ionisationskammern veränderte Ansprechvermögen auf. Diese Einflüsse werden durch den Korrektionsfaktor k_q berücksichtigt. Der Wert dieses Korrektionsfaktors steht in Abhängigkeit vom Strahlungsqualitätsindex, welcher die spektrale Teilchenflussdichte klassifiziert.

Sowohl nationale als auch internationale Leitlinien [3, 5, 23] beschreiben Methoden, um die Strahlenqualität zu ermitteln, die unter bestimmten Referenzbedingungen durchzuführen sind.

Die IAEA empfiehlt in der Technical Report Series 398 [5], wie auch die DIN 6800-2 [23] eine Bestimmung von der Strahlenqualität nach dem Gewebe-Phantom-Verhältnis 20 cm zu 10 cm (Tissue-Phantom Ratio, $TPR_{20,10}$). $TPR_{20,10}$ ist definiert als das Verhältnis der gemessenen Dosis in 20 cm (D_{20}) zu 10 cm (D_{10}) Tiefe in Wasser bei einem konstanten Quell-Detektor-Abstand von 100 cm und einer Feldgröße von 10x10 cm² in der Messebene:

$$TPR_{20,10} = {}^{D_{20cm}}/_{D_{10cm}}$$

Die Taskgroup 51 der AAPM [3] dagegen empfiehlt eine Bestimmung der Strahlenqualität nach dem relativen Dosiswert der auf das Maximum normierten Tiefendosiskurve (*TDK*) in einer Tiefe von 10 cm (%dd). Die Messbedingungen für die *TDK* sind eine Feldgröße von 10x10 cm² in 100 cm Abstand bei einem Quell-Phantomoberflächen-Abstand von ebenfalls 100 cm.

Insbesondere die Feldgröße als auch der Quell-Detektor-Abstand sind an den TomoTherapy Bestrahlungsgeräten nicht einstellbar. In dieser Arbeit wird die Bestimmung von der Strahlenqualität unter Nichtreferenzbedingungen mit Monte-Carlo-Berechnungen verifiziert [36].

1.2.2. MONTE-CARLO-METHODE

Die Monte-Carlo-Methode ist eine numerische Methode, um komplexe Gleichungen oder Integrale mittels Zufallszahlen zu lösen [75].

In der Strahlentherapie wird der Transport der Photonen, Elektronen, Positronen, Neutronen oder Schwerionen durch Materie simuliert, um absorbierte Energiedosis zu berechnen. Ein viel zitiertes und in dieser Arbeit genutztes Programmpaket ist EGSnrc (Elektron Gamma Shower), entwickelt vom National Research Center of Canada [44, 45]. Grundlage für die simulierten Wechselwirkungen der Photonen, Elektronen und Positronen sind die energie- und materialabhängigen Wechselwirkungsquerschnitte des National Institute of Standards and Technology (NIST) [10, 11].

Mit dem Anwendercode von BEAMnrc [68] können, in Kooperation mit den Herstellern, Beschleunigerkopfmodelle erstellt werden. So können Bremsstrahlungsspektren genau berechnet werden und realistische Photonen- und Elektronenspektren des Linearbeschleunigers ermittelt werden. Dazu ist es notwendig, alle Geometrien mit entsprechenden Materialien zu definieren. Anschließend müssen folgende Parameter iterativ ermittelt werden:

- primäre Elektronenenergie bzw. -energieverteilung vor dem Target
- Intensitätsverteilung der Elektronen auf dem Target
- Richtungsverteilung der Elektronen auf dem Target

Dieser Prozess erfolgt üblicherweise über einen Vergleich zwischen simulierter und gemessener Tiefendosiskurven und Querprofilen in einem Wasserphantom [2, 18, 76, 83, 85, 86].

Das Ergebnis von BEAMnrc-Simulationen sind PhaseSpace-Dateien, in denen die Teilchen in gewünschter Ebene mit Eigenschaften wie Art des Teilchens, Ortskoordinaten, Impuls, Ladung, Energie etc. gespeichert sind. Diese können a) statistisch analysiert werden, um Energiespektren auszulesen, und b) für Simulationen in weiterführenden Anwender-Codes, wie „sprrznrc“ [67] und „egs_chamber“ [90] als Quelldatei genutzt werden.

1.2.3. PATIENTENBEZOGENE QUALITÄTSSICHERUNG

Die DIN 6875-3 [24] gibt eine Empfehlung für eine patientenbezogene Qualitätssicherung für IMRT-Pläne. Die bekanntesten Phantome für die helikale TomoTherapy sind das ArcCheck von Sun Nuclear (Melbourne, USA) und das Delta4 von Scandidos (Uppsala, Schweden) [25, 30, 61, 62, 69]. Die Detektorarrays beider zylindrischen Phantome bestehen aus mehreren hundert Si-Dioden. So kann die Integraldosis eines helikalen Bestrahlungsplans mit einer hohen räumlichen Auflösung detektiert werden.

Im ArcCheck ist das Detektor-Array auf einer Mantelfläche drei Zentimeter unter der Oberfläche des Phantoms positioniert. In der Auswertung der Qualitätssicherung werden berechnete und gemessene Dosiswerte verglichen.

Das Delta4 bietet den Vorteil, dass die physikalische Dosismessung direkt im interessierenden Hochdosisgebiet erfolgen kann – im Zylinder kreuzen sich zwei Diodenarrays orthogonal. So können Dosisgradienten um das Hochdosisgebiet und eine mediane Dosisabweichung innerhalb des Hochdosisgebiets für jeden Patientenplan verifiziert werden.

Die Anzeige der Absolutdosis einer jeden einzelnen Diode (*D(i)*) ist nach einer Kalibrierprozedur (*kal*) der Diodenarrays möglich. Dafür wird ein absoluter Kalibrierfaktor (kal_{abs}) für jedes Detektorboard durch eine Ionisationskammer bestimmt. Des Weiteren wird für jede Diode ein relativer Kalibrierfaktor ($kal_{rel}(i)$) ermittelt, der unterschiedliche Ansprechvermögen der Dioden korrigiert. Die folgenden Korrektionsfaktoren werden derzeit im Delta4 berücksichtigt, um die Unsicherheiten der Messergebnisse zu minimieren [74]:

- Temperaturkorrektionsfaktor (k_{temp}), da die Sensitivität der Dioden von der Temperatur abhängt (≈Δ 1% der Dosis bei Δ 3 °C)
- Diodenpositionskorrektionsfaktor (k_{pos}). Die Ansprechvermögen der Dioden hängen ab von der Messtiefe, dem Abstand von der Feldkante, sofern sie sich außerhalb des Feldes befinden, und dem Einstrahlwinkel. Diese drei Unsicherheiten werden durch k_{pos} minimiert.
- Feldgrößenkorrektionsfaktor (k_{fg}). Ein Überschätzen der Dosis bei einem großen Hochdosisbereich durch erhöhte niederenergetische sekundäre Streubeiträge wird durch k_{fg} korrigiert.

$$D_i = M \cdot kal_{abs} \cdot kal_{rel} \cdot k_{temp} \cdot k_{pos} \cdot k_{fg}$$

Die IAEA veröffentlichte 2017 in der Technical Report Series 483 [64] Korrektionsfaktoren, unter anderem für Dioden bei kleinen Feldern. Helikale TomoTherapy-Bestrahlungspläne bestehen aus einer Vielzahl kleiner Felder, mit Feldgrößen bis hinunter zu 0.625 x 1.0 cm^2, was in den Korrektionsfaktoren im Delta4 jedoch nicht berücksichtigt wird.

In dieser Arbeit wird der Einfluss der Subfeldgrößen auf das Ansprechvermögen der Delta4-Dioden untersucht [37].

2. EIGENE ARBEITEN

In diesem Kapitel werden die drei Arbeiten vorgestellt, die dieser kumulativen Promotionsschrift zu Grunde liegen.

2.1. GANZKÖRPERBESTRAHLUNG MIT TOMODIRECT

Die neue Bestrahlungstechnik TomoDirect bietet die Möglichkeit einer robusten Ganzkörperbestrahlung mit einer homogenen Dosis und einem integrierten Niedrigdosisvolumen bzw. Dosisschonungsvolumen im Bereich der Lungen.

Es wird eine Methode vorgestellt, mit der acht Ganzkörperpatienten mit einer Gesamtdosis von 12 Gy im Ganzkörperzielgebiet und einer reduzierten Dosis von 8 Gy im Lungengewebe in der klinischen Routine bestrahlt wurden. Patienten, die größer als 1.35 m waren, wurden mit einem cranialen Plan (von Kopf bis Oberschenkel) und einem caudalen Plan (von Fuß bis Oberschenkel) bestrahlt. Beide Pläne überlappten sich durch diametrale, flache Dosisgradienden im Bereich der Oberschenkel. So verursachten kleine Lagerungsunsicherheiten vernachlässigbare Unter- bzw. Überdosierungen im Anschlussbereich.

Die Einflüsse der Planungsparameter Modulationsfaktor (MF), Pitch, Y-Blendenöffnung und Dosisraster während der Optimierung auf die Planergebnisse wurden untersucht und ausgewertet. Es wurde gezeigt, dass die Wahl des MFs zwischen 1 und 2 den größten Einfluss auf die Dosisverteilung, bezüglich Homogenität und Konformität, und die Bestrahlungszeit besitzt. Der Planvergleich verschiedener Y-Blendenöffnungen zeigte lediglich einen Unterschied in der Bestrahlungszeit. Der Einfluss des Pitchs war sowohl in der Dosisverteilung als auch in der Bestrahlungszeit vernachlässigbar.

Eine Dosisverifikation der Bestrahlungspläne erfolgte durch:

a) Dosimetrie mittels Thermo-Lumineszenz-Detektoren (TLD) in einem RANDO-Phantom. Abweichung zwischen Messung und Rechnung: 0.7% ± 2.3%, maximale Abweichung < 5%.
b) Verifikationsmessungen mit dem Delta4 im Thoraxbereich: mediane Dosisabweichung: 1.5%.
c) patientenindividuelle Qualitätssicherungsmessungen mit der Ionisationskammer A1SL (SunNuclear) im Cheesephantom (Accuray): Abweichungen zwischen Messung und Rechnung: < 2.2% ± 1.8% für verschiedene Körperregionen.

Ein Vergleich mit der Translationstechnik zeigt eine deutliche Verbesserung der Homogenität im Ganzkörperzielgebiet und eine besseren Schonung der Lungen bei einer Dosis > 10 Gy.

Salz H, Bohrisch B, Howitz S, Banz N, Weibert K, Wiezorek T, Wendt TG; Intensity-modulated Total Body Irradiation (TBI) with TomoDirect™; Radiat Oncol. 2015 Mar 6;10:58. doi: 10.1186/s13014-015-0362-3.

Impact-Factor: 2.466

Eigenanteil an dieser Arbeit: 40%

Mitgestaltung des Zielgedankens und Methodik, technische Realisierung, Durchführung der Messungen und Auswertungen, Unterstützung beim Erstellen des Manuskripts

2.2. Bestimmung des Strahlenqualitätsindexes für die TomoTherapy mit Monte-Carlo-Methoden

Sauer [73] stellt eine Methode vor, die Strahlenqualität aus $TPR_{20,10}(s)$-Messungen kleiner Felder mit einer quadratischen Kantenlänge *(s)* zu bestimmen. Hierfür wird ein Fit empfohlen, der sich größtenteils aus $TPR_{20,10}(s)$-Messungen aus dem Suppelement BJR25 [13] ableitet. Diese Dosisverhältnisse wurden in 6-MV und 15-MV-Photonenstrahlen ermittelt, erzeugt von klinischen Linearbeschleunigern mit Ausgleichfiltern. Der 6-MV-Photonenstrahl der TomoTherapy dagegen ist ausgleichsfilterfrei. Damit sind die Phantom-Streudosisbeiträge nicht vergleichbar, was einen Einfluss auf den Tiefendosiskurvenverlauf und damit auf $TPR_{20,10}$ hat. Sauer empfiehlt, für die TomoTherapy $TPR_{20,10}$ nicht in Abhängigkeit von der quadratischen Kantenlänge s zu berechnen, sondern berücksichtigt die fehlenden Streubeiträge durch eine äquivalente quadratische Kantenlänge $s_{eq,fff}$.

Das analytische Modell wurde durch verschiedene Monte-Carlo-Methoden verifiziert. In Kooperation mit Accuray wurde dafür ein Strahlerkopfmodell in BEAMnrc modelliert und kommissioniert. Die durch Monte Carlo berechneten und die messtechnisch ermittelten Strahlenqualitätsindizes variierten nicht mehr als ± 0.5%. Die Unsicherheit des resultierenden Korrektionsfaktors k_q ist damit kleiner 0.1%.

Howitz S, Schwedas M, Wiezorek T, Zink K; Experimental and Monte Carlo-based determination of the beamquality specifier for TomoTherapyHD treatment units;
Z Med Phys. 2018 Apr;28(2):142-149. doi: 10.1016/j.zemedi.2017.09.006.

Impact-Factor: 2.322

Eigenanteil an dieser Arbeit: 90%

Festlegung der Zielsetzung, Kooperationsvertrag mit Accuray für das Strahlerkopfmodell, Monte-Carlo-Simulationen, Dosimetrie, Auswertung und Diskussion der Ergebnisse, Erstellung des Manuskripts

2.3. Fluenzgewichtete mittlere Subfeldgröße in der helikalen TomoTherapy

Kleine Strahlenfelder (< 4x4 cm²) stellen die klinische Dosimetrie vor messtechnische Herausforderungen [9, 19, 21]. Im Optimierungsprozess der Bestrahlungsplanung der helikalen TomoTherapy ist es nicht möglich, einen Schwellwert für kleinste Felder zu definieren. Es wurde untersucht, ob das Ansprechvermögen des Delta4-Messsystems, welches in der klinischen Patientenqualitätssicherung eingesetzt wird, durch einen hohen Anteil zu kleiner Felder beeinflusst wird.

Für die helikale TomoTherapy wurde erstmalig eine mittlere Subfeldgröße definiert. Der Einfluss von Planungsparametern wie Pitch, Modulationsfaktor (MF) und Anzahl der Iterationen auf das Planergebnis wurde für verschiedene Zielgebiete untersucht. Als Planergebnis wurden die Subfeldgrößen, die klinischen Dosisverteilungen und verschiedene Maschinencharakteristika wie LOT, Bestrahlungszeit und Gantryperiode analysiert. Der MF und die Anzahl der Iterationen der Optimierung zeigten den größten Einfluss auf die Subfeldgröße. Während die Subfelder der Pläne bei großen MF und vielen Iterationen signifikant kleiner wurden, verbesserte sich ebenfalls die klinische Dosisverteilung. Damit wurde auf die Herausforderung aufmerksam gemacht, klinisch bessere Pläne auf Kosten einer steigenden Anzahl kleinster Subfelder zu planen.

Das Ansprechvermögen des Delta4-Messsystems zeigte in dieser Studie keine Abhängigkeit von der mittleren Subfeldgröße. Die Planverifikationen aller Pläne erfüllten die Anforderungen für eine klinische Akzeptanz: mediane Dosisabweichung im Zielgebiet ≤ ± 0.7%, gamma passing rate (3% / 3 mm) > 99.5%.

Howitz S, Wiezorek T, Wittig A, Vorwerk H, Zink K, Fluence-weighted average subfield size in helical TomoTherapy,
Z Med Phys 29 (2019) 337–348 doi: 10.1016/j.zemedi.2019.03.003

Impact-Factor: 2.322

Eigenanteil an dieser Arbeit: 90%

Festlegung der Zielsetzung, Definition mittlere Subfeldgröße für helikale TomoTherapy, Berechnung und Auswertung der Planvergleiche, Durchführung und Auswertung der Dosimetrie, Auswertung und Diskussion der Ergebnisse, Erstellung des Manuskripts

3. DISKUSSION

Das primäre Ziel der Medizinischen Physik im Gebiet der onkologischen Strahlentherapie besteht darin, die Energie der ionisierenden Strahlung präzise im Tumorgebiet zu applizieren und umliegendes gesundes Gewebe so gut es geht zu schonen. Klinische Forschungsgruppen erreichen Fortschritte diesbezüglich durch Verbesserung der Absolut– und Relativdosimetrie. Darüber hinaus tragen ingenieurstechnische Entwicklungen der Bestrahlungsgeräte durch immer mehr Freiheitsgrade zu einer präziseren Bestrahlungsplanung und entsprechender Applikation hochenergetischer Photonen bei. Die Herausforderung für die Medizinische Physik besteht darin, Vorteile neuer Bestrahlungstechniken zu nutzen und am Patienten anzuwenden.
Durch die patientenbezogene Qualitätssicherung wird verifiziert, dass das Bestrahlungsgerät in der Lage ist, die hochkomplexen Pläne abzustrahlen. Dafür werden mit geeigneten Dosimetriesystemen gemessene Dosisverteilungen mit den in Planungssystemen berechneten Dosisverteilungen verglichen.

Im Planungsprozess muss immer zwischen einer hochpräzisen Dosisverteilung und Robustheit abgewogen werden. Dabei gilt es, intra– und interfraktionelle Bewegungen von Patienten zu berücksichtigen und zu gewährleisten, dass die Zielgebiete trotz aller Lagerungsunsicherheiten mit der geplanten Dosis versorgt werden, bzw. die Lagerungsunsicherheiten minimiert werden.
Bei Ganzkörperbestrahlungen ist abzuwägen, mit welchen Lagerungshilfen der Patient immobilisiert werden kann, oder ob durch eine robuste Bestrahlungsplanung Lagerungsunsicherheiten zu klinisch vernachlässigbaren Dosisabweichungen im Patienten führen.

3.1. GANZKÖRPERBESTRAHLUNG MIT TOMODIRECT

Das Bestrahlungsgerät TomoTherapyHD von Accuray ermöglicht erstmals eine Bestrahlung des Patienten durch die Technik TomoDirect. Diese Technik versprach eine neue und qualitativ höherwertige Ganzkörperbestrahlung bezüglich der Dosisverteilung im Patienten, als auch der Robustheit. In dieser Arbeit wurde erstmalig mit der Ganzkörperbestrahlung durch TomoDirect eine neue Einsatzmöglichkeit des Bestrahlungsgerätes TomoTherapyHD untersucht und beurteilt.

Auch wenn sich die berechneten Dosisverteilungen zwischen TomoDirect und TomoHelical nur unwesentlich voneinander unterscheiden, wird TomoDirect in dieser Arbeit aus folgenden Gründen bevorzugt:

a) Die mittlere Dosisleistung wird durch eine Vielzahl von nacheinander abstrahlbaren Stehfeldern mit vordefinierten Gantrywinkeln (maximal zwölf) mit TomoDirect reduziert. Dadurch sinkt das Risiko einer Pneumonitis.
b) Die Dosishomogenität in zirkulierenden Blutzellen wird verbessert [58].
c) Die Strahlkantenaufweitung trägt zu einer größeren Robustheit bei. Dadurch führen Ungenauigkeiten der Lagerung im Bereich von bis zu 2 cm nicht zu Unter- oder Überdosierungen. Die Patientenlagerung erfolgte in einer Vakuummatte, ohne Kopfmaske. Verifikationsscans zeigten nach der Fusionierung eine Abweichung kleiner 5 mm im Hals Kopfbereich.

Erste Berechnungsvergleiche zeigten den Einfluss der Bestrahlungsplanungsparameter Modulationsfaktor (MF), Pitch, und Feldgröße auf die Dosisverteilung und die Bestrahlungszeit. Der MF hat einen maßgeblichen Einfluss auf die Dosishomogenität und die Bestrahlungszeit. Erlaubt man im Optimierungsprozess einen MF > 2,

verlängert sich die Bestrahlungszeit wesentlich, während keine weitere Verbesserung der Dosisverteilung erreicht werden kann. Die Feldgröße beeinflusst vorwiegend die Bestrahlungszeit, während der Einfluss des Pitchs vernachlässigbar ist.

Ein Vergleich der Dosisberechnungen zwischen der Translationstechnik mit Lungenblöcken und TomoDirect zeigte wesentliche Verbesserungen der Dosishomogenität in den Planungszielvolumina Ganzkörper und Lunge.

Die Dosishomogenität und –konformität für Ganzkörperbestrahlungen zu verbessern, war auch Schwerpunkt folgender Forschungsarbeiten.
Kasai et al [42] untersuchten verschiedene TomoTherapy-Techniken, um Ganzkörperbestrahlungen zu optimieren. Die Ergebnisse von TomoHelical und TomoDirect unterscheiden sich ab drei Einstrahlwinkeln nicht signifikant bezüglich Dosishomogenität und der Maximaldosis (D_2). Die umschließende Dosis (D_{98}) ist jedoch erst ab vier Einstrahlrichtungen akzeptabel. Der Unterschied zwischen TomoHelical und TomoDirect ist ab sieben Einstrahlwinkeln dann auch bezüglich des D_{98}-Wertes vernachlässigbar.
Wilhelm-Buchstab et al [89] zeigten auch mit TomoHelical eine deutliche Verbesserung der Lungenschonung, ohne dabei Kompromisse an der Zielgebietsdosis von Ganzkörperbestrahlungen einzugehen. Das zeigt Möglichkeiten einer Dosiseskalation auf das Zielvolumen, während die biologisch effektiven Dosen für strahlensensible Organe wie Lunge, Augen oder Nieren nicht erhöht werden. Mit einer fluenzmodulierten Bestrahlungstechnik für Ganzkörper, wie dieser hier vorgestellten, sind simultanintegrierte Boostbestrahlungen möglich, beispielsweise auf das Knochenmark [35, 41].

Für die dosimetrische Qualitätssicherung dieser Ganzkörperbestrahlung mit TomoDirect kamen verschiedene Dosismessverfahren zum Einsatz. Mit dem Delta4-Messsystem wurde die hochmodulierte Dosisverteilung im Thoraxbereich verifiziert. Durch die hohe Auflösung der Anordnung der Messdioden ermöglicht dieses Messsystem eine Verifikation der geplanten Dosisgradienten zwischen den Lungen und dem Mediastinum. Eine präzise Applikation der im Bestrahlungsplanungssystem berechneten Dosisgradienten konnte so nachgewiesen werden.

Mittels TLD Messungen im RANDO-Phantom wurde die berechnete Dosis in den Regionen: Hals und Kopf, Mediastinum, Lungen und Abdomen unter Berücksichtigung der Dichteunterschiede im Phantom verifiziert. Die Abweichungen waren kleiner als 5%.

Alle Patientenpläne wurden auf das homogene Festwasserphantom „Cheesephantom“, Accuray, gerechnet und mit der A1SL Ionisationskammer, Standard Imaging, gemessen. Weiterführende Studien zeigten Ergebnisse einer größeren Anzahl von 28 Patienten QA Messungen mit einer sehr guten Übereinstimmung zur Dosisberechnung: Mediastinum: 0.0% ± 1.1% und Lunge: 0.3% ± 1.8% [70].

TomoDirect ermöglicht für Kinder bis hin zu Erwachsenen mit hohem Body-Maß-Index eine robuste Ganzkörperbestrahlung mit einer wesentlich verbesserten Dosisverteilung im Vergleich zur bis dato verwendeten Translationstechnik und hat sich in dem Universitätsklinikum Jena als Methode der Wahl etabliert.

3.2. Dosimetrische Untersuchungen

Die TomoTherapy stellt spezielle Anforderungen an die Dosimetrie [22, 82]. So ist eine Absolutdosimetrie unter Referenzbedingungen, nach DIN6800-2 [23] definiert, nicht möglich.
Außerdem stellt die dynamische Bestrahlung Dosimetriesysteme vor die Herausforderung, Korrektionsfaktoren für Feldgröße, Energie, Sättigungseffekte und Richtungsabhängigkeit anzuwenden.
Mit diesen zwei Schwerpunkten beschäftigt sich diese Arbeit.

Alfonso et al [1] veröffentlichte 2008 einen Formalismus und führte einen maschinenspezifischen Referenzkorrektionsfaktor ein. Dieser Faktor berücksichtigt veränderte Ansprechvermögen von Ionisationskammern durch die maschinenbezogenen Referenzbedingungen in Bezug zu den Kalibrierbedingungen. Für die TomoTherapy werden so Einflüsse durch abweichende Feldgrößen (20x5 cm^2), anderer Strahlqualität (6-MV-Photonenstrahl, ausgleichsfilterfrei) und beschränkten Quell-Fokus-Abstand (85 cm) einbezogen.
Die Ansprechvermögen können experimentell ermittelt werden, beispielsweise mit Alanindosimetern zur Referenz.
Weitere Möglichkeiten bieten Monte-Carlo-Simulationen. Für die rechenbasierten Untersuchungen werden detaillierte Modelle von den strahlformenden Beschleunigerköpfen und Dosimetern erstellt. Für die Kommissionierung solcher Modelle sind sowohl umfassende Informationen zum Aufbau (Geometrien, Materialien) als auch ein hoher Simulationsaufwand notwendig. Das Ansprechvermögen ergibt sich aus der berechneten Dosis in sensitiven Messvolumen zur berechneten Dosis in einem kleinsten Wasservoxel unter definierten Strahlbedingungen, wie Energie, Feldgröße, Messtiefe und Quell-Detektor-Abstand.

Nach diesen Methoden wurden TomoTherapy-spezifische Korrektionsfaktoren für Ionisationskammern für ausgewählte Detektoren berechnet [52, 79, 91].

Die deutsche Dosimetrienorm DIN 6800-2 [23] beschreibt Korrektionsfaktoren in Abhängigkeit des Strahlenqualitätsindex für eine in der Praxis große Auswahl eingesetzter Detektoren. Die Bestimmung muss unter definierten Referenzbedingungen erfolgen, die, wie bereits beschrieben, mit der TomoTherapy nicht möglich sind. Sauer [73] publizierte eine analytische Methode, den Strahlenqualitätsindex messtechnisch unter Nichtreferenzbedingungen zu bestimmen. Diese wurde in dieser Arbeit durch unabhängige Monte-Carlo-Methoden für das Bestrahlungsgerät TomoTherapHD verifiziert.

Dafür wurde der TomoTherapyHD Strahlerkopf nach Herstellerangaben, herausgegeben durch einen Kooperationsvertrag mit Accuray, in dem Monte Carlo Code BEAMnrc [68] modelliert und kommissioniert. Elektronenenergie und -strahlfläche auf dem Target wurden dabei iterativ bestimmt, bis simulierte und gemessene Dosisprofile übereinstimmten.

Durch die folgenden Monte-Carlo-Berechnungen wurde der Strahlungsqualitätsindex nach den Methoden von Sauer [73] und Palmans et al [63], verifiziert:

- Vergleich zwischen Monte-Carlo-Methoden berechneten Stoßbremsvermögen Wasser zu Luft und analytisch ermittelten Stoßbremsvermögen, die in direkter Abhängigkeit zum Strahlungsqualitätsindex stehen [4].
- Monte-Carlo Berechnung des Gewebe-Phantom-Verhältnis $TPR_{20,10}$ unter Referenzbedingungen

Der Strahlungsqualitätsindex nach der Methode von Sauer [73] und Palmans et al [63] wurde mit einer Genauigkeit von 0.5% verifiziert. Diese Ungenauigkeit entspricht einer Unsicherheit von nur 0.1% für den

Strahlungsqualitätskorrektionsfaktor entsprechend der DIN 6800-2 [23] für Ionisationskammern.
Das für diese Arbeit kommissionierte Strahlerkopfmodell wurde in weiteren Arbeiten [15, 29] weiterentwickelt, um helikale TomoTherapy-Pläne mit EGSnrc simulieren zu können. Damit ermöglicht es eine unabhängige Planverifikation oder weitere strahlenphysikalische Untersuchungen.

Neben dem maschinenspezifischen Referenzkorrektionsfaktor beschreibt Alfonso et al [1] einen planklassenspezifischen und einen klinischen Korrektionsfaktor. Messsysteme, die aufgrund einzelner Planparameter oder einer Kombination verschiedener Planparameter ein verändertes Ansprechvermögen aufweisen, werden so korrigiert. Ein planklassenspezifisches Referenzfeld entspricht einer Zusammensetzung vieler Felder, die mit klinischen Plänen vergleichbar sind.
Gago-Arias et al [28] generiert ein planklassenspezifisches Referenzfeld auf ein zylinderförmiges Zielgebiet, 8 cm Durchmesser und 10 cm Länge, mit einer homogenen Dosisverteilung von 2 Gy in einem zylindrischen Festwasserphantom. Der helikale Bestrahlungsplan hat einen MF von 1.807, eine Feldgröße von 5 cm und einen Pitch von 0.287. Zwei klinische Pläne, die in dieser Studie untersucht wurden, unterscheiden sich zum planklassenspezifischen Referenzfeld sehr stark bezüglich Einzeldosis: 1.6 & 18 Gy, Pitch: 0.1 & 0.287, Feldgröße: 2.5 cm und MF 1.322 & 2.167. Die Korrektionsfaktoren wurde für die A1SL Ionisationskammer experimentell durch einen Vergleich mit Alanindosimetrie ermittelt. Ein Vergleich zwischen maschinenspezifischen, planklassenspezifischen und klinischen Korrektionsfaktoren zeigte trotz der großen planparametrischen Unterschiede eine sehr kleine Abweichung ≤0.5%.

Eine Auswertung der Patienten-Qualitätssicherung für die ersten 500 helikalen TomoTherapy-Bestrahlungspläne mit dem Delta4 Phantom am

Universitätsklinikum Jena zeigte im Mittel eine mediane Dosisabweichung von 0.1% zum Bestrahlungsplan mit einer Standardabweichung von 1.5%. Erste Untersuchungen zeigten einen signifikanten Zusammenhang zwischen der Dosisabweichung von Messung und Rechnung zum Volumen der Hochdosis. Als mögliche Ursache kann eine Änderung des Energiespektrums mit dem Hochdosisvolumen gesehen werden. Je größer das Hochdosisvolumen ist, desto größer der Anteil niederenergetischer Photonen, die zur Gesamtdosis beitragen. Eine Überbewertung der niederenergetischen ionisierenden Strahlung durch die im Delta4 verbauten Dioden wurde daraufhin mit einem Dosis-Volumen-abhängigen Korrektionsfaktor ab der Softwareversion „November-2014“ korrigiert.

In den letzten Jahren wurden viele Arbeiten veröffentlich, die detektorspezifische Korrektionsfaktoren für kleine Stehfelder experimentell oder durch Monte-Carlo Verfahren ermittelten. Dabei wurden Ionisationskammern, Dioden und Diamanddetektoren untersucht [6, 9, 20, 26, 50].

Ein Einfluss der Subfeldgröße von IMRT-Plänen auf Ansprechvermögen von Detektoren oder einzelner Messsysteme wurde dagegen kaum untersucht.

Der von Laub et al [49] beschriebene Volumeneffekt für IMRT-Pläne mit kleinen Feldern, kann eine Änderung des Ansprechvermögen hervorrufen, besonders für große Ionisationskammern.

Vereinfacht betrachtet bestehen Pläne der helikalen TomoTherapy aus einer Summe vieler Stehfelder, die sich wiederrum aus kleinen Subfeldern zusammensetzen (0.66 … 3.25 cm^2). In dieser Arbeit wurde erstmalig eine mittlere äquivalente Subfeldgröße für die helikale TomoTherapy definiert. Diese Größe liefert eine neue Möglichkeit, die Komplexität der Bestrahlungspläne darzustellen. So zeigte sich, dass Optimierungen mit vielen Iterationen und ein hoher MF zu Plänen mit sehr kleinen Subfeldern führen.

Für das diodenbasierte Dosimetriesystem Delta4 zeigte sich kein Einfluss der Subfeldgröße auf das Ansprechvermögen.

Eine systematische Untersuchung des Einflusses der äquivalenten Subfeldgröße auf das Ansprechvermögen weiterer Dosimetriesysteme, wie das ArcCheck, oder einzelner Ionisationskammern muss noch erfolgen.

QUELLENVERZEICHNIS

1. Alfonso, R., et al., *A new formalism for reference dosimetry of small and nonstandard fields.* Med Phys, 2008. 35(11): p. 5179-86.
2. Almberg, S.S., et al., *Monte Carlo linear accelerator simulation of megavoltage photon beams: independent determination of initial beam parameters.* Med Phys, 2012. 39(1): p. 40-7.
3. Almond, P.R., et al., *AAPM's TG-51 protocol for clinical reference dosimetry of high-energy photon and electron beams.* Med Phys, 1999. 26(9): p. 1847-70.
4. Andreo, P. *Improved calculations of stopping power ratios and their correlation with the quality of therapeutic photon beams*. in *Measurement Assurance in Dosimetry*. 1994. Vienna: IAEA.
5. Andreo, P., et al., *Absorbed Dose Determination in External Beam Radiotherapy. Technical Reports Series No. 398*, W. IAEA, PAHO and ESTRO, Editor. 2000.
6. Azangwe, G., et al., *Detector to detector corrections: a comprehensive experimental study of detector specific correction factors for beam output measurements for small radiotherapy beams.* Med Phys, 2014. 41(7): p. 072103.
7. Balog, J., T. Holmes, and R. Vaden, *A helical tomotherapy dynamic quality assurance.* Med Phys, 2006. 33(10): p. 3939-50.
8. Beavis, A.W., *Is tomotherapy the future of IMRT?* Br J Radiol, 2004. 77(916): p. 285-95.
9. Benmakhlouf, H., J. Sempau, and P. Andreo, *Output correction factors for nine small field detectors in 6 MV radiation therapy photon beams: a PENELOPE Monte Carlo study.* Med Phys, 2014. 41(4): p. 041711.
10. Berger, M.J., et al., *Stopping-power and range tables for electrons, protons, and helium ions, NIST Standard Reference Database 124.* 2017.
11. Berger, M.J., et al., *XCOM: Photon cross section database (version 1.5)(2010).* URL http://physics. nist. gov/xcom. 2017.
12. Binny, D., et al., *Effects of changing modulation and pitch parameters on tomotherapy delivery quality assurance plans.* J Appl Clin Med Phys, 2015. 16(5): p. 5282.
13. BJR-25, *Central Axis Depth Dose Data for Use in Radiotherapy*, Br. J. o. Radiology (suppl 25). 1996.
14. Bragg, W.H., *Studies in Radioactivitiy*. Macmillan and Company, limited. 1912.
15. Buck, C., *Implementierung des binären TomoTherapy MLC im Monte-Carlo EGSnrc User Code*, in *UKJ Klinik für Strahlentherapie und Radioonkologie*. 2017, TU Ilmenau.

16. Buschmann, M., et al., *Advanced optimization methods for whole pelvic and local prostate external beam therapy.* Phys Med, 2016. 32(3): p. 465-73.
17. Chen, M., et al., *Theoretical analysis of the thread effect in helical TomoTherapy.* Med Phys, 2011. 38(11): p. 5945-60.
18. Chibani, O., B. Moftah, and C.M. Ma, *On Monte Carlo modeling of megavoltage photon beams: a revisited study on the sensitivity of beam parameters.* Med Phys, 2011. 38(1): p. 188-201.
19. Cranmer-Sargison, G., et al., *Experimental small field 6 MV output ratio analysis for various diode detector and accelerator combinations.* Radiother Oncol, 2011. 100(3): p. 429-35.
20. Czarnecki, D. and K. Zink, *Monte Carlo calculated correction factors for diodes and ion chambers in small photon fields.* Phys Med Biol, 2013. 58(8): p. 2431-44.
21. Das, I.J., G.X. Ding, and A. Ahnesjo, *Small fields: nonequilibrium radiation dosimetry.* Med Phys, 2008. 35(1): p. 206-15.
22. De Ost, B., et al., *Reference dosimetry for helical tomotherapy: Practical implementation and a multicenter validation.* Medical Physics, 2011. 38(11): p. 6020-6026.
23. DIN6800-2, *Dosismessverfahren nach der Sondenmethode f\"ur Photonen- und Elektronenstrahlung; Teil 2: Dosimetrie hochenergetischer Photonen- und Elektronenstrahlung mit Ionisationskammern*. 2008.
24. DIN6875-3, *Special radiotherapy equipments - Part 3: Intensity-modulated radiation therapy - Characteristics, test methods and rules for clinical application*. 2008.
25. Feygelman, V., et al., *Evaluation of a new VMAT QA device, or the "X" and "O" array geometries.* J Appl Clin Med Phys, 2011. 12(2): p. 3346.
26. Francescon, P., et al., *Monte Carlo simulated correction factors for machine specific reference field dose calibration and output factor measurement using fixed and iris collimators on the CyberKnife system.* Phys Med Biol, 2012. 57(12): p. 3741-58.
27. Franco, P., et al., *TomoDirect: an efficient means to deliver radiation at static angles with tomotherapy.* Tumori, 2011. 97.
28. Gago-Arias, A., et al., *Correction factors for A1SL ionization chamber dosimetry in TomoTherapy: machine-specific, plan-class, and clinical fields.* Med Phys, 2012. 39(4): p. 1964-1970.
29. Gebser, F., *Implementierung der helikalen Tomotherapie in die Monte Carlo Simulation mittels EGSnrc*, in *UKJ Strahlentherapie und Radioonkologie*. 2016, University of Applied Science Mittweida.
30. Geurts, M., J. Gonzalez, and P. Serrano-Ojeda, *Longitudinal study using a diode phantom for helical tomotherapy IMRT QA.* Med Phys, 2009. 36(11): p. 4977-83.

31. Goyal, S. and T. Kataria, *Image guidance in radiation therapy: techniques and applications.* Radiol Res Pract, 2014. 2014: p. 705604.
32. Gray, L.H. and E. Rutherford, *The absorption of penetrating radiation.* Proc. R. Soc. Lond. A, 1928. 122(790): p. 647-668.
33. Gray, L.H. and E. Rutherford, *An ionization method for the absolute measurement of γ-ray energy.* Proc. R. Soc. Lond. A, 1936. 156(889): p. 578-596.
34. Gruen, A., et al., *Total Body Irradiation (TBI) using helical tomotherapy in children and young adults undergoing stem cell transplantation.* Radiation Oncol, 2013. 8.
35. Hill-Kayser, C.E., et al., *TBI during BM and SCT: review of the past, discussion of the present and consideration of future directions.* Bone Marrow Transplant, 2011. 46(4): p. 475-84.
36. Howitz, S., et al., *Experimental and Monte Carlo-based determination of the beam quality specifier for TomoTherapyHD treatment units.* Z Med Phys, 2018. 28(2): p. 142-149.
37. Howitz, S., et al., *Fluence-weighted average subfield size in helical TomoTherapy.* Z Med Phys, 2019.
38. Hui, S.K., et al., *Feasibility study of helical tomotherapy for total body or total marrow irradiation.* Med Phys, 2005. 32.
39. Jacob, V., et al., *A planning comparison of dynamic IMRT for different collimator leaf thicknesses with helical tomotherapy and RapidArc for prostate and head and neck tumors.* Strahlenther Onkol, 2010. 186(9): p. 502-10.
40. Jeraj, R., et al., *Radiation characteristics of helical tomotherapy.* Med Phys, 2004. 31(2): p. 396-404.
41. Kal, H.B., et al., *Biologically effective dose in total-body irradiation and hematopoietic stem cell transplantation.* Strahlenther Onkol, 2006. 182.
42. Kasai, Y., et al., *Dose evaluation indices for total body irradiation using TomoDirect with different numbers of ports: A comparison with the TomoHelical method.* J Appl Clin Med Phys, 2019. 20(2): p. 129-135.
43. Katayama, S., et al., *Accelerated tomotherapy delivery with TomoEdge technique.* J Appl Clin Med Phys, 2015. 16(2): p. 4964.
44. Kawrakow, I., *Accurate condensed history Monte Carlo simulation of electron transport. I. EGSnrc, the new EGS4 version.* Med Phys, 2000. 27(3): p. 485-498.
45. Kawrakow, I., et al., *The EGSnrc Code System: Monte Carlo Simulation of Electron and Photon Transport*, in *NRCC Report PIRS-701*. 2016.
46. Kissick, M.W., et al., *The helical tomotherapy thread effect.* Med Phys, 2005. 32(5): p. 1414-23.

47. Langen, K.M., et al., *The use of megavoltage CT (MVCT) images for dose recomputations.* Phys Med Biol, 2005. 50(18): p. 4259-76.
48. Langen, K.M., et al., *QA for helical tomotherapy: report of the AAPM Task Group 148.* Med Phys, 2010. 37(9): p. 4817-53.
49. Laub, W.U. and T. Wong, *The volume effect of detectors in the dosimetry of small fields used in IMRT.* Med Phys, 2003. 30(3): p. 341-7.
50. Lechner, W., et al., *Detector comparison for small field output factor measurements in flattening filter free photon beams.* Radiother Oncol, 2013. 109(3): p. 356-60.
51. Lissner, S., et al., *A method for testing the performance and the accuracy of the binary MLC used in helical tomotherapy.* Z Med Phys, 2013. 23(2): p. 153-61.
52. Lopes, M.D.C., et al., *Application of the TRS 483 code of practice for reference and relative dosimetry in tomotherapy.* Med Phys, 2019. 46(12): p. 5799-5806.
53. Mackie, T.R., *History of tomotherapy.* Phys Med Biol, 2006. 51(13): p. R427-53.
54. Mackie, T.R., et al., *Tomotherapy: a new concept for the delivery of dynamic conformal radiotherapy.* Med Phys, 1993. 20(6): p. 1709-19.
55. Mackie, T.R., et al., *Tomotherapy: Optimized Planning and Delivery of Radiation-Therapy.* International Journal of Imaging Systems and Technology, 1995. 6(1): p. 43-55.
56. Meeks, S.L., et al., *Performance characterization of megavoltage computed tomography imaging on a helical tomotherapy unit.* Med Phys, 2005. 32(8): p. 2673-2681.
57. Mildenberger, P., M. Eichelberg, and E. Martin, *Introduction to the DICOM standard.* European Radiology, 2002. 12(4): p. 920-927.
58. Molloy, J.A., *Statistical analysis of dose heterogeneity in circulating blood: implications for sequential methods of total body irradiation.* Med Phys, 2010. 37.
59. Murai, T., et al., *Intensity-modulated radiation therapy using static ports of tomotherapy (TomoDirect): comparison with the TomoHelical mode.* Radiation Oncol, 2013. 8.
60. Murthy, V., et al., *Helical tomotherapy for head and neck squamous cell carcinoma: dosimetric comparison with linear accelerator-based step-and-shoot IMRT.* J Cancer Res Ther, 2010. 6(2): p. 194-8.
61. Neilson, C., et al., *Delivery quality assurance with ArcCHECK.* Med Dosim, 2013. 38(1): p. 77-80.
62. Nilsson, G., *Delta4-A new IMRT QA device.* Medical Physics, 2007. 34(6): p. 2432-2432.
63. Palmans, H., *Determination of the beam quality index of high-energy photon beams under nonstandard reference conditions.* Med Phys, 2012. 39(9): p. 5513-5519.

64. Palmans, H., et al., *Dosimetry of small static fields used in external photon beam radiotherapy: Summary of TRS-483, the IAEA-AAPM international Code of Practice for reference and relative dose determination.* Med Phys, 2018. 45(11): p. e1123-e1145.
65. Quast, U., *Total body irradiation--review of treatment techniques in Europe.* Radiother Oncol, 1987. 9(2): p. 91-106.
66. Quast, U. and H. Sack, *Ganzkörper-Strahlenbehandlung vor Stammzell-Transplantation*, D. DEGRO, Editor. 2002.
67. Rogers, D.W.O., et al., *NRC user codes for EGSnrc National Research Council of Canada Report PIRS-702*. 2005.
68. Rogers, D.W.O., B. Walters, and I. Kawrakow, *NRCC Report PIRS-0509: BEAMnrc Users Manual.* National Research Council of Canada, 2013.
69. Sadagopan, R., et al., *Characterization and clinical evaluation of a novel IMRT quality assurance system.* J Appl Clin Med Phys, 2009. 10(2): p. 2928.
70. Salz, H., *Ganzkörperbestrahlung mit TomoDirect - Erfahrungsbericht nach vier Jahren im klinischen Einsatz*, in *DGMP*, C. Bert, M. Wucherer, and F.B. Laun, Editors. 2018.
71. Salz, H., et al., *Intensity-modulated Total Body Irradiation (TBI) with TomoDirect™.* Radiation Oncology, 2015. 10(1): p. 58.
72. Sarkar, V., et al., *Quality assurance of the multileaf collimator with helical tomotherapy: design and implementation.* Med Phys, 2007. 34(7): p. 2949-56.
73. Sauer, O.A., *Determination of the quality index (Q) for photon beams at arbitrary field sizes.* Med Phys, 2009. 36(9): p. 4168-4172.
74. Scandidos, *Manual Delta4 Phantom+.* 2016.
75. Seco, J. and F. Verhaegen, *Monte Carlo Techniques in Radiation Therapy*. 2013: Taylor & Francis Group.
76. Sheikh-Bagheri, D. and D.W. Rogers, *Sensitivity of megavoltage photon beam Monte Carlo simulations to electron beam and other parameters.* Med Phys, 2002. 29(3): p. 379-90.
77. Shimizu, H., et al., *Analysis of modulation factor to shorten the delivery time in helical tomotherapy.* J Appl Clin Med Phys, 2017.
78. Squires, M., et al., *Static beam tomotherapy as an optimisation method in whole-breast radiation therapy (WBRT).* J Med Radiat Sci, 2017. 64(4): p. 281-289.
79. Sterpin, E., T.R. Mackie, and S. Vynckier, *Monte Carlo computed machine-specific correction factors for reference dosimetry of TomoTherapy static beam for several ion chambers.* Medical Physics, 2012. 39(7): p. 4066-4072.
80. Sterpin, E., C. Verboomen, and S. Vynckier, *Impact of the number of discrete angles used during dose computation for TomoTherapy treatments.* Medical Physics, 2012. 39(11): p. 6947-6956.

81. Sterzing, F., et al., *Dynamic jaws and dynamic couch in helical tomotherapy.* Int J Radiat Oncol Biol Phys, 2010. 76(4): p. 1266-73.
82. Thomas, S.J., et al., *Reference dosimetry on TomoTherapy: an addendum to the 1990 UK MV dosimetry code of practice.* Phys Med Biol, 2014. 59(6): p. 1339-1352.
83. Tzedakis, A., et al., *Influence of initial electron beam parameters on Monte Carlo calculated absorbed dose distributions for radiotherapy photon beams.* Med Phys, 2004. 31(4): p. 907-13.
84. Van Gestel, D., et al., *RapidArc, SmartArc and TomoHD compared with classical step and shoot and sliding window intensity modulated radiotherapy in an oropharyngeal cancer treatment plan comparison.* Radiat Oncol, 2013. 8: p. 37.
85. Verhaegen, F. and J. Seuntjens, *Monte Carlo modelling of external radiotherapy photon beams.* Phys Med Biol, 2003. 48(21): p. R107-64.
86. Wang, L.L. and K. Leszczynski, *Estimation of the focal spot size and shape for a medical linear accelerator by Monte Carlo simulation.* Med Phys, 2007. 34(2): p. 485-488.
87. Webb, S., *The physical basis of IMRT and inverse planning.* Br J Radiol, 2003. 76(910): p. 678-89.
88. Wiezorek, T., et al., *Rotational IMRT techniques compared to fixed gantry IMRT and tomotherapy: multi-institutional planning study for head-and-neck cases.* Radiat Oncol, 2011. 6: p. 20.
89. Wilhelm-Buchstab, T., et al., *Total body irradiation: Significant dose sparing of lung tissue achievable by helical Tomotherapy.* Z Med Phys, 2019.
90. Wulff, J., K. Zink, and I. Kawrakow, *Efficiency improvements for ion chamber calculations in high energy photon beams.* Med Phys, 2008. 35(4): p. 1328-1336.
91. Zeverino, M., et al., *Determination of the correction factors for different ionization chambers used for the calibration of the helical tomotherapy static beam.* Radiother Oncol, 2011. 100(3): p. 424-8.

Salz et al. Radiation Oncology (2015) 10:58
DOI 10.1186/s13014-015-0362-3

RADIATION ONCOLOGY

RESEARCH Open Access

Intensity-modulated Total Body Irradiation (TBI) with TomoDirect™

Henning Salz*, Babette Bohrisch, Simon Howitz, Nico Banz, Kirsten Weibert, Tilo Wiezorek and Thomas G Wendt

Abstract

Background: The new TomoDirect™ modality offers a non-rotational option with discrete beam angles. We have investigated this mode for TBI with the intention to test the feasibility and to establish it as a clinical routine method. Special foci were directed onto treatment planning, dosimetric accuracy and practical aspects.

Patients and methods: TBI plans were calculated with TomoDirect™ for a Rando™ phantom and all patients with an intended fractionated total body irradiation between November 2013 and May 2014 (n = 8). Finally, four of these patients were irradiated with TomoDirect™. Additionally we studied variations in the modulation factor, pitch, field width of Y-jaws and dose grid during optimization. Dose measurements were performed using thermoluminescent rods in the Rando™ phantom, with the Delta4® and with ionization chambers in a solid water phantom.

Results: For all eight calculated plans with a prescribed dose of 12 Gy Dmean was 12.09-12.33 Gy (12,25 ± 0.08 Gy), D98 11.2-11.6 Gy (11.45 ± 0.12 Gy) and D2 12.6-13.1 Gy (12.94 ± 0.13 Gy). Dmean of inner lungs was 8.73 ± 0.22 Gy on the left side and 8.69 ± 0.27 Gy on the right side.
When single planning parameters are varied with otherwise constant parameters, the modulation factor showed the greatest impact on dose homogeneity and treatment time. The impact of the pitch was marginally, and almost equal homogeneity can be obtained with field width of Y-jaws 5 cm and 2.5 cm.
Measurements with thermoluminescent rods (n = 25) in the Rando™ phantom showed a mean dose deviation between measured and calculated dose of 0.66 ± 2.26%. 18 of 25 TLDs had a deviation below 3%, seven of 25 TLDs between 3% and 5%.

Conclusion: TBI with TomoDirect™ allows a superior homogeneity compared to conventional methods, where lung blocks are widely accepted. The treatment is performed only in supine position and is robust and comfortable for the patient.
TomoDirect™ allows the implementation of organ-specific dose prescriptions. So the discussion about the balance between the need for aggressive treatment and limited toxicity can be renewed with the new potentials of TomoDirect™ - for children as well as for adults – and possibly yield a better clinical outcome in the future.

Keywords: Total body irradiation, IMRT, Tomotherapy, TomoDirect

Introduction

Total body irradiations (TBI) are a special challenge for treatment planning and dose application. The large target size hampers the use of modern methods of radio-oncology, like IMRT. Therefore conventional methods are widely used, such as treatments with large source-surface distances, arc techniques [1,2] and translational methods [3,4]. Most of the current methods follow the recommendations from the European group for Blood and Marrow Transplantation (EBMT) [5], which suggest to check the dose homogeneity along the patient's midline at several points and which specify the lung dose at a point which is representative for more than 50% of the lung volume. The use of physical blocks to reduce dose to the lung, which includes lower dose under the blocks, is widely accepted.

In recent years some TBI techniques such as arc techniques have been enhanced [6,7]. According [7], the use of an inverse optimization algorithm improves the dose

* Correspondence: henning.salz@med.uni-jena.de
Department of Radiation Oncology, University Hospital Jena, Bachstr. 18, 07749 Jena, Germany

homogeneity in comparison to conventional forward-planned arc techniques. There, the achieved percentage of the PTV which received 90-110% of the prescribed dose was 75.8-90.2% (n = 4). With these arc techniques TBI can be performed even in normal treatment rooms.

The TomoTherapy® system (Accuray Inc., Sunnyvale, USA) overcomes the geometrical limitations of classical accelerators and allows the use of the advantages of IMRT even for total body irradiation. First experiences using the helical delivery mode have already been reported by other groups [8-10]. Using this technique, Gruen et al. reported an average dose received by 95% of the target (D95%) for all patients (n = 10) of 11.7 Gy for a prescription dose of 12Gy [9]. With the new TomoDirect™ modality, TomoTherapy® offers a non-rotational option with discrete beam angles. This method is different in some aspects from the helical mode. The dose is applied through maximum twelve fixed beams, while the table is moved through to the gantry. So it is comparable with an IMRT with very large field lengths. First studies showed that TomoDirect™ might be an efficient means to deliver radiation at static angles for different indications [11,12], and for craniospinal irradiation it is recommended [13]. In our department this method is not used as an alternative to the linac-based IMRT except for cases with very large target volumes.

TomoDirect™ has the potential to improve TBI even in comparison with the helical mode: (I) Because of the fact that multiple fields are used, the treatment time from the beginning to the end of the irradiation of the lung is extended, which has the potential to decrease the risk of interstitial pneumonitis. (II) TomoDirect™ allows a beam expansion on both edges by a maximum of 5 leaves each (3.125 cm at isocenter). This allows to ensure a sufficient dose distribution even in the case of dislocations up to 2 cm of the surface.

We have investigated the TomoDirect™ mode for TBI with the intention to test its feasibility and to establish it in clinical routine for children as well as for adults even with higher body mass indexes (BMI). Special foci were directed onto treatment planning, dosimetric accuracy and practical aspects. This work describes the new method and the results in detail and discusses differences to helical tomotherapy and to our previous translational method with lung blocks as well.

Materials and methods

Patient selection and dose prescription

All patients (7 adults, one child) with an intended TBI between November 2013 and April 2014 (n = 8) underwent the planning process for TomoDirect™ to assess the feasibility. Two of them were finally treated with the conventional translational technique, four with TomoDirect™, and two were not irradiated because of changing clinical conditions. Detailed characteristics of the patient selection are shown in Table 1.

The prescribed dose for the total body was 12 Gy, the dose per fraction was 2 Gy for children (twice a day) and 3 Gy for adults (one fraction per day). The prescribed total lung dose was 8 Gy.

Immobilization and planning CT

Patients were immobilized in supine position in a vacuum cushion (UNGER Medizintechnik GmbH&Co KG). Masks for head and neck fixation were not used. CTs were performed at a wide-bore CT scanner Optima CT580W (General Electric). Two CT scans (one head-first, one feet-first) were necessary for patients taller than 1.45 m because of limited table motion capacities of the CT and TomoTherapy®.

Contouring

Contouring was performed with Oncentra® (Elekta AB), treatment planning was performed with TomoHD™, Version 1.2.1. The following structures were created: outer body contour, planning target volume (PTV) consisting of body without skin (distance to the surface 5 mm), eyes, spinal cord, lung and central lung (distance to thoracic wall 10 mm for adults). Additionally, a help target structure was defined which consisted of the PTV, a small connection of the left and the right leg and a safety margin near the shoulder and superior of the head. If the irradiation was split into a head-first and a feet-first part, two "overlap regions" covering a length of 3 cm each were added beyond the PTVs. The upper overlap region should obtain 2/3 of the prescribed dose from the head-first plan and 1/3 from the feet-first plan, the lower one 1/3 from the head-first plan and 2/3 from the feet-first plan. By this a gradual dose gradient was created to minimize the risk of over- or underdosage by misplacement.

Treatment planning

The treatment planning was performed on the TomoTherapy® planning station. The defined targets were in the order of their priority settings in the inverse planning (1 = highest priority): (1) left eye, (2) right eye, (3) spinal cord, (4) total body, (5) left inner lung, (6) right inner lung, (7) "overlap 8 Gy", (8) "overlap 4 Gy", (9) second target (with the connection between leg contours). Table 2 shows the constraints which have to be fulfilled. Additionally a sufficient dose on the skin is also demanded.

Due to the technical limitation of the TomoTherapy® table the possible table motion in long direction depends on the table height. Therefore the table height was selected (I) high enough to encompass the complete thorax contour in the scan and (II) low enough to allow a large table motion range.

Table 1 Patient characteristics

Patient no.	Age (years)	Sex	Diagnosis	Body length (cm)	Body weight (kg)	Body mass index (kg/m^2)	Used treatment technique
1	40	f	ALL recurrence	176	70	22.6	translational technique
2	48	m	ALL	188	116	32.8	translational technique
3	5	f	ALL recurrence	104	18,3	16.9	TomoDirect
4	34	m	AML	174	85	28.1	TomoDirect
5	41	m	ALL	172	65	22.0	not treated
6	52	m	AML	175	97	31.7	TomoDirect
7	33	f	AML	172	85	28.7	not treated
8	37	m	AML	185	77	22.5	TomoDirect

For adults, the maximum possible number of beams –12- with equally spaced angles were used for the head-first-plan (see Figure 1), four fields for the feet-first plan. TomoDirect™ allows to expand the beam angle on both edges by a maximum of 5 leaves each (3.125 cm at isocenter). This expansion is limited when leaves at the end of the MLC are already in use. As a precaution against dislocation of the patient or patient movement, for every plan the maximum possible beam expansion was chosen.

Treatment plans were analysed according to ICRU 83 [14] including D2 (near-max dose), D98 (near-min dose), mean and median dose, homogeneity index (difference between D2 and D98 divided by the median dose), mean doses of left and right inner lung and treatment time.

For a better understanding of the treatment planning, we studied the effect of variations of the modulation factor (MF), pitch, field width of Y-jaws (FW) and dose grid during optimization for an adult case.

Backup concept

In clinical routine, the translational method was used as a backup concept so it can be switched to it if a breakdown of the treatment unit occurs. Individual lung blocks were manufactured for every patient before the first fraction.

Dosimetric measurements

The following dosimetric studies were performed: (I) Planning and irradiation of a RANDO™ phantom (Radiology Support Devices, Inc., Long Beach, USA) containing thermoluminescent rods (TLDs), (II) verification of a planned case with a Delta4® system (Scandidos AB, Uppsala, Sweden). In clinical routine the following measurements were performed for every patient: (III) recalculation of planned cases in a cylindrical solid water phantom ("Cheese phantom", TomoTherapy®) and measurements with ion chambers Exradin® A1SL (Standard Imaging Inc.) in regions representing lung, mediastinum and leg, (IV) in-vivo dosimetry with TLDs (ten positions with 3 TLDs each). They are positioned in different regions, especially in those where a higher risk of possible dislocations can be expected (shoulder, overlap regions).

Table 2 Constraints of the targets and organs-at-risk which have to be fulfilled for an accepted plan

Organ	Constraints	corresponds at 12 Gy (lung 8 Gy) to
Total body	D98 > 90%	D near-min > 10.8 Gy
	D2 < 110%	D near-max < 13.2 Gy
Inner lungs	D med < 75%	D median < 9 Gy
	V prescr dose > 90%	V 8 Gy > 90%
Eyes	D max < 105%	D max < 12,6 Gy

Patient setup verification

Phantoms and patients were positioned using the MVCT scanner of the TomoTherapy® system before delivery of every fraction. The scans were taken from the caudal edge of the eyes to the pelvis. The images were automatically fused with the kV planning CT and verified manually in all views. Besides the position of the patient outline and vertebral bodies, critical structures like eyes and lung were particularly monitored.

Results

Treatment planning

All calculated dose plans were in agreement with the defined constraints (Table 3). D near-min (D98) was 11.45 ± 0.12 Gy (mean ± S.D.) for the head-first plans and 11.72 ± 0.18 Gy for the feet-first plans, the near-maximum dose (D2) was 12.94 ± 0.13 Gy for the head-first plans and 12.78 ± 0.19 Gy for the feet-first plans. Dmean for the left and right inner lung were 8.73 ± 0.22 Gy and 8.69 ± 0.27 Gy.

The treatment time per fraction was 45.7-68.9 min for the head first plans and 12.3-16.0 min for the feet-first plans of the adults (fractional dose 3 Gy).

Variations in the MF, pitch and FW for head-first plans (fractional dose 3 Gy) with twelve beams and with otherwise constant parameters yield different dose-volume-histograms (DVH) and treatment times (see Figure 2). If the planned modulation factor was between 1.25 and 2

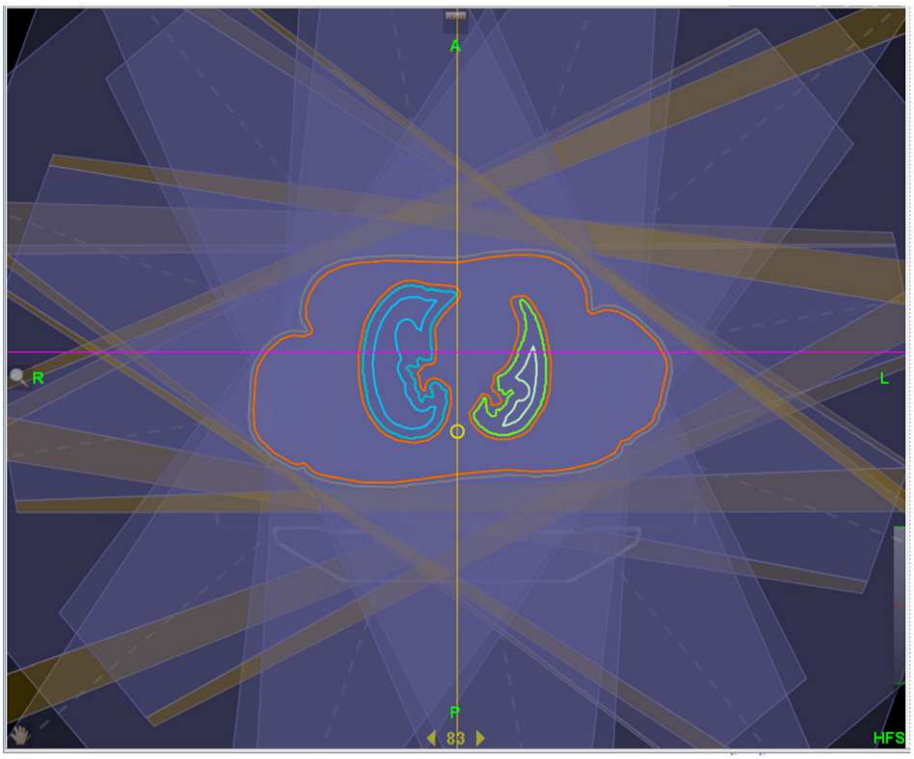

Figure 1 Twelve beams with equally spaced angles were used for the head-first-plan. The beams were expanded (yellow part of the beam) laterally on both edges by a maximum of 5 leaves each (3,125 cm at isocenter). This expansion is limited if leaves on the end of the MLC are already used because of the patient size.

Table 3 DVH results (hf = head-first plan, ff = feet-first plan, HI = homogeneity index = difference between D2 and D98 divided by the median dose, see [14])

Patient no. head/ feet first	Dose per fraction [Gy]	Time per fraction [min]	D98 [Gy]	D2 [Gy]	D50 [Gy]	HI	Dmean [Gy] inner lung left	Dmean [Gy] inner lung right
1 – hf	3 Gy	59.6	11.5	13.1	12.37	0.129	8.68	8.43
2 – hf	3 Gy	68.9	11.4	13.0	12.23	0.131	8.91	8.76
3 – hf	2 Gy	29.1	11.2	12.7	12.13	0.124	8.29	8.22
4 – hf	3 Gy	50.9	11.5	12.9	12.30	0.114	8.76	8.65
4 – ff	3 Gy	13.5	11.4	13.1	12.30	0.138		
5 – hf	3 Gy	45.7	11.5	13.0	12.35	0.121	8.64	8.69
5 – ff	3 Gy	12.3	11.8	12.7	12.09	0.074		
6 – hf	3 Gy	59.0	11.6	13.0	12.38	0.113	9.03	9.11
6 – ff	3 Gy	14.7	11.8	12.7	12.12	0.074		
7 – hf	3 Gy	45.7	11.5	13.0	12.34	0.122	8.69	8.70
7 – ff	3 Gy	16.0	11.8	12.8	12.19	0.082		
8 – hf	3 Gy	49.9	11.4	12.8	12.25	0.114	8.86	8.93
8 – ff	3 Gy	13.9	11.8	12.6	12.18	0.066		
Range hf		45.7-68.9 (without pat. 3)	11.2-11.5	12.7-13.1	12.13-12.37	0.114-0.131	8.20-9.03	8.22-9.11
Range ff		12.3-16.0	11.4-11.8	12.6-13.1	12.09-12.30	0.066-0.138		
Average hf		54.2 (without pat. 3)	11.45	12.94	12.29	0.121	8.73	8.69
Average ff		14.1	11.72	12.78	12.18	0.087		

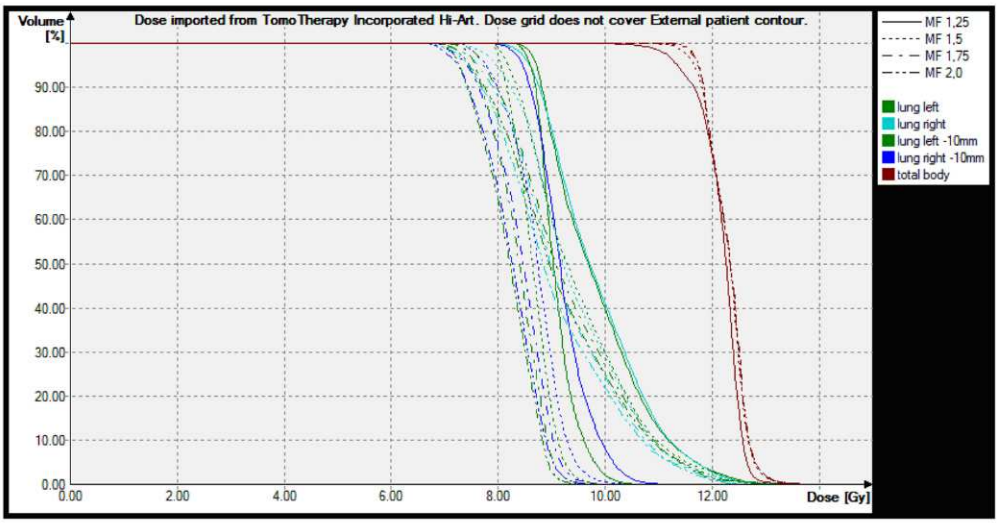

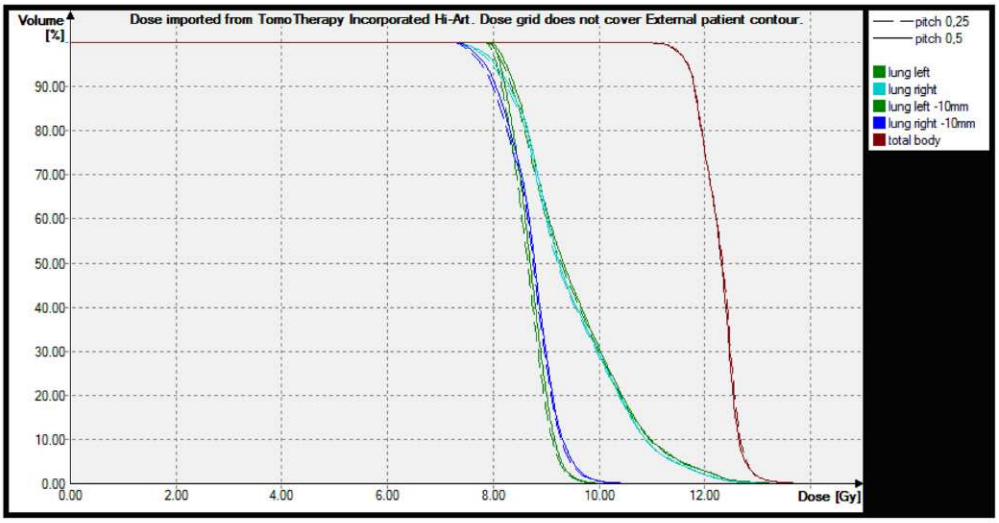

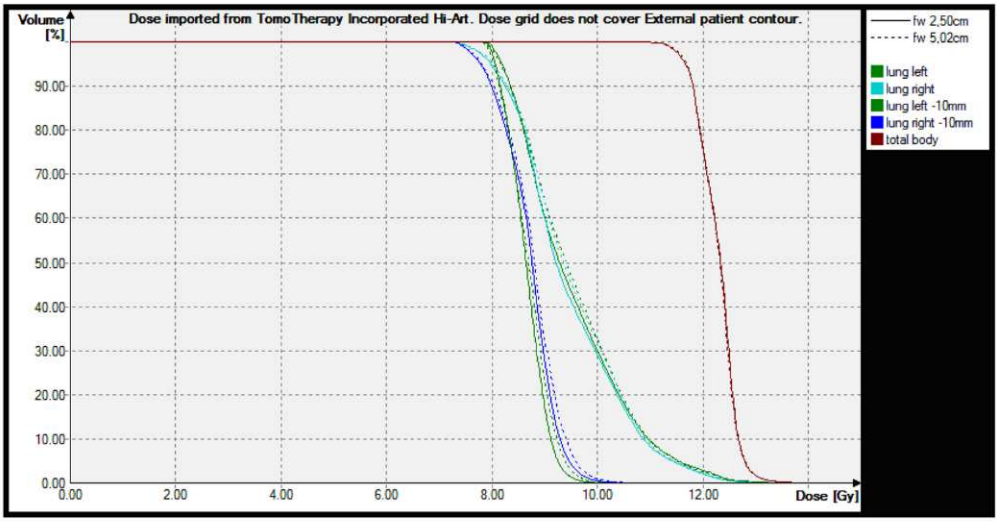

Figure 2 Dose volume histograms of total body (head-first plan), lung and inner lung as a function of modulation factor (MF), pitch and field width of Y-jaws (FW). Values, if not varied are: MF = 1.5, pitch = 0.25, FW = 2.5 cm.

Table 4 Results of TLD measurements in the Rando™ phantom (negative values mean a lower dose in the calculated plan)

Region	No of TLDs	Mean [%]	Standard deviation	dev. >5%	dev. >3%
Head and neck	4	−3.47	1.11	0	3
Thorax without lung	7	−1.19	1.15	0	0
Lung	10	1.11	1.84	0	2
Abdomen	4	−1.40	2.10	0	2
All	25	−0,66	2.26	0	7

(pitch was 0.25, FW was 2.5 cm), the DVH of the target showed an increased homogeneity with increasing MF, while the treatment time per fraction was also increased (MF planned 1.25, finally 1.44: 40.8 min, MF = 1.5/1.72: 45.7 min, MF = 2.0/2.26: 60.3 min, MF = 5/5.58: 145 min). If the planned MF was greater than 2, the dose homogeneity was not improved with increasing MF, while the treatment time became longer.

If the pitch changed from 0.25 to 0.5 (MF was 1.5, FW was 2.5 cm), there were only small differences determinable in the DVHs, and treatment times changed only minimally (45.7 vs. 45.8 min). In some cases we observed fewer hot or cold spots if the pitch was smaller. Modification of the field width had considerable influence on the treatment time (FW = 2.5 cm: 45.7 min, FW =

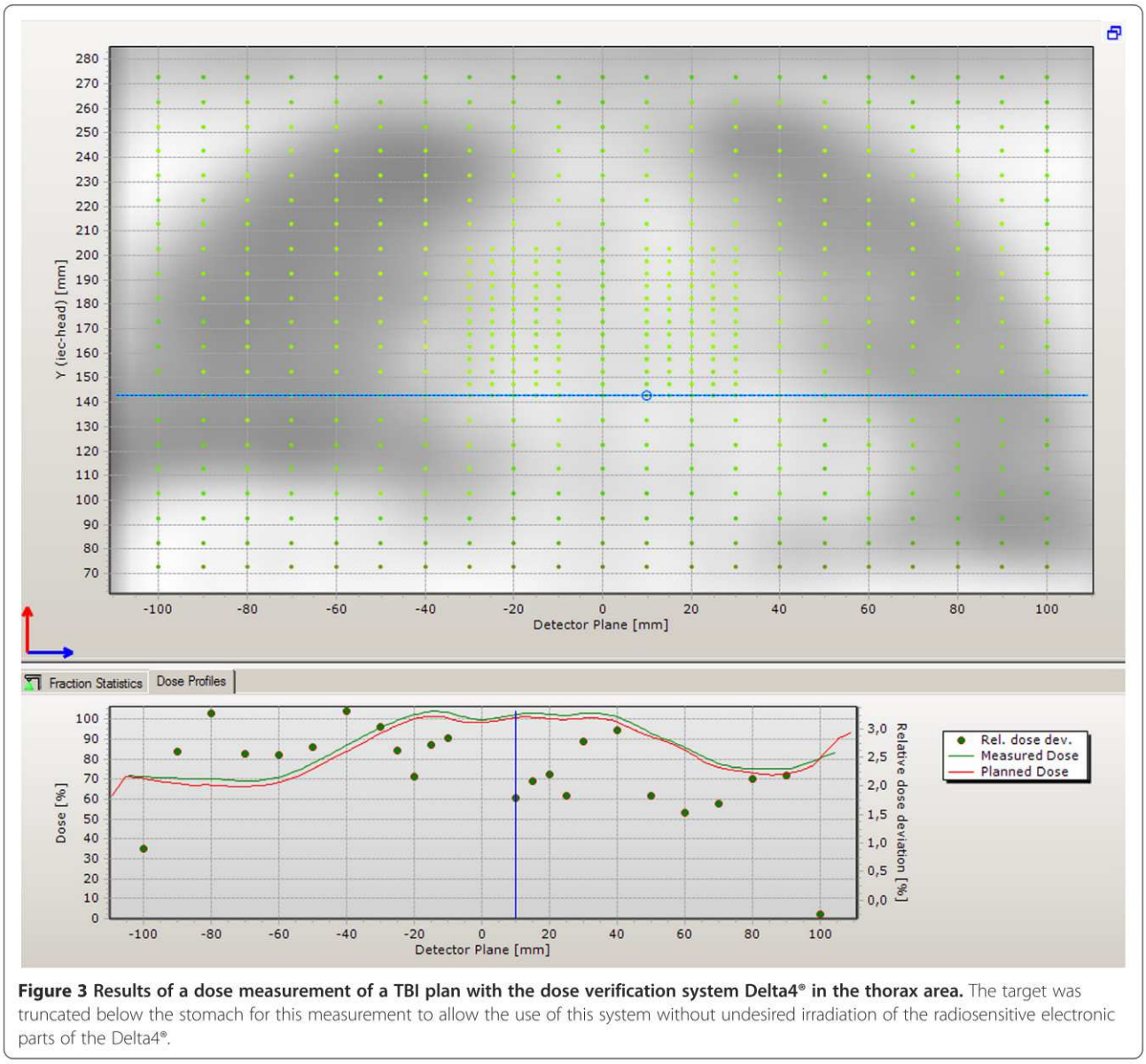

Figure 3 Results of a dose measurement of a TBI plan with the dose verification system Delta4® in the thorax area. The target was truncated below the stomach for this measurement to allow the use of this system without undesired irradiation of the radiosensitive electronic parts of the Delta4®.

5 cm: 24.0 min), while the quality of the DVH was nearly constant.

A critical point can be the dose grid. It was observed that differences between the calculated dose distribution before and after final dose calculation can locally amount to 1 Gy if the optimization was not performed with the fine dose grid, which should be taken into account for the optimization. This is especially important for small organs with strong maximum criteria as the lens.

Dose verification measurements

Planning and irradiation of a RANDO phantom with thermoluminescent rods showed a mean deviation of 0.66 ± .2.26% between calculation and measurement (Table 4). 18 of 25 TLDs showed a deviation smaller than 3%, no TLD showed a deviation larger than 5%.

The dose measurements with the dose verification system Delta4® in the thorax (see Figure 3) showed a median dose deviation of 1.5%. The dose deviation was less than 3% for 89% of the diodes in the high-dose area and in the lung. Figure 3 shows a line dose from the left to the right side in the thorax.

The measurements with the ion chamber in a cylindrical phantom ("Cheese phantom", TomoTherapy®) showed a mean error in the mediastinum of 1.1 ± 1.5%, in the lung of 2.2 ± 1.8% and in the leg of 1.8% ± 0.7% of the calculated dose.

Patient immobilization and setup verification

Patient immobilization and setup verification were well tolerated. For the correction of set-up errors the main focus was on a correct positioning of the cranio-thoracic area (vertebrae, lung). Setup errors in the head area after correction amounted to 5 mm or less.

Discussion

The introduction of intensity modulated TBI techniques has the potential to homogenize the dose to the target and to reduce the prescribed dose on specified organs (see Figure 4). A comparison with the conventional translation method with lung blocks reveals a much higher homogeneity in the target with TomoDirect™ (Figure 5). Irradiation in prone position is not necessary, which is more comfortable for the patient.

The limited table motion capacity of the table of both TomoTherapy® and CT has to be considered carefully. We decided to start in head-first position, then to turn the vacuum cushion and subsequently treat feet-first. So we have two target volumes: one in the head-first CT beginning from the head and one in the feet-first CT (legs, feet) with a defined distance to each other. The definition of two "overlap regions" with an extension of three cm each enables smooth dose gradients in each plan to avoid critical overdosage and underdosage. The cumulative dose in this region was measured in-vivo with TLDs.

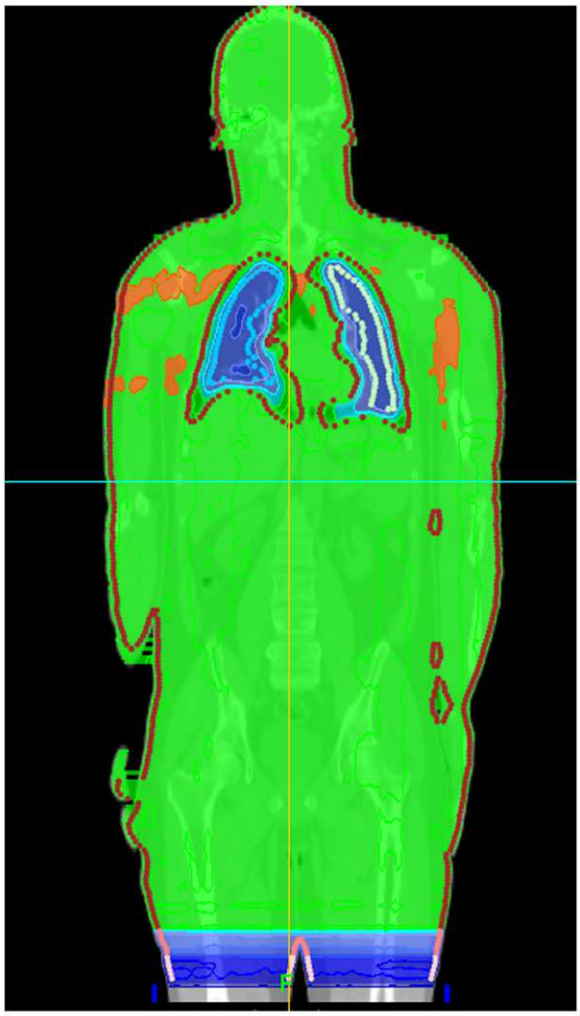

Figure 4 Dose distribution (in Gy) of a TBI head-first treatment plan. Isodoses: 14 Gy (red), 13 Gy (orange), 12 Gy (green), 11 Gy (green), 10 Gy (light blue), 9 – 8 – 6 – 4 – 2 Gy blue (stepwise).

Treatment planning

Treatment plans with a very good dose homogeneity can be obtained with different parameters.

Our studies showed that the modulation factor (MF) has the most prominent impact on dose homogeneity and treatment time especially if it is between 1 and 2. Beyond these values, the treatment time is prolonged without an effect on treatment plans. For that reason the planned modulation factor should be smaller than 2. A small pitch can be helpful for patients with a large diameter to avoid few small underdosage regions near the skin. No noteworthy differences were seen for smaller patients.

Comparing treatment plans calculated with a field width of 5 cm and 2.5 cm, the treatment time differs by a factor

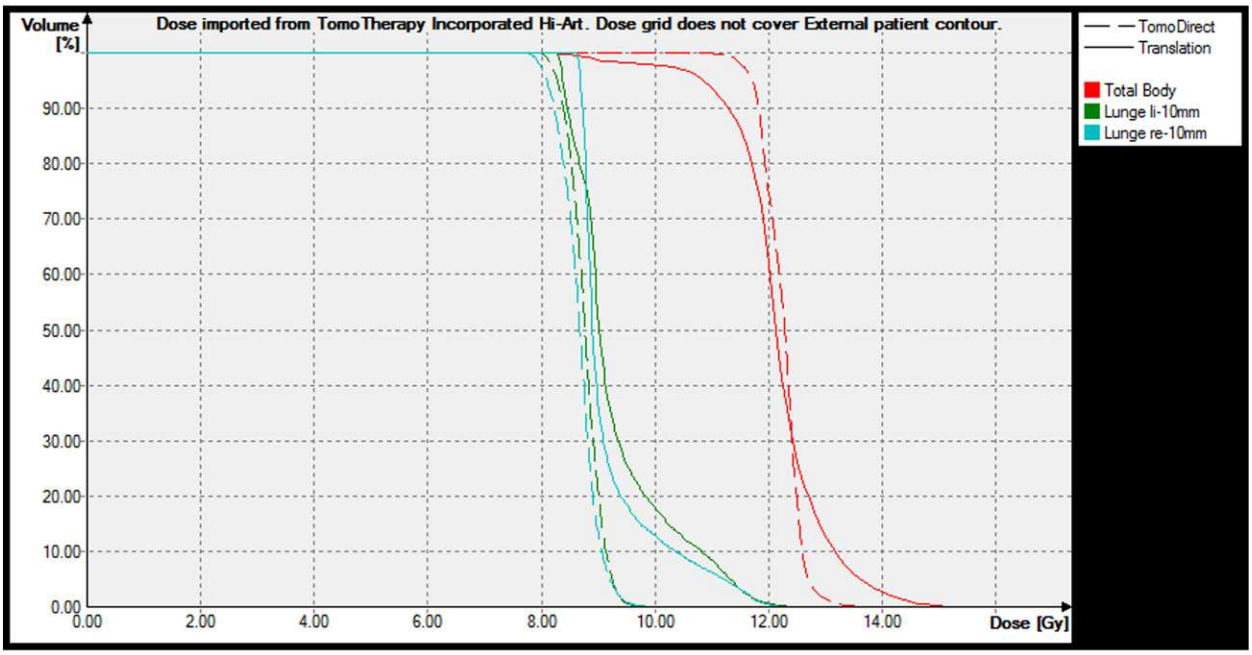

Figure 5 Comparison of dose-volume-histograms for the translational method with lung blocks and TomoDirect™. The DVH of the treatment plan of the translational technique was calculated with Oncentra, the comparison is done with Oncentra as well.

of 2 whereas almost equal homogeneity can be obtained. We prefer a treatment time of approximately one hour for adults in this study as a compromise between a lower mean dose rate in the lung and the patient's comfort. Because of the above-named considerations, a MF of 1.5, a pitch of 0.25, a field width of 2.5 cm and a fine dose grid already during inverse planning are used now as default values.

Patient immobilization and setup verification

TomoDirect™ requires a higher accuracy in patient positioning than conventional methods. On the other hand, the use of a vacuum cushion and the MVCT option ensure a sufficient accuracy.

Because the beams include up to five additional open leaves at the edges, set-up errors up to 2 cm can be tolerated. Therefore no masks for head and neck were used.

Comparison between static and helical tomotherapy

The main difference between static and helical TomoTherapy® is that with TomoDirect™ the body gets the dose from up to 12 fixed beams. So it is similar to a linac-based IMRT but with a very large field length. Taking into account that for the irradiation of one beam between 3.5 min and 5 min are needed, the irradiation time for single organs or points in the body is 30–60 min. With helical TomoTherapy®, the full fractional dose per point is given in one portion with a duration less than one minute. According to [15] the toxicity to the lung is more dependent on the average dose rate than on the maximum or instantaneous dose rate. An irradiation with several beams prolongs the treatment time per fraction of the lung and can be less toxic than one beam, but there is no clinical evidence up to now.

A second point of view is the dose heterogeneity in circulating blood. Malloy et al. [16] showed that the blood dose heterogeneity is improved by the use of longer treatment times and reduced dose rates for sequential techniques like IMRT and TomoTherapy®. It is reported furthermore, that the dose heterogeneity is on the order of magnitude of + – 10% for a treatment time of 20 min and a (theoretical) 2 min (125 s) perfusion period, which corresponds to heterogeneity values that are typically considered acceptable when evaluating traditional TBI [16].

Considering these results, dose heterogeneity in circulating blood cells is improved with TomoDirect™ compared to helical TomoTherapy® for typical treatment times, perfusion rates and cell types.

The third difference are the additional open leaves at the edges of the beam. In helical mode it is not possible to create such a beam expansion. So set-up errors up to 2 cm can be tolerated and masks for head and neck can be omitted.

Independent of that, a voxel based dose algorithm as reported in [17] has the potential to implement adaptive radiotherapy and to improve the robustness for helical TomoTherapy®.

Finally, the dose distribution is sufficient with both techniques, perhaps with less hot spots with TomoDirect™.

In [9] dose peaks of up to 130% were observed in small volumes with helical TomoTherapy®. For most cases we did not find dose maxima larger than 120% with TomoDirect™. The near-max dose D2 was between 12.7 and 13.1 Gy for all cases.

Potential use

TomoDirect™ allows the implementation of organ-specific dose prescriptions. So the dose to sensitive structures can be lowered which has the potential to reduce acute and chronic morbidity. Otherwise it is supposed [18,19] that "more dose in the target is better" if the biologically effective doses in lung, kidney and eyes are not increased. So this technique may allow delivery of higher doses or dose escalation with limited toxicity to normal critical structures. Irradiation with simultaneous integrated boost, e.g. for bone marrow, are in the realm of possibilities for TBI now.

Conclusion

With the new TomoDirect™ modality, the TomoTherapy® system combines the conventional translational method for TBI with the possibilities of IMRT. There are clear advantages compared to conventional methods which make it very attractive: excellent homogeneity, dose sparing of specific organs and comfort can be assumed to be for the benefit of the patient. The discussion about the "delicate balance" [18] between the need for aggressive treatment and limited toxicity can be renewed with the new potentials of TomoDirect™ - for children as well as for adults – and possibly yield a better clinical outcome in the future.

Competing interests

The authors declare that they have no competing interests.

Authors' contributions

HS conceived and developed the project, HS, BB, SH, NB and TW planned and performed the project, HS and BB performed the treatment planning analysis, HS, BB, SH, NB and KW performed dosimetric measurements, HS prepared the manuscript, BB, SH, NB, KW, TW and TGW revised the manuscript. All authors read and approved the final manuscript.

Received: 30 June 2014 Accepted: 17 February 2015
Published online: 06 March 2015

References

1. Chui CS, Fontenla DP, Mullokandov E, Kapulsky A, Lo YC, Lo CL. Total body irradiation with an Arc and a gravity-oriented compensator. Int J Radiat Oncol Biol Phys. 1997;39:1191–5.
2. Hussein S, El-Khatib E. Total body irradiation with a sweeping 60Cobalt beam. Int J Rad Onc Biol Phys. 1995;33:493–7.
3. Quast U. Physical treatment planning of total body irradiation: patient translation and beam zone method. Med Phys. 1985;12:567–74.
4. Quast U. Total body irradiation–review of treatment techniques in Europe. Radiother Oncol. 1987;9:91–106.
5. Sanchez-Doblado F, Quast U, Arrans R, Errazquin L, Sanchez-Nieto B, Terron JA. Total body irradiation prior to bone marrow transplantation. Report of European Group for Blood and Marrow Transplantation. Sevilla; 1995.
6. Jahnke A, Jahnke L, Molina-Duran F, Ehmann M, Kantz S, Steil V, et al. Arc therapy for total body irradiation - a robust novel treatment technique for standard treatment rooms. Radiother Oncol. 2014;110:553–7.
7. Kirby N, Held M, Morin O, Fogh S, Pouliot J. Inverse-planned modulated-arc total-body irradiation. Med Phys. 2012;39:2761–4.
8. Hui SK, Kapatoes J, Fowler J, Henderson D, Olivera G, Manon RR, et al. Feasibility study of helical tomotherapy for total body or total marrow irradiation. Med Phys. 2005;32:3214–24.
9. Gruen A, Ebell W, Wlodarczyk W, Neumann O, Kuehl JS, Stromberger C, et al. Total Body Irradiation (TBI) using helical tomotherapy in children and young adults undergoing stem cell transplantation. Radiation Oncol. 2013;8:92.
10. Zhuang AH, Liu A, Schultheiss TE, Wong JY. Dosimetric study and verification of total body irradiation using helical tomotherapy and its comparison to extended SSD technique. Med Dosim. 2010 Winter;35:243–9.
11. Franco P, Catuzzo P, Cante D, La Porta MR, Sciacero P, Girelli G, et al. TomoDirect: an efficient means to deliver radiation at static angles with tomotherapy. Tumori. 2011;97:498–502.
12. Murai T, Shibamoto Y, Manabe Y, Murata R, Sugie C, Hayashi A, et al. Intensity-modulated radiation therapy using static ports of tomotherapy (TomoDirect): comparison with the TomoHelical mode. Radiation Oncol. 2013;8:68.
13. Langner UW, Molloy JA, Gleason Jr JF, Feddock JM. A feasibility study using TomoDirect for cranial irradiation. J Appl Clin Med Phys. 2013;14:104–14.
14. International Commission on Radiation Units and Measurements. Prescribing, recording, and reporting photon-beam intensity-modulated radiation therapy (IMRT). ICRU Report 83. J ICRU. 2010;10:1–106.
15. Lehnert S, Rybka WB. Dose rate dependence of response of mouse lung to irradiation. Br J Radiol. 1985;58:745–9.
16. Molloy JA. Statistical analysis of dose heterogeneity in circulating blood: implications for sequential methods of total body irradiation. Med Phys. 2010;37:5568–78.
17. Chao M. Voxel-based dose reconstruction for total body irradiation with helical tomotherapy. Int J Radiat Oncol Biol Phys. 82:1575–83.
18. Hill-Kayser CE, Plastaras JP, Tochner Z, Glatstein E. TBI during BM and SCT: review of the past, discussion of the present and consideration of future directions. Bone Marrow Transplant. 2011;46:475–84.
19. Kal HB, Loes van Kempen-Harteveld M, Heijenbrok-Kal MH, Struikmans H. Biologically effective dose in total-body irradiation and hematopoietic stem cell transplantation. Strahlenther Onkol. 2006;182:672–9.

Experimental and Monte Carlo-based determination of the beam quality specifier for TomoTherapyHD treatment units

Simon Howitz[1,2,3,*], **Michael Schwedas**[1], **Tilo Wiezorek**[1], **Klemens Zink**[2,4,5]

[1] University Hospital Jena, Department of Radiation Oncology, Germany
[2] Institute for Medical Physics and Radiation Protection IMPS, University of Applied Science – THM, Giessen, Germany
[3] Philipps-University, Marburg, Germany
[4] University Medical Center Giessen-Marburg, Department of Radiation Oncology, Germany
[5] Frankfurt Institute for Advanced Studies (FIAS), Frankfurt, Germany

Received 12 April 2017; accepted 18 September 2017

Abstract

Reference dosimetry by means of clinical linear accelerators in high-energy photon fields requires the determination of the beam quality specifier $TPR_{20,10}$, which characterizes the relative particle flux density of the photon beam. The measurement of $TPR_{20,10}$ has to be performed in homogenous photon beams of size $10 \times 10\,cm^2$ with a focus-detector distance of 100 cm. These requirements cannot be fulfilled by TomoTherapy treatment units from Accuray. The TomoTherapy unit provides a flattening-filter-free photon fan beam with a maximum field width of 40 cm and field lengths of 1.0 cm, 2.5 cm and 5.0 cm at a focus-isocenter distance of 85 cm.

For the determination of the beam quality specifier from measurements under nonstandard reference conditions Sauer and Palmans proposed experiment-based fit functions. Moreover, Sauer recommends considering the impact of the flattening-filter-free beam on the measured data.

To verify these fit functions, in the present study a Monte Carlo based model of the treatment head of a TomoTherapyHD unit was designed and commissioned with existing beam data of our clinical TomoTherapy machine. Depth dose curves and dose profiles were in agreement within 1.5% between experimental and Monte Carlo-based data.

Based on the fit functions from Sauer and Palmans the beam quality specifier $TPR_{20,10}$ was determined from field sizes $5 \times 5\,cm^2$, $10 \times 5\,cm^2$, $20 \times 5\,cm^2$ and $40 \times 5\,cm^2$ based on dosimetric measurements and Monte Carlo simulations. The mean value from all experimental values of $TPR_{20,10}$ resulted in $\overline{TPR_{20,10}} = 0.635 \pm 0.4\%$. The impact of the non-homogenous field due to the flattening-filter-free beam was negligible for field sizes below $20 \times 5\,cm^2$. The beam quality specifier calculated by Monte Carlo simulations was $TPR_{20,10} = 0.628$ and $TPR_{20,10} = 0.631$ for two different calculation methods.

The stopping power ratio water-to-air $s^{\Delta}_{w,a}$ directly depends on the beam quality specifier. The value determined from all experimental $TPR_{20,10}$ data was $s^{\Delta}_{w,a} = 1.126 \pm 0.1\%$, which is in excellent agreement with the value directly calculated by Monte Carlo simulations. The agreement is a good indication that the equations proposed by Sauer and Palmans are able to calculate the beam quality specifier under reference conditions from measurements in arbitrary photon field sizes with high accuracy and are applicable for the TomoTherapyHD treatment unit.

Keywords: TomoTherapyHD, Monte Carlo simulation, Beam quality specifier, Photon dosimetry

* Corresponding author: S. Howitz, University Hospital Jena, Department of Radiation Oncology, Germany.
E-mail: simon.howitz@med.uni-jena.de (S. Howitz).

1 Introduction

According to national and international dosimetry protocols [1–3], clinical reference dosimetry for medical accelerators is based on the experimental determination of the beam quality index (BQI). Regarding high energy photon beams there are two different beam quality specifiers in use: the tissue-phantom ratio at a depth of 20 cm and 10 cm ($TPR_{20,10}$) [1,2] and the value of a normalized depth dose curve at the depth of 10 cm (*%dd*) [3]. In both cases the beam quality index has to be determined under reference conditions, meaning a field size of $10 \times 10\,cm^2$ with a homogenous fluence distribution and a source-axis-distance (SAD) of 100 cm or a source-surface-distance of 100 cm (SSD). For TomoTherapy treatment units these reference conditions cannot be realized, the field length is limited to 5 cm and the SAD is 85 cm. Moreover, as there is no flattening filter in the beam, the resulting beam profiles are non-homogenous [4–6].

To overcome the field size problem, Sauer [7] and Palmans [8] proposed different fit functions to calculate the beam quality specifier $TPR_{20,10}(10 \times 10\,cm^2)$ from measurements in arbitrary field sizes. Both fit functions are based on experimental data, mainly taken from BJR Suppl.25 [9].

However, these fit functions are based on flattened photon beams. Their applicability to the unflattened beam of a TomoTherapy unit will be investigated in this study by Monte Carlo simulations. Many authors have proven that especially within the Monte Carlo codes PENELOPE and EGSnrc [10,11] the transport of photons and charged particles (electrons and positrons) is adequately implemented and both codes are able to calculate the ion chamber response with an accuracy of 0.1% relative to its own cross-sections, even in the case of complex geometries. In the present study we have applied the EGSnrc [12] and BEAMnrc [13] Monte Carlo system to build the complete treatment head of a TomoTherapyHD unit. With this model Monte Carlo based *TPR*-values for different field sizes were calculated and compared with experimental values. Applying the equations from Sauer and Palmans the beam quality specifier BQI was calculated. The Monte Carlo model of the TomoTherapy unit also facilitates in calculation of the *TPR* under reference conditions, i.e. the direct determination of the beam quality specifier *TPR*.

2 Material and methods

2.1 Determination of beam quality in arbitrary field sizes

The photon beam quality specifier as defined in national or international codes of practice, like DIN 6800-2 [1] or IAEA TRS-398 [2], equals the tissue phantom ratio $TPR_{20,10}(10 \times 10\,cm^2)$,[1] which is the ratio of measured dose values determined in a water phantom in depths of 20 cm (D_{20}) and 10 cm (D_{10}), in a constant source-to-detector distance (SDD) of 100 cm and a field size of $10 \times 10\,cm^2$ at the SDD plane (Eq. (1)):

$$TPR_{20,10} = \frac{D_{20}}{D_{10}} \tag{1}$$

Due to the mentioned design, TomoTherapy users can only determine *TPR* values in smaller fields, since the maximal square field length (s) available at these machines is $s = 5$ cm. In 2009 Sauer [7] published a method to determine the beam quality specifier $TPR_{20,10}(10 \times 10\,cm^2)$ from measured $TPR_{20,10}(s)$ data. Based on published $TPR_{20,10}(s)$ data [9] for square field lengths $4\,cm < s < 40\,cm$ and own measurements for 6 MV and 10 MV photon beams ($2\,cm < s < 40\,cm$) he derived a fit for the beam quality specifier *BQI*:

$$TPR_{20,10}(10 \times 10\,cm^2) = \frac{TPR_{20,10}(s) - b_1 - A_1(1 - e^{-s/t})}{b_2 + A_2(1 - e^{-s/t})} \tag{2}$$

with

s: length of the square field,
A_1, A_2, b_1, b_2, t: fit parameters (see Table 1).

Table 1
Parameters for Eq. (2) valid for $0.62 < Q < 0.8$ taken from Sauer [7].

b_1:	-0.208 ± 0.022	A_1:	$+0.625 \pm 0.036$	t:	$+19.5 \pm 2$ cm
b_2:	$+1.213 \pm 0.030$	A_2:	-0.679 ± 0.050		

According to Sauer, the fit is applicable for square field lengths $4\,cm < s < 40\,cm$ and values of the beam quality specifier $0.62 < TPR_{20,10} < 0.8$. In all cases, the difference in *TPR* determined from a small field and applying Eq. (2) from the measured value at the field size $10 \times 10\,cm^2$ was not larger than 1% [7] for conventional linacs. For rectangular fields with side lengths a, b the equivalent square field lengths (s_{eq}) according to the conversion table A.2 listed in BJR Suppl.25 [9] may be applied.

The fit from Sauer was simplified by Palmans [8]:

$$TPR_{20,10} = \frac{TPR_{20,10}(s) + 0.0165(10 - s)}{1 + 0.0165(10 - s)} \tag{3}$$

[1] The German dosimetry protocol DIN 6800-2 defines Q as the beam quality index for high energy photon beams, i.e. $Q = TPR_{20,10}$. In contrast, international codes of practice (CoP) like IAEA TRS-398 uses the symbol Q only as a general symbol to indicate the quality of a radiation beam independent of the type of radiation. The beam quality index for high energy photon beams is $TPR_{20,10}$.

Eq. (3) is valid for a smaller range of field lengths $4\,cm < s < 12\,cm$ and nominal photon energies $4\,MV < E < 12\,MV$ with a maximum relative difference to the values of Eq. (2) of 0.24%.

2.2 Impact of non-flattened beams

The expressions described above (Eqs. (2) and (3)) were derived using measured depth dose data from flattened photon beams. The non-uniformity of the dose profile in a beam generated without a flattening filter (FFF beam) results to differences in phantom scatter that would influence the dose variation with increasing depth. These can be of the order of 4% in 6MV field size of $40 \times 40\,cm^2$ [14,15].

According to Sauer [7] the difference in phantom scatter for both types of photon beams can be taken into account by a modified equivalent square field length $s_{eq,FFF}$ in FFF beams. The modification proposed by Sauer is based on a model function for the scatter contribution on the central axis for circular fields published in BJR Suppl.25 [9]:

$$S_r = S_\infty(1 - e^{-(ar/r_{1/2})} - \mu r \frac{a}{r_{1/2}} e^{-(ar/r_{1/2})}) \tag{4}$$

with:

S_r: normalized central axis scatter dose in a field of radius r;
S_∞: normalized central axis scatter dose in a field of infinite radius;
r: field radius;
$r_{1/2}$: radius of a field giving a scatter dose on central axis of $S_\infty/2$;
μ: energy-dependent parameter.

According to Tab. A.II in BJR Suppl.25, the parameter μ for 6 MV photons equals zero and $r_{1/2}$ is 4.6 cm. The parameter a can be determined with the help of Fig.(A.1) in BJR Suppl.25, where the ratio S_r/S_∞ is plotted as a function of $r/r_{1/2}$. For $r = r_{1/2}$ the resulting value S_r/S_∞ equals 0.5. Based on these data, the parameter a is just $a = \ln(2)$ and for our case Eq. (4) is simply:

$$S_r/S_\infty = 1 - e^{-(\ln(2)r/4.6\,cm)} \tag{5}$$

To apply Eq. (5), the equivalent square field lengths must first be converted into equivalent circular field sizes r_{eq}. This can be done by applying Tab. A.1 from BJR Suppl. 25, which was done in the present study or by using the approximation $r_{eq} \approx s_{eq}/(0.9 \cdot 2)$. To consider the impact of unflattened dose profiles, i.e. the changed phantom scatter contributions, the equivalent field radius r_{eq} has to be modified. Sauer [7] assumed that the off-axis ratio at half of the equivalent radius r_{eq} in a depth of 10 cm, $OAR(r_{eq}/2)$, is approximately equal to the phantom scatter reduction:

$$OAR\left(\frac{r_{eq}}{2}\right) \cdot \frac{S_{r_{eq}}}{S_\infty} = \frac{S_{r_{eq,FFF}}}{S_\infty} = 1 - e^{-(\ln(2)r_{eq,FFF}/4.6cm)} \tag{6}$$

resulting in an expression for the equivalent field radius $r_{eq,FFF}$, correcting the reduced scatter contribution in FFF beams:

$$r_{eq,FFF} = \ln\left(\frac{1}{(1 - S_{r_{eq,FFF}}/S_\infty)}\right) \frac{4.6\,cm}{\ln(2)} \tag{7}$$

Finally the flattening-filter-free circular field radius ($r_{eq,FFF}$) must be converted into an equivalent square side length ($s_{eq,FFF}$) (see above).

The addendum to the 1990 United Kingdom dosimetry code of practice recommends the application of Eq. (3) for TomoTherapy machines [16] for a field of $10 \times 5\,cm^2$ and ignores the influence of the non-flattened beam. The verification of this recommendation is also goal of the present study.

2.3 Dosimetric measurements

The experiments were done in the PTW MP3T water phantom, which has a size of $60 \times 50 \times 34\,cm^3$. In all measurements it was ensured that there was at least a thickness of 7 cm backscatter material. Preliminary experiments were conducted to verify that this thickness is sufficient for backscatter equilibrium.

2.3.1 Experimental determination of beam quality specifier

$TPR_{20,10}$ measurements were performed in photon fields of sizes $5 \times 5\,cm^2$, $10 \times 5\,cm^2$, $20 \times 5\,cm^2$ and $40 \times 5\,cm^2$ with a source-to-detector distance (*SDD*) of 85 cm. To investigate a possible impact of the ion chamber on measured *TPR* values, three different chambers were used: PTW-31016 PinPoint (sensitive volume $V = 0.016\,cm^3$), SunNuclear A1SL ($V = 0.053\,cm^3$) and PTW-31003 Semiflex ($V = 0.125\,cm^3$). In this way we were able to exclude the influence of flattening-filter-free-related volume-averaging effects [17] on the *TPR* measurements. The dosimeter readings were corrected for air pressure and temperature. In a preliminary study possible saturation effects of the ion chambers were investigated. The saturation correction k_s for the PTW chambers was determined experimentally at water depths 10 and 20 cm using the two-voltage method [18] according to the German code of practice DIN 6800-2 [1] applying a voltage ratio of 400 V/100 V. For the PTW-31016 PinPoint chamber the saturation effect was up to 0.7%, but as there was no difference of k_s between the measurement depths 10 cm and 20 cm for all chambers and

field sizes the correction was not taken into further consideration for *TPR* measurements. According to McEwen [19] the polarity effect for the PinPoint chamber is negligible and was therefore also not considered.

Regarding the impact of the FFF beam on scattered dose (see Eq. (6)), isocentric dose profiles at a depth of 10 cm and a *SDD* of 85 cm were measured with the PTW-31016 PinPoint for each field size: $5 \times 5\,cm^2$, $10 \times 5\,cm^2$, $20 \times 5\,cm^2$ and $40 \times 5\,cm^2$.

2.3.2 *Commissioning of the Monte Carlo based accelerator*

For the commissioning of the Monte Carlo model, relative profiles and depth dose curve measurements with *SSD* of 85 cm and depths of 5 cm, 10 cm and 20 cm for the field size of $20 \times 5\,cm^2$ were performed. Profiles for the field sizes $10 \times 5\,cm^2$, $40 \times 5\,cm^2$, $10 \times 2.5\,cm^2$, $20 \times 2.5\,cm^2$ and $40 \times 2.5\,cm^2$ were additionally measured at a depth of 10 cm. All these depth dose and profile measurements were performed with a PTW-30106 PinPoint chamber.

2.4 Monte Carlo simulations

The EGSnrc code system [12] was used for all Monte Carlo simulations. A model of a TomoTherapyHD treatment head was commissioned with the BEAMnrc user code [13] for static beams with jaw openings of 2.5 cm and 5.0 cm. The treatment head was modeled according to detailed design information supplied by Accuray. The unknown parameters such as the energy of the primary electrons hitting the target and the electron spot size on the target were determined iteratively by comparison of measured and simulated profiles at a depth of 5 cm for the field size $20 \times 5\,cm^2$ in a water phantom sized $60 \times 60 \times 60\,cm^3$ and an *SSD* of 85 cm.

Additionally, a PDD for the same field size and further profiles in depths of 10 and 20 cm were calculated. Furthermore, profiles and PDDs for the field sizes $10 \times 5\,cm^2$, $40 \times 5\,cm^2$, $10 \times 2.5\,cm^2$, $20 \times 2.5\,cm^2$ and $40 \times 2.5\,cm^2$ in 10 cm depth also with an *SSD* of 85 cm were simulated. Moreover $TPR_{20,10}(s)$ simulations for field sizes $5 \times 5\,cm^2$, $10 \times 5\,cm^2$, $20 \times 5\,cm^2$ and $40 \times 5\,cm^2$ were performed. To calculate $TPR_{20,10}$ under reference conditions, the jaw and primary collimator opening of our virtual TomoTherapyHD Monte Carlo model were adjusted to the appropriate field size of $10 \times 10\,cm^2$ at the *SDD* plane. All these simulations were performed with the EGSnrc user code egs_chamber [20], using the modeled TomoTherapy treatment head as the source. The chamber used for all the measurements (PTW PinPoint 31016) was included in the Monte Carlo simulations. This chamber was already used in several Monte Carlo studies of our group, chamber details may be found in Czarnecki and Zink [21].

To account for a potential impact of the ion chamber on calculated dose values, the *TPR* calculations were additionally performed in a small water voxel of radius $r = 0.15$ cm and height $h = 0.3$ cm at the different depths in the water phantom. This voxel size is a good approximation for the necessary point dose in the non-homogenous beam of the TomoTherapy unit, i.e. a further reduction of voxel size did not change the calculated dose value D_w [22].

The stopping power ratio water-to-air $s^{\Delta}_{w,a}$ is directly related to the beam quality specifier $TPR_{20,10}$. According to Andreo [23] eq. (8) holds and may be applied to compare and evaluate the experimental and Monte Carlo-based values for the beam quality specifier:

$$s^{\Delta}_{w,a} = 1.3614 - 1.2963 \cdot TPR_{20,10} + 2.5302 \cdot (TPR_{20,10})^2 - 1.6896 \cdot (TPR_{20,10})^3 \quad (8)$$

For that reason $s^{\Delta}_{w,a}$ was calculated applying the user code SPRRZnrc [24] under reference conditions, i.e. at a depth of 10 cm with a field size of $10 \times 10\,cm^2$. The air- or water-filled cavity used for this calculation was a cylinder with $r = 0.05$ cm and $h = 0.01$ cm in a water phantom with a radius of 30 cm and a height of 60 cm. A phase-space file from our virtual TomoTherapyHD unit generated with BEAMnrc was used as the source for this calculation.

For all Monte Carlo simulations using the codes egs_chamber and SPRRZnrc the threshold/cut-off energies for the particle transport was set to ECUT = AE = 521 keV for electrons as well as positrons and PCUT = AP = 10 keV for photons. The BEAMnrc simulations were performed with values ECUT = AE = 700 keV and PCUT = AP = 10 keV in favor of calculation time.

3 Results

3.1 Commissioning of the TomoTherapyHD Monte Carlo model

A comparison of Monte Carlo calculated and measured depth dose curves and profiles is shown in Fig. 1. The best agreement of the depth dose curves was achieved with a Gaussian spectral distribution of the primary electrons with a full width at half maximum (FWHM) of 0.126 MeV and a mean energy of 5.0 MeV. Compared with published data from Thomas et al. [25] ($E_0 = 5.6$ MeV) and Jeraj et al. [5] ($E_0 = 6.0$ MeV) our determined primary electron energy is considerably smaller, but one has to keep in mind that these published values were determined for the older TomoTherapy HiArt machines. The TomoTherapyHD unit investigated here has a different target design and newer publications [26,27] confirm our finding that the energy of the primary electrons is well below 6 MeV.

As shown by Wang et al. [28], the penumbra of the dose profiles strongly depends on the focal spot size. Therefore the spot size was optimized by comparing the measured and Monte Carlo-based penumbra size of the $5 \times 20\,cm^2$ field in the lateral (x) and longitudinal (y) directions at a depth of

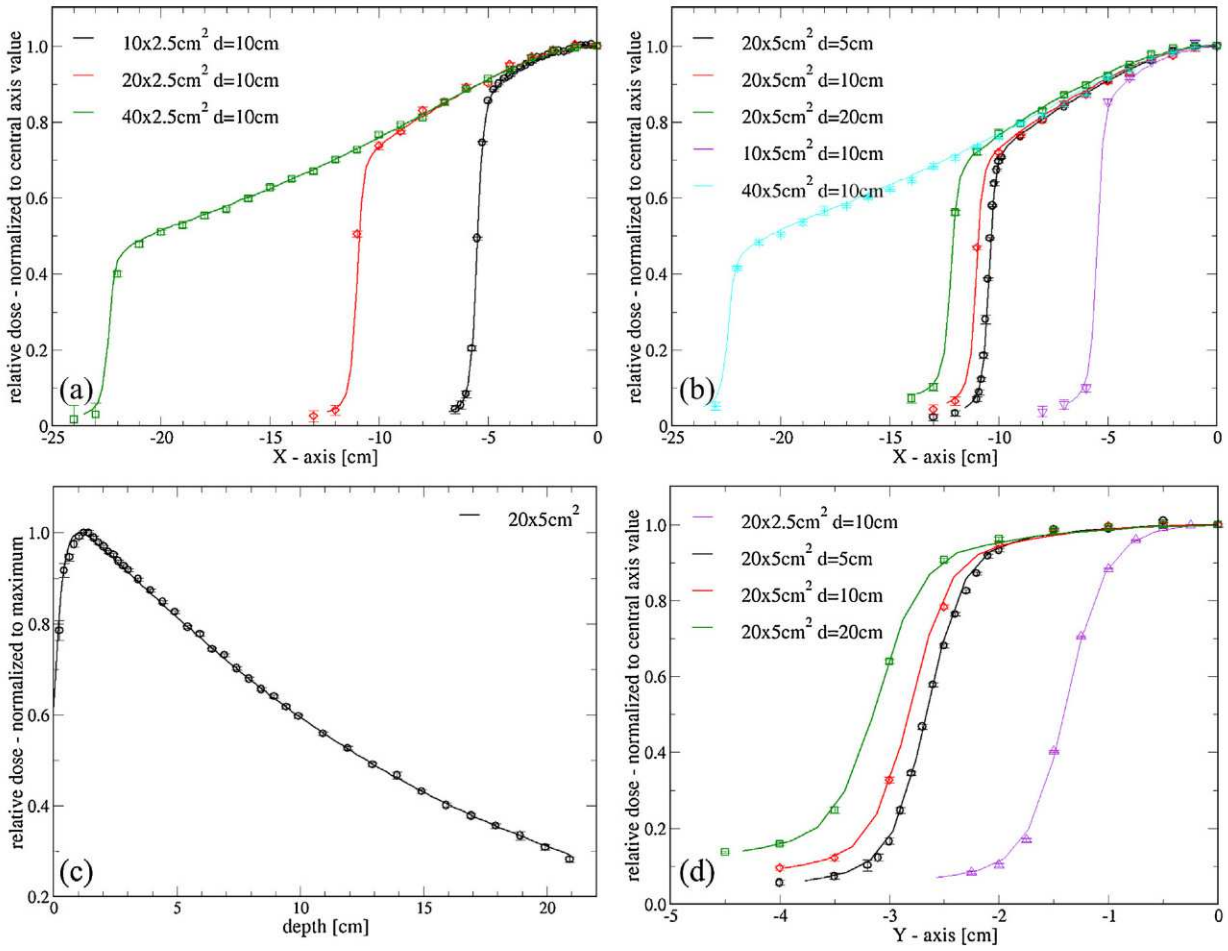

Figure 1. Comparison of Monte Carlo calculated (symbols) and measured (lines) profiles and depth dose curves of the commissioned TomoTherapyHD treatment unit. (a) x-Profiles for jaw opening 2.5 cm at a depth of 10 cm. (b) x-Profiles for jaw opening 5.0 cm at depths 5 cm, 10 cm and 20 cm. (c) Depth dose curves for field size $5 \times 20\,cm^2$. (d) y-Profiles for field size of $5 \times 20\,cm^2$ at depths of 5 cm, 10 cm and 20 cm and field size $2.5 \times 20\,cm^2$ at 10 cm depth. The error bars for the Monte Carlo data indicate the type-B uncertainties; within the field they correspond to the symbol width.

5 cm. The best results were accomplished with an elliptical spot size with Gaussian distributions in both directions. In the x direction the determined FWHM value was 0.18 cm, in the y direction 0.10 cm. For the field size used for optimization, measured and simulated profiles and depth dose curves agree better than $\Delta D/\Delta d = 1\%/1$ mm.

With the determined parameters the profiles and PDD's for the field sizes $10 \times 5\,cm^2$, $40 \times 5\,cm^2$, $10 \times 2.5\,cm^2$, $20 \times 2.5\,cm^2$ and $40 \times 2.5\,cm^2$ were evaluated; the agreement in all cases was almost better than $\Delta D/\Delta d = 1\%/1$ mm.

3.2 Determination of beam quality index

The equivalent field sizes for our measurements at the TomoTherapyHD unit and the impact of the non-flattened beam according to Eq. (7) are summarized in Table (2).

Fig. 2 shows the measured and Monte Carlo-based $TPR_{20,10}(s)$ values as well as the resulting beam quality specifier according to the different approaches described in Section 2.1.

As expected, the measured and Monte Carlo-based $TPR_{20,10}$ values as a function of the equivalent field length s increase with increasing field size (open symbols in Fig. 2). The experimental data taken with the three different ion chambers agree within 0.5%.

Regarding the Monte Carlo-based $TPR_{20,10}$ values, only those including the ion chamber (PTW 31016) during simulations are shown in Fig. 2. The $TPR_{20,10}$ values calculated in the water cylinder agree within statistical uncertainty with those including the chamber, proving that the chamber has no impact on TPR measurements. For clarity the water voxel data are omitted in Fig. 2.

The agreement between experimental and Monte Carlo-based $TPR_{20,10}$ values is $\Delta < 0.8\%$ and therewith a further proof for the correct modeling of the TomoTherapyHD treatment head.

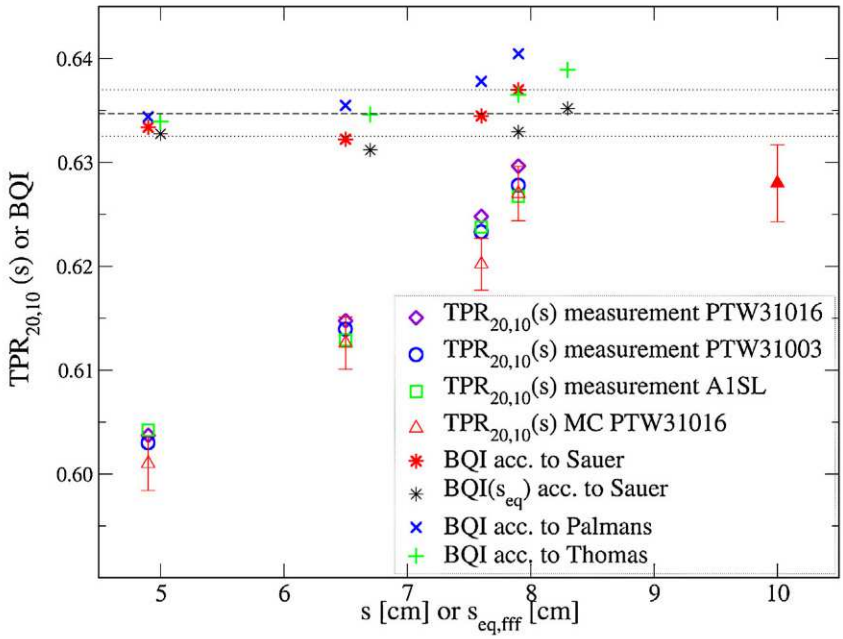

Figure 2. Measured and Monte Carlo-based $TPR_{20,10}$ values as a function of the equivalent square field length s and resulting data for the beam quality specifier (BQI) according to the different approaches given in Section 2.1. The data point for $s = 10$ cm, $TPR_{20,10}(10 \times 10\,\text{cm}^2)$ was calculated under reference conditions, i.e. with the field size of $10 \times 10\,\text{cm}^2$ at an $SDD = 100$ cm. For all Monte Carlo data the ion chamber PTW-31016 PinPoint was included in the simulations. The horizontal lines represent the mean value and standard deviation of all experimental based BQI values. The error bars for the Monte Carlo data indicate the type-B uncertainties.

Applying Eqs. (2) or (3) and accounting for the impact of the FFF beam (see Eq. (7) and Table 2) the beam quality specifier was calculated based on the experimental measured $TPR_{20,10}$ values. These results are shown as bold stars and crosses in Fig. 2. Neglecting the impact of the FFF beam as recommended by Thomas et al. [16], the BQI values are somewhat smaller, shown as pluses (3) and thin stars (2). The largest deviation between the different methods to determine the beam quality specifier and applying different field sizes is below 1.0%, even when the impact of FFF beams is neglected. The average of BQI regarding all experimental data sets is $\overline{TPR_{20,10}} = 0.635$ with a standard deviation of $\pm 0.4\%$, shown by the dashed horizontal line in Fig. 2.

Additionally Fig. 2 includes the Monte Carlo calculated value for the beam quality specifier which was calculated under reference conditions, i.e. with an SDD of 100 cm and a field size of $10 \times 10\,\text{cm}^2$ at SDD plane. The numerical values are $\overline{TPR_{20,10}} = 0.628 \pm 0.6\%$, calculated with the PTW-31016 PinPoint chamber and $\overline{TPR_{20,10}} = 0.631 \pm 0.34\%$ calculated within the water cylinder. As one can see, these values are somewhat smaller than those determined from true TPR measurements. However, regarding the uncertainties of the different values, the experimental BQI-value is in good agreement with our Monte Carlo-based value determined under reference conditions.

Using the experimental BQI value $\overline{TPR_{20,10}} = 0.635$ and applying Eq. (8) a value for the stopping power ratio $s^{\Delta}_{w,a} = 1.126 \pm 0.1\%$ is obtained. The Monte Carlo-based value, calculated with the user code SPRRZnrc using a phase space file from our modeled TomoTherapyHD unit with jaw openings of $10 \times 10\,\text{cm}^2$ and a SDD of 100 cm is $s^{\Delta}_{w,a} = 1.126 \pm 0.1\%$, which is in perfect agreement with the experimental value.

Table 2
Geometrical and effective field sizes for the TomoTherapyHD unit and impact of the unflattened beam on the equivalent field size.

Geometrical field size in cm^2	s_{eq} in cm	r_{eq} in cm	$OAR(r_{eq}/2)$ relative	$r_{eq,FFF}$ in cm	$s_{eq,FFF}$ in cm
5×5	5.0	2.80	0.97	2.71	4.9
10×5	6.7	3.75	0.97	3.62	6.5
20×5	7.9	4.40	0.97	4.22	7.6
40×5	8.3	4.60	0.97	4.37	7.9

4 Discussion

According to all present dosimetry protocols [1–3] clinical photon beam dosimetry is based on reference conditions which cannot be fulfilled with TomoTherapy treatment units. The determination of the photon beam quality specifier $BQI = TPR_{20,10}$ requires measurements within a water phantom with a field size of $10 \times 10\,\text{cm}^2$ and a source-to-detector distance of 100 cm. Both conditions cannot be realized at TomoTherapy treatment units, since the maximum field size at these machines in one direction is limited to 5 cm and the

source-to-axis distance for these machines is 85 cm. Moreover, due to the absence of a flattening filter TomoTherapy units are not able to create homogenous dose profiles, which is a prerequisite for the application of present dosimetry codes of practice. Mainly based on data from BJR Suppl.25 [9] Sauer [7] and Palmans [8] developed fit functions to determine *BQI* from *TPR* measurements in arbitrary photon field sizes. Additionally Sauer suggests a method to include the impact of flattening-filter-free beams in the determination of *BQI*. The determination of the beam quality specifier based on $TPR_{20,10}$ measurements and Monte Carlo simulations for different field sizes and the application of the approximations proposed by Sauer [7] and Palmans [8] given in Eqs. (2) and (3) resulted in consistent *BQI* values varying by no more than ±0.5%, with the exception of the largest field size ($40 \times 5\,cm^2$) when Eq. (3) is applied. In that case a deviation from the mean value of about 1% was determined. As can be seen in Fig. 2, the consideration of the impact of the FFF beam on the resulting *BQI* as proposed by Sauer is negligible for the field sizes used in the present study. This result is in agreement with the findings of Thomas et al. [16], warranting the recommendation in the United Kingdom code of practice [16].

The impact of the above mentioned variation of the determined *BQI* value of ±0.5% on the resulting beam quality correction factor k_Q and therefore on measured dose-to-water in the energy range investigated here is around 0.1%, which is negligible for clinical dosimetry. Therefore, from a practical clinical point of view the correction of the equivalent field length (see Section 2.2) can be omitted as long as small-volume ion chambers ($V \leq 0.125\,cm^3$) in field sizes $\geq 5 \times 5\,cm^2$ are used.

The present study is based on experimental data and Monte Carlo simulations and the comparison of both data sets. The results, which couldn't be gained by experiments alone once again show the usefulness of Monte Carlo simulations to solve dosimetric problems.

5 Conclusion

The present study confirmed that the method developed by Sauer and developed further by Palmans can be used for the determination of the beam quality index of TomoTherapy treatment units from measured *TPR* values under the nonstandard reference conditions. Furthermore it was confirmed that the change in phantom scatter as a result of the non-flat beam in FFF beams does not influence the determination of the *BQI* value with this method.

References

[1] DIN6800-2. Dosismessverfahren nach der Sondenmethode für Photonen- und Elektronenstrahlung; Teil 2: Dosimetrie hochenergetischer Photonen- und Elektronenstrahlung mit Ionisationskammern, Report; 2008.

[2] Andreo P, Burns D, Hohlfeld K, Huq MS, Kanai T, Laitano F, et al. Absorbed dose determination in external beam radiotherapy. In: Technical reports series no. 398, report. 2000.

[3] Almond PR, Biggs PJ, Coursey BM, Hanson WF, Huq MS, Nath R, et al. AAPM's TG-51 protocol for clinical reference dosimetry of high-energy photon and electron beams. Med Phys 1999;26:1847–70, http://dx.doi.org/10.1118/1.598691.

[4] Mackie TR. History of tomotherapy. Phys Med Biol 2006;51(13): R427–53, http://dx.doi.org/10.1088/0031-9155/51/13/R24 http://www.ncbi.nlm.nih.gov/pubmed/16790916.

[5] Jeraj R, Mackie TR, Balog J, Olivera G, Pearson D, Kapatoes J, et al. Radiation characteristics of helical tomotherapy. Med Phys 2004;31(2):396–404 http://www.ncbi.nlm.nih.gov/pubmed/15000626.

[6] Meeks SL, Harmon J, Langen JFKM, Willoughby TR, Wagner TH, Kupelian PA. Performance characterization of megavoltage computed tomography imaging on a helical tomotherapy unit. Med Phys 2005;32(8):2673–81 http://www.ncbi.nlm.nih.gov/pubmed/16193798.

[7] Sauer OA. Determination of the quality index (Q) for photon beams at arbitrary field sizes. Med Phys 2009;36(9):4168–72 http://www.ncbi.nlm.nih.gov/pubmed/19810490.

[8] Palmans H. Determination of the beam quality index of high-energy photon beams under nonstandard reference conditions. Med Phys 2012;39(9):5513–9, http://dx.doi.org/10.1118/1.4745565 http://www.ncbi.nlm.nih.gov/pubmed/22957618.

[9] BJR-25. British Journal of Radiology, report; 1996.

[10] Kawrakow I. Accurate condensed history Monte Carlo simulation of electron transport. I. EGSnrc, the new EGS4 version. Med Phys 2000;27(3):485–98 http://www.ncbi.nlm.nih.gov/pubmed/10757601.

[11] Kawrakow I. Accurate condensed history Monte Carlo simulation of electron transport. II. Application to ion chamber response simulations. Med Phys 2000;27(3):499–513, http://dx.doi.org/10.1118/1.598918 http://www.ncbi.nlm.nih.gov/pubmed/10757602.

[12] Kawrakow I, Mainegra-Hing E, Rogers D, Tessier F, Walters B. The EGSnrc code system: Monte Carlo simulation of electron and photon transport. Report; 2016.

[13] Rogers DW, Faddegon BA, Ding GX, Ma CM, We J, Mackie TR. BEAM: a Monte Carlo code to simulate radiotherapy treatment units. Med Phys 1995;22(5):503–24 http://www.ncbi.nlm.nih.gov/pubmed/7643786.

[14] Richmond N, Allen V, Daniel J, Dacey R, Walker C. A comparison of phantom scatter from flattened and flattening filter free high-energy photon beams. Med Dos 2015;40(1):58–63, http://dx.doi.org/10.1016/j.meddos.2014.10.001 http://www.ncbi.nlm.nih.gov/pubmed/25454113.

[15] Kragl G, af Wetterstedt S, Knausl B, Lind M, McCavana P, Knoos T, et al. Dosimetric characteristics of 6 and 10MV unflattened photon beams. Radiother Oncol 2009;93(1):141–6, http://dx.doi.org/10.1016/j.radonc.2009.06.008 http://www.ncbi.nlm.nih.gov/pubmed/19592123.

[16] Thomas SJ, Aspradakis MM, Byrne JP, Chalmers G, Duane S, Rogers J, et al. Reference dosimetry on TomoTherapy: an addendum to the 1990 UK MV dosimetry code of practice. Phys Med Biol 2014;59(6):1339–52, http://dx.doi.org/10.1088/0031-9155/59/6/1339 http://www.ncbi.nlm.nih.gov/pubmed/24583900.

[17] Sudhyadhom A, Kirby N, Faddegon B, Chuang CF. Technical note: preferred dosimeter size and associated correction factors in commissioning high dose per pulse, flattening filter free x-ray beams. Med Phys 2016;43(3):1507–13, http://dx.doi.org/10.1118/1.4941691 http://www.ncbi.nlm.nih.gov/pubmed/26936734.

[18] Karger CP, Hartmann GH. Correction of ionic recombination for pulsed radiation according to DIN 6800-2 and TRS-398. Z Med Phys 2004;14(4):260–6 http://www.ncbi.nlm.nih.gov/pubmed/15656108.

[19] McEwen MR. Measurement of ionization chamber absorbed dose k(Q) factors in megavoltage photon beams. Med Phys 2010;37(5):2179–93 http://www.ncbi.nlm.nih.gov/pubmed/20527552.

[20] Wulff J, Zink K, Kawrakow I. Efficiency improvements for ion chamber calculations in high energy photon beams. Med Phys 2008;35(4):1328–36 http://www.ncbi.nlm.nih.gov/pubmed/18491527.
[21] Czarnecki D, Zink K. Monte carlo calculated correction factors for diodes and ion chambers in small photon fields. Phys Med Biol 2013;58:2431–44, http://dx.doi.org/10.1088/0031-9155/58/8/2431.
[22] Kawrakow I. On the effective point of measurement in megavoltage photon beams. Med Phys 2006;33(6):1829–39.
[23] Andreo P. Improved calculations of stopping power ratios and their correlation with the quality of therapeutic photon beams. In: Measurement assurance in dosimetry, IAEA. 1994. p. 335–59 http://www.iaea.org/inis/collection/NCLCollectionStore/_Public/25/069/25069718.pdf.
[24] Rogers DWO, Kawrakow I, Walters BRB, Mainegra-Hing E. NRC user codes for EGSnrc National Research Council of Canada Report PIRS-702, report; 2005.
[25] Thomas SD, Mackenzie M, Rogers DWO, Fallone BG. A Monte Carlo derived TG-51 equivalent calibration for helical tomotherapy. Med Phys 2005;32(5):1346–53, http://dx.doi.org/10.1118/1.1897084, <Go to ISI>://WOS:000229274300014.
[26] Gago-Arias A, Rodriguez-Romero R, Sanchez-Rubio P, Miguel Gonzalez-Castano D, Gomez F, Nunez L, et al. Correction factors for A1SL ionization chamber dosimetry in TomoTherapy: machine-specific, plan-class, and clinical fields. Med Phys 2012;39(4):1964–70, http://dx.doi.org/10.1118/1.3692181 http://www.ncbi.nlm.nih.gov/pubmed/22482617.
[27] Bailat CJ, Buchillier T, Pachoud M, Moeckli R, Bochud FO. An absolute dose determination of helical tomotherapy accelerator, TomoTherapy High-Art II. Med Phys 2009;36(9):3891–6, http://dx.doi.org/10.1118/1.3176951 http://www.ncbi.nlm.nih.gov/pubmed/19810461.
[28] Wang LL, Leszczynski K. Estimation of the focal spot size and shape for a medical linear accelerator by Monte Carlo simulation. Med Phys 2007;34(2):485–8 http://www.ncbi.nlm.nih.gov/pubmed/17388165.

Fluence-weighted average subfield size in helical TomoTherapy

Simon Howitz[1,2,3,*], **Tilo Wiezorek**[1], **Andrea Wittig**[1], **Hilke Vorwerk**[3], **Klemens Zink**[2,4,5]

[1] University Hospital Jena, Department of Radiation Oncology, Germany
[2] Institute for Medical Physics and Radiation Protection IMPS, University of Applied Science – THM, Giessen, Germany
[3] Philipps-University, Marburg, Germany
[4] University Medical Center Giessen-Marburg, Department of Radiation Oncology, Germany
[5] Frankfurt Institute for Advanced Studies (FIAS), Frankfurt, Germany

Received 13 November 2018; accepted 30 March 2019

Abstract

Introduction: *Helical TomoTherapy allows a highly conformal dose distribution to complex target geometries with a good protection of organs at risk. However, the small field sizes associated with this method are a possible source of dosimetrical uncertainties. The IAEA has published detector-specific field output correction factors for static fields of the TomoTherapy in the TRS483. This work investigates the average subfield size of helical TomoTherapy plans.*

Material and methods: *A new parameter for helical TomoTherapy was defined – the fluence-weighted average subfield size.*
The subfield sizes were extracted from the leaf-opening time sinograms in the RT-plan files for 30 clinical prostate and head and neck plans and were put in relation to Delat4 Phantom+ measurement results.
Additionally the influence of planning parameters on the subfield size was studied by varying the modulation factor, number of iterations and pitch in the dose optimization and calculation for three different clinical indications H&N, prostate and rectum cancer. Selected plans were dosimetrically verified by Delta4 measurements to examine the reliability in dependence of the average subfield size.
Furthermore, the impact of the planning parameters on a) the dose distribution, with regard to the planning target volume and regions at risks, and b) machine characteristics such as delivery time, actual modulation factor and leaf-opening times were evaluated.

Results: *The average equivalent square subfield lengths ($\bar{s}_{eq}$) of the two investigated indications did not differ significantly – prostate plans: 2.75 ± 0.14 cm and H&N plans: 2.70 ± 0.16 cm, both with a jaw width of 2.5 cm. No correlation between field size and measured dose deviation was detected.*
The number of iterations and the modulation factor have a considerable influence on the average subfield size. The higher the planned modulation factor and the more iterations are used during optimization, the smaller is the subfield size. In our pilot study plans were calculated with field sizes $\bar{s}_{eq}$ between 4.2 cm and 1.7 cm, with a jaw width of 2.5 cm. Again, the measurement results of Delta4 showed no significant deviation from the doses calculated by the TomoTherapy planning system for the whole range of subfield sizes, and no significant correlation between field sizes and dose deviations was found. As expected, the clinical dose distribution improved with increasing modulation factor and an increasing number of iterations.
The compromise between an improved dose distribution and smaller $\bar{s}_{eq}$ was shown.

* Corresponding author: S. Howitz, University Hospital Jena, Department of Radiation Oncology, Germany.
E-mail: simon.howitz@med.uni-jena.de (S. Howitz).

Conclusion: *In this work, a method was presented to determine the average subfield size for helical TomoTherapy plans. The response of the Delta4 did not show any dependence on field size in the range of the field sizes covered by the studied plans.*
The influence of the subfield sizes on other dosimetry systems remains to be investigated.

Keywords: Helical TomoTherapy, Small field dosimetry, Subfield size, Modulation factor, Numbers of iteration

1 Introduction

Helical TomoTherapy (Accuray, Madison) is a fluence-modulated radiation therapy technique using a rotating radiation source in combination with a continuous treatment table increment, moving the patient through the gantry bore in longitudinal direction. During irradiation, the beam is shaped dynamically by the binary multi-leaf collimator [1,2]. This specific method of fluence modulation enables a highly conformal dose distribution to the target, especially for complex target geometries, with a good protection of organs at risk, as proven in several previous investigations [3,4,5–8].

It is essential in radiation therapy to ensure that calculated dose distributions can be applied correctly to the patient. For this purpose, the accuracy and precision of the irradiation machines is essential. The impact of the leaf opening time on the reliability of helical TomoTherapy radiation has been investigated by several studies [9–11]. It has been shown that the actual leaf opening times differ from the planned leaf opening times, which leads to uncertainty in dosimetric measurements and, most importantly, the application. Very short or very long leaf opening times – relative to the projection time – should be avoided by optimizing the pitch and/or the jaw opening width [9].

A second source of possible uncertainties are the small field sizes contained in the TomoTherapy irradiation plans. The International Atomic Energy Agency (IAEA) published field output correction factors for TomoTherapy for static small fields in the Technical Report Series 483 [12]. According to Crop et al. [13] the largest perturbations of small field dosimetry were caused by the volume averaging effect and the difference between the mass density of the ion chamber sensitive volume and that of the medium water [14].

However, no absolute dosimetry of static small fields is mandatory for TomoTherapy users. Even the commissioning of the TomoTherapy machine against the golden beam data, on which the planning systems are based, is done by dosimetric measurements of some helical TomoTherapy plans with ionization chambers. The smallest possible field size in TomoTherapy plans is 0.625 cm × 1.0 cm with one opened leaf and the smallest Y-Jaw opening. This would lead to correction factors greater than 1.02, according to TRS 483 [12]. It is not possible to avoid such small field sizes in a simple way, e.g. defining a minimum field size in the Treatment Planning Station (Accuray, Madison). Additionally, the amount of such small fields, e.g. one opened leaf, is unapparent.

This work is focused on the uncertainties of dose distribution verification caused by the dosimetry of small fields [15,16] for helical TomoTherapy. The goal of the present work was to investigate the influence of field size on dosimetry results for clinical quality assurance according to DIN6875-3 [17].

For this purpose, a new parameter was defined to describe the complexity of helical TomoTherapy plans: the fluence-weighted average subfield size. It was investigated how the reliability of the measurement system Delta^4 Phantom+ (Scandidos, Uppsala) depends on this average subfield size. Furthermore, we investigated the impact of three planning parameters – pitch, modulation factor and the number of iterations – on the average field size. Additionally, the influence of these planning parameters on the clinical dose distribution and machine characteristics was examined.

2 Material and methods

2.1 Average subfield size

There is still no definition of a subfield size for helical TomoTherapy irradiation plans. In the following section, a detailed definition for a fluence-weighted average subfield and an explanation of how the subfield size can be extracted from the TomoTherapy RT-Plan DICOM file will be given.

2.1.1 Definition of average subfield size

The definition of the average subfield size is based on a simplification that is used by the Planning Station (Accuray, Madison) as well: one gantry rotation is divided into 51 equidistant gantry directions, which are called projections. During each projection the fluence modulation is realized by individual leaf-opening times (*LOT*), each open leaf of each projection defining one beamlet. These opening times are summarized in form of a sinogram in the RT-Plan DICOM file, a two-dimensional data array consisting of rows representing projections and 64 columns representing the leaves. This simplification is discussed in detail by Sterpin et al. [18].

In this work the subfield was defined as a rectangular area shaped by the adjacent open leaves in lateral direction (x), and the jaws in longitudinal direction (y), projected into the isocentric plane. Since every leaf has an individual *LOT*, the pattern of subfields changes not only between projections but also within each projection (since some leaves open or close earlier than others).

The contribution of each subfield to the total planned dose depends on its photon fluence. To take this into account, we introduce a new parameter: the fluence-weighted average subfield size. This value was obtained by averaging the field size of all subfields, weighted with their respective photon fluence, over the whole treatment procedure. The average longitudinal length (y) was equal to the jaw width. Dynamic jaws were not considered in this work, because they were not available in our institution at this time. The average subfield width ($\bar{x}$) depended on the number of adjacent open leaves. The photon fluence was related to the opening time of the leaves forming the subfield. Two additional influences on the fluence were taken into account: (a) the inhomogeneous photon emission probability of the target for flattening-filter-free LINACS and (b) the field-size-dependent output factor.

a) Because of the flattening-filter-free (*fff*) mode of the linac, the open leaves at the edge of the maximum field have a lower photon fluence compared to central leaves with the same *LOT*. To take this effect into account, lateral beam profiles were measured for the field size $40 \times 2.5\,cm^2$ with a PinPoint chamber 31016 (PTW, Freiburg) in the water phantom MP3-T (PTW, Freiburg) with a source-to-surface distance of 75 cm in a depth of 10 cm. The measured lateral dose profile was normalized to one in the isocenter and divided into beamlets. In this way, for each beamlet a specific flattening-filter-free (*fff*) correction factor was obtained.
b) The output factor (*OF*) is defined as the ratio of the central dose of a field with an arbitrary field size and the dose of a square field with a length of typically 10 cm.

However, in this work, the reference field was $40 \times 2.5\,cm^2$ (all leaves open). Output factors were measured for rectangular fields in the range of 1–64 open leaves (n_{ol}) (corresponding to a field width of 0.625 cm to 40 cm) and a longitudinal jaw width of 2.5 cm in solid water phantom slabs in the TomoTherapy isocenter, i.e. at a source-to-surface distance of 75 cm, in a depth of 10 cm and interpolated by a symmetrical sigmoid function. In this way we were able to determine the *OF* for each field size ($OF_{n_{ol}}$). Due to its small sensitive volume and advantages in small field dosimetry, the microDiamond detector 60019 (PTW, Freiburg) was used [19]. Preliminary experiments showed that the *OF* on the central axis is within 0.8% equal to the *OF* in the periphery of the radiation field at 15 cm distance from the isocenter, i.e. the dependence of the output factor on the lateral field position was neglected.

2.1.2 Determination of average subfield size

A MATLAB tool was developed to analyze the sinogram information in the RT-Plan DICOM files. The scheme in Fig. 1 and the following section explain the methods of this developed tool. First the *LOT*s were extracted from the private tag

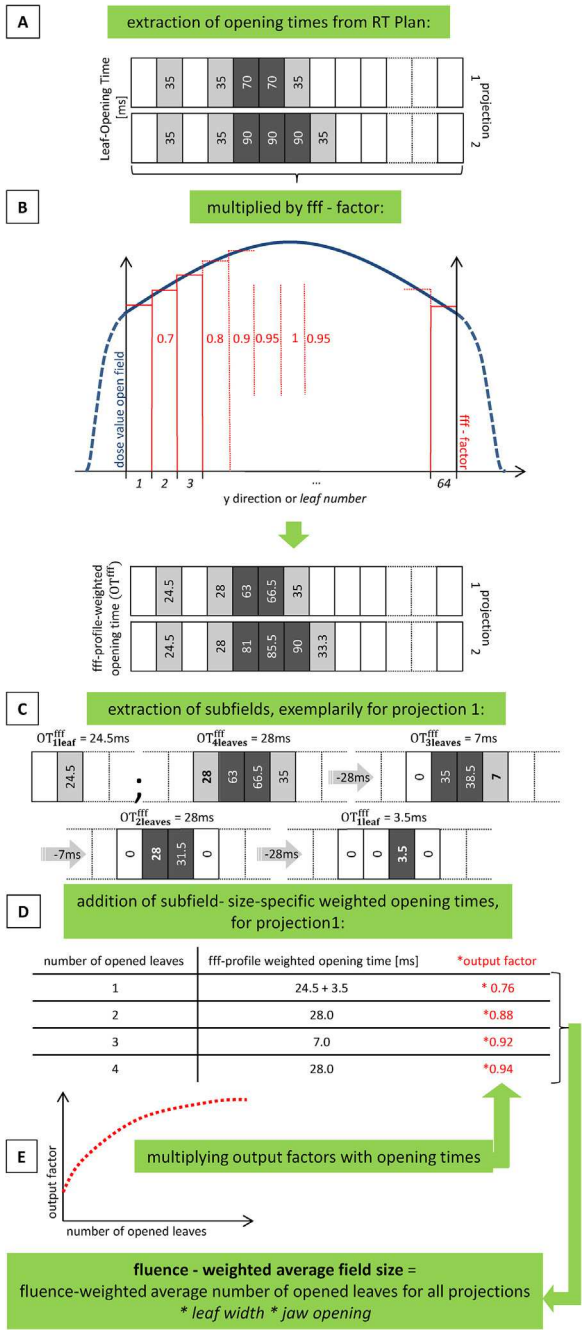

Fig. 1. Illustration of the definition and determination of the fluence-weighted average subfield size for TomoTherapy. The fluence-weighted average field size for projection one according to the illustrated example is $3.9\,cm^2$ with a jaw opening of 2.5 cm and the leaf width of 0.625 cm. All quantities are exemplary and are chosen to facilitate the understanding.

and translated into ASCII, see Fig. 1 part A. The *LOT* of each beamlet in the sinogram was multiplied by the *fff* factor to take the inhomogeneous photon emission probability into account, see Fig. 1 part B. Thus, the modified sinogram contained the fff-profile-weighted opening time (OT^{fff}) for each beamlet. Subsequently the subfields were extracted depending on their smallest connected OT^{fff}, Fig. 1 part C. The OT^{fff} were added up for each subfield size, i.e. for each number of adjacent open leaves (n_{ol}), over all (m) projections (pr), see Fig. 1 part D. Finally, these weighted opening times, summed for each subfield size ($OT^{fff}_{n_{ol}}$), were multiplied by the corresponding output factor ($OF_{n_{ol}}$), see Fig. 1 part E. For each subfield size, i.e. n_{ol}, the fluence-weighted opening time ($OT^{FW}_{n_{ol}}$) resulted:

$$OT^{FW}_{n_{ol}} = \sum_{1\ pr}^{m\ pr} OT^{fff}_{n_{ol}} \cdot OF_{n_{ol}} \tag{1}$$

Hence, the average number of open leaves ($\overline{n^{FW}_{ol}}$) for the whole treatment plan was determined by:

$$\overline{n^{FW}_{ol}} = \frac{\sum_{n_{ol}1}^{n_{ol}64}(OT^{FW}_{n_{ol}} \cdot n_{ol})}{\sum_{n_{ol}1}^{n_{ol}64} OT^{FW}_{n_{ol}}} \tag{2}$$

Finally, the average subfield width in x-direction ($\bar{x}$) was obtained by multiplying the average number of adjacent open leaves by the leaf width (0.625 cm):

$$\bar{x} = \overline{n^{FW}_{ol}} 0.625\ \text{cm} \tag{3}$$

The subfield length in y-direction (y) was given by the jaw opening, which was constant during the whole radiation, due to the used fixed jaws.

From these fluence-weighted average subfield parameters $\bar{x}$ and y, the rectangular area can be calculated by simple multiplication of $\bar{x}$ and y. In this work, the fluence-weighted average subfield size is described by the dosimetrically relevant parameter, the equivalent square subfield lengths ($\bar{s}_{eq}$) according to Worthley [20]:

$$\bar{s}_{eq} = \frac{2\bar{x}y}{\bar{x} + y} \tag{4}$$

In addition to the mean subfield size, the distribution of subfield sizes was also statistically evaluated. For this, the fluence-weighted opening times for each subfield size used in the plan were evaluated and plotted cumulatively. Thus the dose contribution applied by small fields can be evaluated.

2.2 Evaluation of clinical plans

First, 30 clinical patient plans from two of the largest groups of patients on our TomoTherapy machine – 15 prostate and 15 head and neck plans – were retrospectively evaluated and the average subfield size parameters $\bar{s}_{eq}$ were determined. These $\bar{s}_{eq}$ were set in relation to the results of the dosimetric plan verification for clinical acceptance according to DIN6875-3 [17]. This quality assurance procedure was performed as follows.

The dose distribution of the Helical TomoTherapy plans was verified by measurements with the biplanar diode array Delta4 Phantom+ (Scandidos), software version *October2016*. The phantom contains 1069 p-Si diodes with a volume of 0.00004 cm^3 with 5 mm spacing in the central area ($6 \times 6\ cm^2$) and 10 mm spacing for areas up to $20 \times 20\ cm^2$, respectively [21–23]. A cross-calibration was done with a simple helical treatment plan before the plan measurements to consider possible output variations of the TomoTherapy machine, according to Salz et al. [24]. The evaluation parameter was the global gamma index with dose deviation and distance to agreement criteria of 3%/3 mm for clinical acceptance [25,26]. Only diodes that received more than 60% of the prescribed dose were used for the analysis, according to our clinical quality assurance procedure. The threshold was chosen because the main goal of our quality assurance is the verification of the prescribed doses in the high dose region.

2.3 Impact of planning parameters

Three different clinical cases were used to investigate the impact of the planning parameters pitch, modulation factor *(MF)* and the number of iterations during optimization on the average subfield size.

Three plans from our database were chosen: a prostate cancer planning target volume (PTV) with 162 cm^3 (78 Gy, 2 Gy/fx), a base of tongue cancer with an integrated boost planning target volume of 176 cm^3 (61.48 Gy, 2.12 Gy/fx) embedded in a lower dose planning target volume of 635 cm^3 for the uninvolved lymph node regions (53.65 Gy, 1.85 Gy/fx), and a rectum cancer planning target volume with adjacent lymph nodes of 2176 cm^3 (45 Gy, 1.8 Gy/fx). The three indications were chosen in order to cover different types of PTV geometries. All chosen plans are in accordance with our clinical and dosimetric constraints.

The pitch is defined as the ratio of couch travel per gantry rotation divided by the fan beam width [27]. Chen et al. [28] and Kissick et al. [29] are recommending pitches of 0.86/n with the integer multiple $n > 1$ to avoid a prominent thread effect.

The *MF* is defined as the ratio of the longest *LOT* and the average nonzero *LOT* [27]. The TomoTherapy planning system exclusively allows determining a maximum MF during the planning process, which is called planned modulation factor *(MF_{plan})*. The higher the parameter MF_{plan} is, the higher is the intensity range that can be reached during optimization.

The number of iterations during optimization has the largest impact on the planning time. The planning time in this study ranged between a few minutes (20 iterations) to several hours (9999 iterations). Helical TomoTherapy is a

fluence-modulated radiation technique, and the treatment plans are obtained by iterative inverse planning [30,31]. During each iteration, the dose distribution is evaluated by means of an objective function based on the dose-volume constraints and weighting parameters, the intensities for all beamlets are updated, and the dose is recalculated.

The planning parameter values that were combined in this plan study were as follows: MF_{plan} = 1.3, 2.0 and 4.0, and the number of iterations = 20, 100, 500 and 9999, with a constant pitch of 0.287. Furthermore the pitch was changed between the values 0.14, 0.287 and 0.43 while the MF_{plan} and the number of iterations were held constant at 2.0 and 100.

The jaw width in longitudinal direction was constant at 2.5 cm with fixed jaws, which is the most frequently used jaw opening for clinical plans. It is often the best compromise between the dose fall-off in longitudinal direction and delivery time as long as dynamic jaws (TomoEDGE^{TM}) are not available [32].

The dose-volume constraints and weighting parameters of the initial three clinically accepted plans were kept at the same values, and the plans were re-optimized with varied planning parameters. Every optimization process of each PTV started with the same set of initial beamlets, which was precalculated. The used optimization constraints and weighting parameters were chosen so strictly that most of them could not be fulfilled, even with the highest modulation. Instead of just trying to reach certain constraints for all organs at risk or other healthy tissue, we tried to save as much dose as possible but to ensure a good dose coverage of the target volumes.

To achieve a good PTV coverage but also a steep dose gradient to the normal tissue, a three-dimensional margin of 5 mm around the PTV was defined. The dose constraints in this region were given a very low weight, while strong constraints were defined for the normal tissue. This results in a steep dose gradient within the 5 mm margin.

The Planning Station software, version 5.1.0.4 (Accuray, Madison), was used for the optimization and dose calculation of the helical TomoTherapyHD plans. For dose calculation TomoTherapy uses a convolution superposition algorithm. During the optimization the dose grid was set to "normal", i.e. half the CT resolution in axial plane (128×128) and CT resolution in longitudinal direction (2.5 mm). The final dose calculation and phantom calculations were based on the "fine" dose grid. Here, the resolution matches the CT voxel resolution (256×256 in the axial plane).

This pilot study included 42 calculated plans with the previously described planning parameters in total. The average subfield sizes were evaluated with MATLAB. The quality assurance measurements were done for the plans with the largest and smallest average subfield size for each case.

Furthermore this study was used to investigate the impact of the planned modulation factor and the number of iterations on clinical dose distribution, see section 2.3.1, and selected machine characteristics, see Section 2.3.2.

2.3.1 Clinical dose distribution

Evaluation metrics such as the homogeneity index *HI*, the conformity index *CI*, the coverage index *COVI* and the different dose-volume constraints for affected organs at risk were used to compare the different plans regarding the clinical dose distribution.

The ratio of dose values delivered to 2% and 98% of the PTV ($D_{2\%}$, $D_{98\%}$) was used to evaluate the dose homogeneity *HI* in this volume:

$$HI = \frac{D_{2\%}}{D_{98\%}} \tag{5}$$

The closer the *HI* is to one, the better the dose uniformity in the PTV.

The conformity index (*CI)* is defined as the ratio of the treated volume that is enclosed by 95% of prescribed isodose (V_{treat}) and the PTV volume (V_{PTV}), originally proposed in ICRU62 [33]:

$$CI = \frac{V_{treat}}{V_{PTV}} \tag{6}$$

The closer the ratio is to one, the smaller the volume of normal tissue receiving the prescribed dose.

The coverage index (*COVI)* is the ratio of PTV volume that is enclosed by 95% of the prescribed isodose ($V_{PTV\text{-}treat}$) and the whole PTV volume (V_{PTV}).

$$COVI = \frac{V_{PTV\text{-}treat}}{V_{PTV}} \tag{7}$$

The closer the *COVI* is to one, the better the dose coverage of the PTV.

For the evaluation of planning target volumes, the indices CI and COVI were considered together. With an optimal coverage of the target area and at the same time highly conformal dose distribution, both indices are equal to one. If more healthy tissue than necessary is irradiated, the COVI may remain 1, but the CI will be >1. On the other hand, if healthy tissue is irradiated with the prescribed dose, but the planning target volume is under-dosed, the CI can still assume the desired value 1, in this case, COVI will be <1.

The evaluation of the head and neck plan relates exclusively to the simultaneously integrated boost, since the evaluation of the low dose planning target volume is influenced by the overlap with the high dose volume.

For the specific plan types, selected organs at risk were evaluated according to the following exemplary parameters and clinically relevant dose constraints. For the prostate cancer plans, the rectum volumes receiving at least 40 Gy ($V_{40\,Gy}$) (RTOG0534) were compared. The head and neck cancer plans were compared with respect to the median dose (D_{med}) of the contra-lateral parotid gland and D_{med} of the mandible. For the rectum cancer plans the mean bladder doses were

compared (RTOG0415). The investigation of these dose volume constraints was intended to illustrate the dependency of the protection of contoured organs at risk on the planning parameters.

2.3.2 Machine characteristics

All machine evaluation parameters were analyzed that are available in the Planning Station software: the delivery time of the treatment, the actual modulation factor (MF_{act}), the average leaf-opening time ($\overline{LOT}$) and the relative number of opened leaves with an *LOT* shorter than 70 ms, which corresponds to one third of the maximum leaf-opening time for the highest gantry rotation speed. A full leaf opening or closing process takes 11–17 ms. Before the final dose is calculated, leaf opening times lower than 20 ms are deleted from the sinogram. Leaf closing times that are too short to be realized by the MLC, i.e. less than 18ms between two projections, will not be considered in the final dose calculation. Thus it is possible that leaves which are assumed to be closed for a short time in the calculation actually remain open during the application.

The MF_{act} is the *LOT* ratio after the final dose calculation, contrary to the planning parameter and threshold value MF_{plan}, used during the optimization process.

The *LOT* information is obtained from the *LOT* histogram, which is available in the Planning Station after the final dose calculation. The smaller the average *LOT* and/or the larger the proportion of opened leaves with a small *LOT* are, the higher the uncertainty of fluence application caused by an imprecise traveling time of the binary MLC becomes, as explained in detail by Lissner et al. [11].

3 Results

3.1 Average subfield size for clinical plans

Fig. 2 shows the evaluated $\bar{s}_{eq}$ of 30 different clinical helical TomoTherapy plans for prostate and head and neck patients in dependency on the results of the quality assurance measurements with the Delta4. The average of $\bar{s}_{eq}$ for the prostate plans is 2.75 cm (standard deviation: ±0.14 cm) and do not differ significantly from the H&N plans with 2.70 cm (standard deviation: ±0.16 cm). The median dose deviation between dose measurement and Planning Station calculation is +0.44% ± 0.4% for prostate plans and 0% ± 0.7% for H&N. In the small range of $\bar{s}_{eq}$ no correlation with the dose deviation was detected.

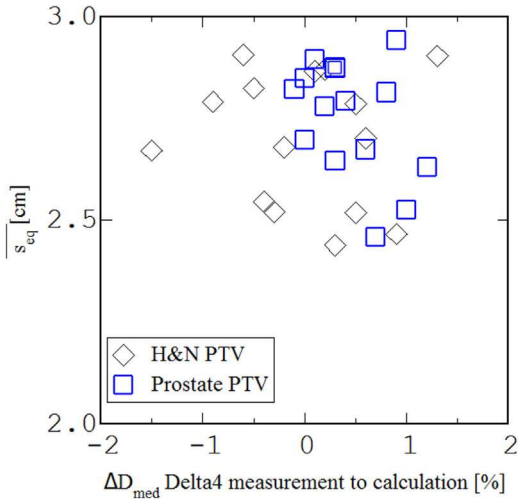

Fig. 2. Average fluence-weighted equivalent square subfield lengths ($\bar{s}_{eq}$) in dependency on the quality assurance measurements with Delta4 for each 15 head and neck and prostate radiation plans.

3.2 Impact of planning parameter

3.2.1 Average subfield size

Fig. 3 shows $\bar{s}_{eq}$ as a function of the MF_{plan}, MF_{act} and the number of iterations for all investigated plans. It was in the range of 1.7 cm (prostate PTV; $MF_{act} = 2.3$; $MF_{plan} = 4$; 9999 iterations) to 4.2 cm (rectum PTV; $MF_{act} = MF_{plan} = 1.3$; 20 iterations), which corresponded to a rectangular subfield area of 3.2 cm^2 to 32.2 cm^2. A strong correlation between the number of iterations and the average subfield size $\bar{s}_{eq}$ was observed.

With an increasing MF_{plan}, or an increasing number of iterations, $\bar{s}_{eq}$ decreased for all investigated treatment plans. MF_{act} showed the same trend, but did not correlate with $\bar{s}_{eq}$ strongly.

The impact of pitch on subfield size was very small. The differences between the $\bar{s}_{eq}$ in dependence on the investigated pitches were smaller than ±0.5 mm.

Further important investigations concerning the subfield size statistics were possible when considering the cumulative fluence as a function of the fluence-weighted subfield size, as shown in Fig. 4. The fraction of photon fluence contributed by each subfield size is added up, beginning with the smallest subfield size. A comparison of two rectum cancer plans, (plan 1) 20 iterations and $MF_{act} = MF_{plan} = 1.3$ and (plan 2) 9999 iterations and $MF_{act} = 3.5$ ($MF_{plan} = 4$), shows that the median of the total fluence is given by a rectangular subfield area ≤32 cm^2 for (plan1) and 2.4 cm^2 for (plan2). The subfield composition of the head and neck and the prostate cancer treatment plan showed comparable results for the investigated parameters. In the rectum cancer plan all the subfield sizes were larger. Furthermore, Fig. 4 shows the large impact of the number of iterations on the subfield sizes contained in the plan.

The median dose deviation (ΔD_{med}) between measurement and dose planning, the passing rate for the gamma criterion 3%/3 mm and the more sensitive criterion 1%/1 mm are tabulated in Table 1 for the plans with the smallest and largest $\bar{s}_{eq}$ of each indication. The measurement results are in sufficient agreement with the calculated dose in the Planning Station. The gamma passing rate is ≥99.7% for each measured plan

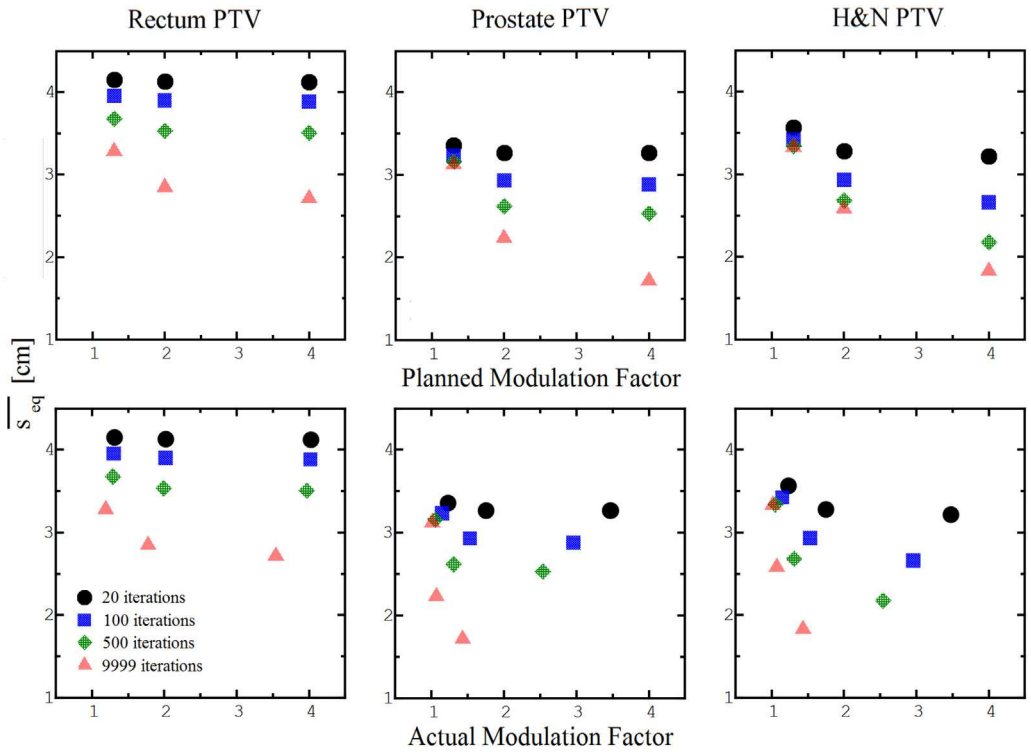

Fig. 3. Average fluence-weighted equivalent square subfield lengths ($\bar{s}_{eq}$) as a function of the planned modulation factor (row one) and actual modulation factor (row two) and the number of optimization iterations.

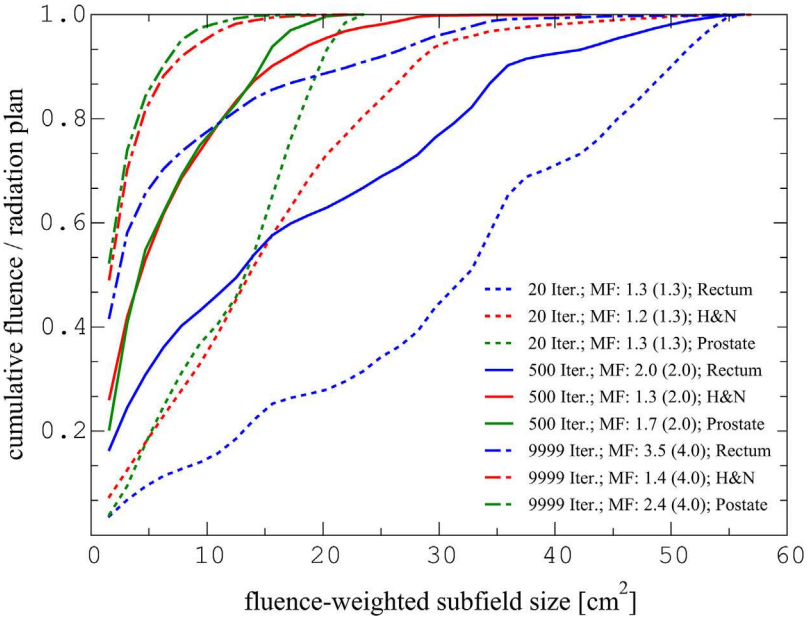

Fig. 4. The fluence contributions of the present rectangular subfield sizes are shown for some selected plans of different complexity, i.e. different number of iterations; actual (planned) modulation factors and planning target volumes.

Table 1
Results of the Delta^4 Phantom+ quality assurance measurements. The median dose deviation from the calculation (ΔD_{med}) and Gamma Index passing rates for two different criteria are shown for six different plans with specific average subfield size ($\bar{s}_{eq}$). The head and neck plan with 9999 iterations was measured on three different days to evaluate the reproducibility.

PTV region	Iterations	MF_{act} (MF_{plan})	$\bar{s}_{eq}$	ΔD_{med}	Passing rate Gamma Index 1%/1 mm	Passing rate Gamma Index 3%/3 mm
Rectum	20	1.3 (1.3)	4.2 cm	−0.7%	75.7%	100.0%
	9999	3.5 (4.0)	2.7 cm	0.2%	94.4%	100.0%
Prostate	20	1.3 (1.3)	3.4 cm	0.7%	68.5%	99.7%
	9999	2.3 (4.0)	1.7 cm	0.2%	90.3%	100.0%
Head and Neck	20	1.2 (1.3)	3.6 cm	−0.3%	83.7%	99.8%
day1	9999	1.4 (4.0)	1.8 cm	0.3%	79.0%	100.0%
day2				0.3%	83.5%	100.0%
day3				0.3%	80.7%	100.0%

with a 3%/3 mm criterion and is therefore clinically acceptable [34]. To evaluate the influence of the *MF* and the number of iterations with a higher accuracy, the gamma criterion was set to 1%/1 mm. Applying the stronger criterion, the passing rate dropped by up to 20%. However, neither the gamma criterion nor the dose deviation of the measurement results showed a significant correlation with $\bar{s}_{eq}$.

In order to exclude daily variations of the TomoTherapy machine and the Delta4 and to investigate the reproducibility, the H&N plan with $MF_{act} = 1.4$ ($MF_{plan} = 4$) and 9999 iterations was measured on three different days. The median dose deviation was 0.3% for all the measurements, taking the daily dose rate correction into account, which varied by about 0.2%.

3.2.2 Clinical dose distribution

Fig. 5a and b shows the homogeneity HI, coverage CI and conformity COVI indices in dependence on MF_{plan}, MF_{act} and the number of iterations for the rectum PTV in row one, the prostate in row two and head and neck high dose planning target volume in row 3, respectively.

The following trends were observed: Optimization with an MF_{plan} of 1.3 resulted in heterogeneous dose distributions in the target volumes and worse target coverages compared with optimizations with $MF_{plan} \geq 2$ for prostate and head and neck PTVs. However homogenous plans with good target coverage were achieved with small MF_{act} for these two indications. For the large-volume rectum PTV, the homogeneity HI and the COVI were independent of the *MF* and the number of iterations.

Furthermore, a considerably decrease of the conformity index CI may be achieved by a higher number of iterations for the rectum cancer PTV. The higher the number of iterations, the better the sparing of the normal tissue, while the PTV coverage remained good for $MF_{plan} \geq 2$. However for the prostate and the head and neck PTV no strong dependency between the number of iterations and an improved CI was observed. The results show an increase of CI with rising MF_{act} and MF_{plan} for these two types of plans.

Fig. 6a and b shows the influence of the number of iterations in combination with the value of MF_{plan} or MF_{act}, respectively, on the dose sparing of selected organs at risk. The best protection was achieved by the highest MF_{plan} and highest number of iterations for each investigated region of interest. The higher MF_{plan}, the higher the influence of the number of iterations; however, from 500 to 9999 iterations it is negligible in nearly all cases. Solely for the bladder in the rectum cancer plan did the increase from 500 to 9999 iterations have a noticeable impact.

When considering MF_{act} instead of MF_{plan} the same behavior is visible.

3.2.3 Machine characteristics

Fig. 7a and b shows the delivery time, average leave-opening time and the number of open leaves with an opening time <70 ms as a function of MF_{plan} and MF_{act}, respectively, and the number of iterations. Additionally Fig. 7a shows the dependency of MF_{act} on MF_{plan} and the number of iterations.

The delivery time depended on the MF_{plan} and may increase by up to a factor of two.

The $\overline{LOT}$ increased with the number of used iterations for the prostate and head and neck plan. With a higher MF_{plan} the impact of the number of iterations on the $\overline{LOT}$ became higher. Particularly for the prostate cancer and head and neck cancer plans the average *LOT* increased to up to 220%. For the large-volume rectum PTV, the $\overline{LOT}$ did not differ.

The relative number of leaves with opening times <70 ms increased with MF_{act} and MF_{plan} for each value of the number of iterations. The number of iterations did not show a systematic influence on the fraction of opened leaves with a short LOT for all three indications. In the rectum PTV plans the fractions of LOT < 70 ms increased with an increasing number of iterations for the whole range of MF_{plan}. The prostate plans had shown this dependency only for the highest MF_{plan}. The head and neck plans showed the smallest fraction of small LOTs for the plans with the highest number of iterations for all values of MF_{plan}.

It was evident that the actual modulation factor MF_{act} depended on the number of optimization iterations, with the exception of the prostate plan with $MF_{plan} = 4$ and 9999 iterations. The higher the number of iterations, the lower MF_{act}

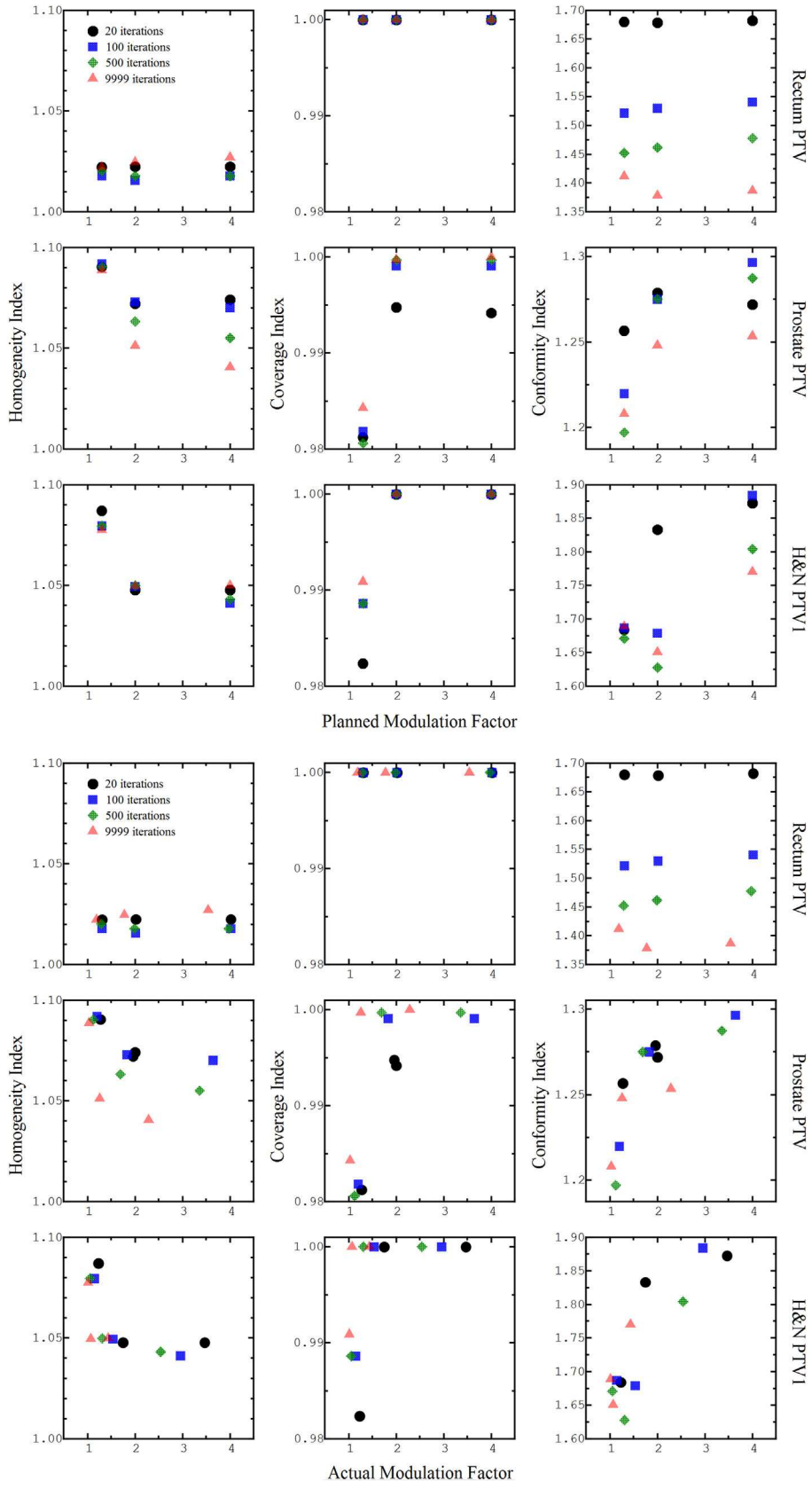
20 iterations
100 iterations
500 iterations
9999 iterations
Homogeneity Index
Coverage Index
Conformity Index
Rectum PTV
Prostate PTV
H&N PTV1
Planned Modulation Factor
Actual Modulation Factor

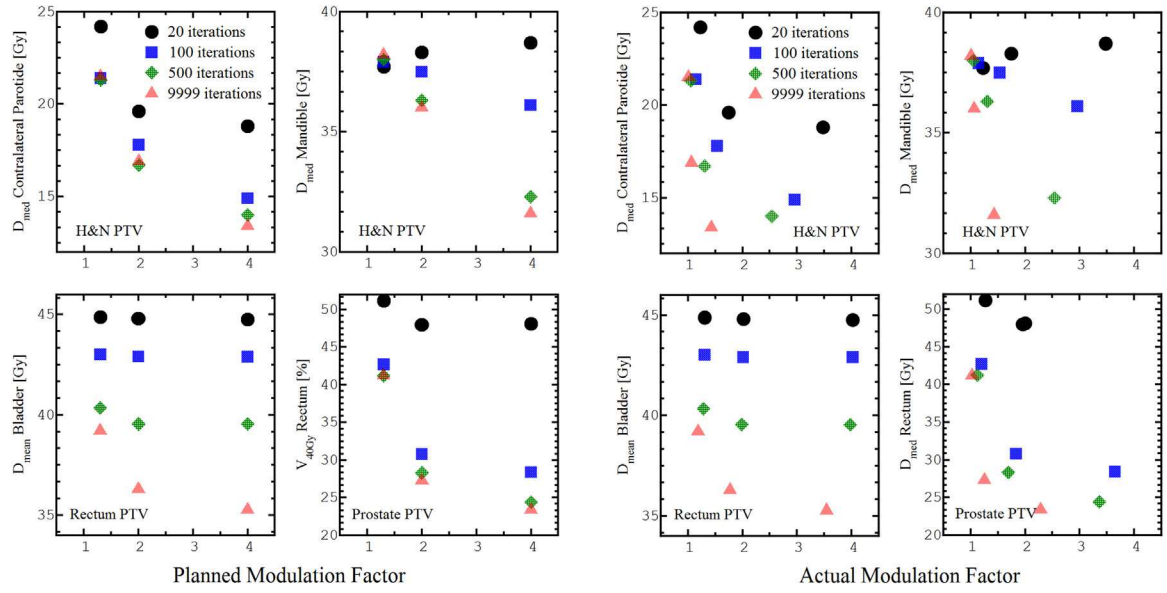

Fig. 6. (a, b) Dose sparing of selected organs at risk – bladder for the rectum cancer plan (top left), rectum for the prostate plan (top right), the mandible and the contra-lateral parotide for the head and neck cancer plan (bottom left and right) – is shown as a function of the planned and actual modulation factor and the number of optimization iterations.

was. This effect was more pronounced with higher planned modulation factors MF_{plan}.

The MF_{act} of the rectum plans showed no strong dependency on the number of iterations between 20, 100 and 500 iterations.

4 Discussion

This work defined for the first time an average subfield size for helical TomoTherapy radiation treatment plans.

The analysis of 30 clinical plans showed an average $\bar{s}_{eq}$ of 2.7 cm with a small standard deviation of ±0.2 cm, regardless of the target area. The field output correction factors are defined in TRS 483, Table 24 [12] for different ionization chambers and diodes. For most solid state detectors listed, the factor is between 0.99 and 1.01 in this field size range. The necessity of field size dependent correction factors is not indicated for this selection of clinical plans for the p-Si diode based detector array of Delta4. The dose difference between the Delta4 measurements and calculations in the planning system showed no significant dependence on the average subfield size. Typical planning parameters for these plans were MF_{plan} of 2.0–2.5, which resulted in MF_{act} of 1.9 with a standard deviation of ±0.3, and about 100–500 iterations. The small standard deviation of the quality assurance results was achieved by a cross calibration before the quality assurance measurement [24].

The good results of the Delta4 measurements may have been caused by using similar irradiation planning parameters MF and number of iterations for all plans. Therefore, non-clinical plans with extreme parameters were created to study the response of the Delat4 more rigorously.

The systematic investigation of the influence of selected planning parameters on the average subfield size has shown a dependency on the number of iterations and on the MF_{plan}.

Although lowly modulated plans with 20 iterations and a planned modulation factor of 1.3 are clinically not relevant, nevertheless they showed the trend of the dependency between MF_{plan} and numbers of iterations on the $\bar{s}_{eq}$, see Fig. 3.

The results of the highly modulated plans illustrate the compromise between an improved clinical dose distribution and a simultaneous increase of the fraction of small subfields. The smallest $\bar{s}_{eq}$ is 1.7 cm. For this field size, a correction factor between 0.976 and 1.017 is recommended for different solid state detectors in static radiation beams, according to the TRS 483 protocol [12]. Overall, the p-Si diodes based dosimetry system Delta4 worked reliable. Even for radiation plans with many small subfield sizes the Delta4 showed no significant deviation from the dose calculated by the Planning Station, for the investigated subfield size range down to $\bar{s}_{eq} = 1.7$ cm. Czarnecki et al. [35] did show an altered dose response for

Fig. 5. (a, b) The three PTV dose-distribution-descriptive indices of homogeneity (column one), coverage (column two) and conformity (column three) are shown as a function of the planned and actual modulation factor and the number of optimization iterations for three different plans: rectum (row one), prostate (row two) and the two head and neck target volumes (rows three and four).

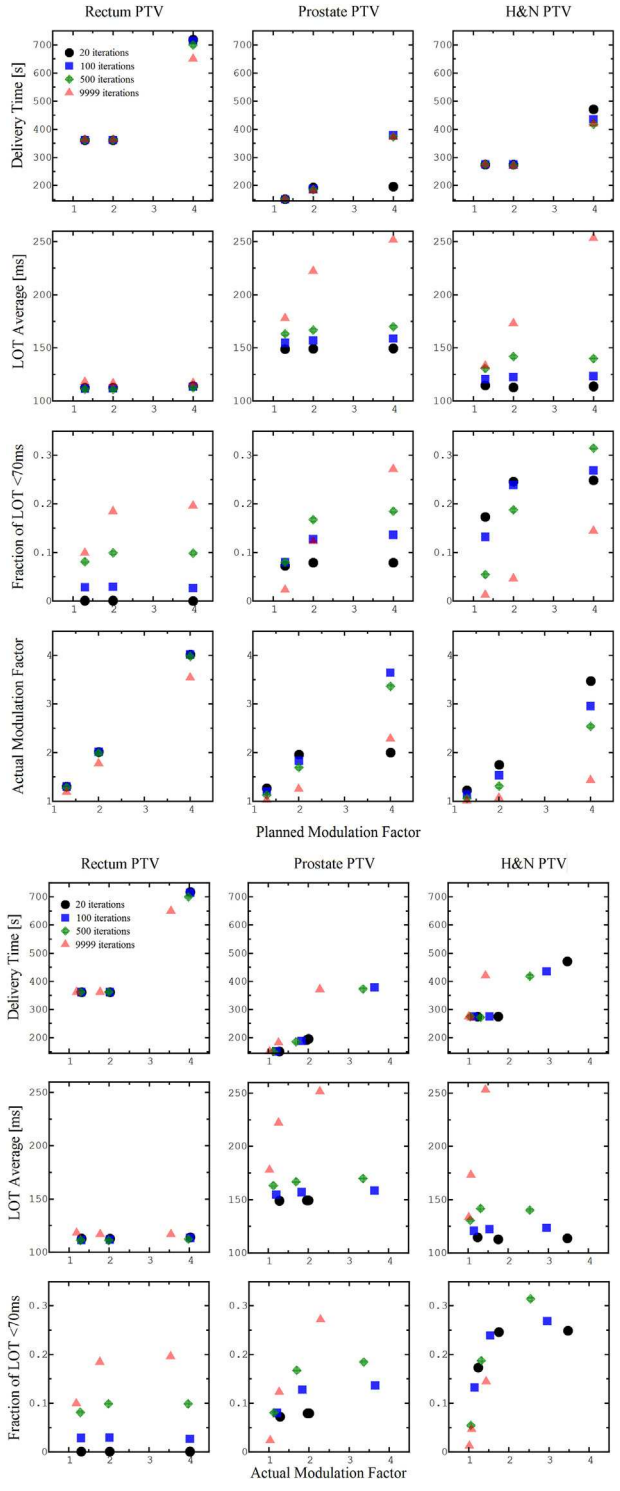

Fig. 7. (a and b) Technical parameters – delivery time, average leaf-opening time *(LOT)*, relative number of open leaves with an opening time <70 ms and actual modulation factor (rows one to four) – are shown as a function of the modulation factors for the given planning target volumes.

shielded and unshielded diodes for field sizes smaller than 2.5 cm. Field size correction factors of static beams may differ from averaged subfield sizes because the proportion of scattered radiation differs significantly. The volume effect should be comparable for subfields and static beams.

The measured dose deviations are independent of the size of the high-dose area. The dose, measured with Delta4 is corrected in the Delta4 software by a factor which depends on the high-dose volume. Thus, the energy dependent over-responsiveness of the diodes for large fields is corrected. The presumably subordinated impact of the volume effect, which would be subfield size dependent, is currently not considered in the Delta4 software.

Measurements of energy doses of small fields are a challenge for dosimetry [15,16]. Even though the Delta4 measurement results were independent of the subfield size, this might not be the case for other dosimetry systems, especially ion chamber based systems. The volume effect should affect the dose response of ion chambers more than that of diodes due to the larger sensitive measurement volume. Correction factors given in the TRS 483 [12] for ion chambers are up to 1.03 for TomoTherapy equivalent square field size of 1.5 cm. The newly introduced quantity fluence-weighted average subfield size may be used to define different plan classes for plan-class-specific correction factors in the TomoTherapy dosimetry according to Alfonso et al. [36].

It can be assumed that the influence of the investigated irradiation parameters on the average subfield size is independent of the jaw opening, i.e. the average number of opened leaves per subfield. This would result in an $\bar{s}_{eq}$ down to 1.1 cm for very highly modulated plans with a jaw opening of 1.0 cm. It is recommended to optimize the objective function during the optimization and start the iterations afresh, especially for the smallest jaw opening. Thus it is possible to avoid too many iterations and consequently too small subfields.

It is noticeable that MF_{act} decreases with the number of iterations and the optimizer did not exploit the full range of MF_{plan}. This suggests that the optimizer of the Planning Station finds more optimal beamlets with an increasing number of iterations.

We had expected that the MF_{act} was a suitable parameter for describing the complexity of the radiation plans. However, the comparison of the actual modulation factor MF_{act} and the percentage of very short *LOT* did not show a clear correlation for all plans, see Fig. 7b. Furthermore $\bar{s}_{eq}$ depends mainly on the combination between MF_{plan} and number of iterations, not on the resulting MF_{act}.

The gantry period limit of 11.8 s is reached for some lowly modulated plans, caused by the small pitch. By optimizing the pitch, the delivery time will be lower for small MF_{plan} and few iterations.

5 Conclusion

For TomoTherapy field size dependent correction factors were defined in TRS 483 [12] but up to date there is no

possibility to determine an average filed size for helical TomoTherapy. Our study described a new parameter, the fluence-weighted average subfield size, and investigated which planning parameters mainly influence the average subfield size.

This will allow TomoTherapy users to decide if correction factors are necessary for the used dosimetry system.

References

[1] Mackie TR, Holmes T, Swerdloff S, Reckwerdt P, Deasy JO, Yang J, et al. Tomotherapy: a new concept for the delivery of dynamic conformal radiotherapy. Med Phys 1993;20(6):1709–19.

[2] Mackie TR, Holmes TW, Reckwerdt PJ, Yang J. Tomotherapy: Optimized Planning and Delivery of Radiation-Therapy. Int J Imag Syst Technol 1995;6(1):43–55.

[3] Buschmann M, Seppenwoolde Y, Wiezorek T, Weibert K, Georg D. Advanced optimization methods for whole pelvic and local prostate external beam therapy. Phys Med 2016;32(3):465–73.

[4] Wiezorek T, Brachwitz T, Georg D, Blank E, Fotina I, Habl G, et al. Rotational IMRT techniques compared to fixed gantry IMRT and tomotherapy: multi-institutional planning study for head-and-neck cases. Radiat Oncol 2011;6:20.

[5] Van Gestel D, Verellen D, Van De Voorde L, de Ost B, De Kerf G, Vanderveken O, et al. The potential of helical tomotherapy in the treatment of head and neck cancer. Oncologist 2013;18(6):697–706.

[6] Van Gestel D, van Vliet-Vroegindeweij C, Van den Heuvel F, Crijns W, Coelmont A, De Ost B, et al. RapidArc, SmartArc and TomoHD compared with classical step and shoot and sliding window intensity modulated radiotherapy in an oropharyngeal cancer treatment plan comparison. Radiat Oncol 2013;8:37.

[7] Murthy V, Master Z, Gupta T, Ghosh-Laskar S, Budrukkar A, Phurailatpam R, et al. Helical tomotherapy for head and neck squamous cell carcinoma: dosimetric comparison with linear accelerator-based step-and-shoot IMRT. J Cancer Res Ther 2010;6(2):194–8.

[8] Jacob V, Bayer W, Astner ST, Busch R, Kneschaurek P. A planning comparison of dynamic IMRT for different collimator leaf thicknesses with helical tomotherapy and RapidArc for prostate and head and neck tumors. Strahlenther Onkol 2010;186(9):502–10.

[9] Hui C, Chen Q, Khandelwal S, Neal B, Watkins W. Detection of dose delivery variations on TomoTherapy using on-board detector based verification. Phys Med Biol 2018;63(14), 14NT02.

[10] Westerly DC, Soisson E, Chen Q, Woch K, Schubert L, Olivera G, et al. Treatment planning to improve delivery accuracy and patient throughput in helical tomotherapy. Int J Radiat Oncol Biol Phys 2009;74(4):1290–7.

[11] Lissner S, Schubert K, Kluter S, Oetzel D, Debus J. A method for testing the performance and the accuracy of the binary MLC used in helical tomotherapy. Z Med Phys 2013;23(2):153–61.

[12] Palmans H, Andreo P, Huq MS, Seuntjens J, Christaki KE. Dosimetry of small static fields used in external beam radiotherapy: an IAEA–AAPM International Code of Practice for reference and relative dose determination /International Atomic Energy Agency, in Technical Report Series No. 483. Vienna: International Atomic Energy Agency; 2017.

[13] Crop F, Reynaert N, Pittomvils G, Paelinck L, De Wagter C, Vakaet L, et al. The influence of small field sizes, penumbra, spot size and measurement depth on perturbation factors for microionization chambers. Phys Med Biol 2009;54(9):2951–69.

[14] Palmans H, Andreo P, Huq MS, Seuntjens J, Christaki KE, Meghzifene A. Dosimetry of small static fields used in external photon beam radiotherapy: summary of TRS-483, the IAEA-AAPM international Code of Practice for reference and relative dose determination. Med Phys 2018;45(11):e1123–45.

[15] Das IJ, Ding GX, Ahnesjo A. Small fields: nonequilibrium radiation dosimetry. Med Phys 2008;35(1):206–15.

[16] Francescon P, Kilby W, Satariano N, Cora S. Monte Carlo simulated correction factors for machine specific reference field dose calibration and output factor measurement using fixed and iris collimators on the CyberKnife system. Phys Med Biol 2012;57(12):3741–58.

[17] DIN6875-3, Special radiotherapy equipments - Part 3: Intensity-modulated radiation therapy - characteristics, test methods and rules for clinical application. 2008.

[18] Sterpin E, Verboomen C, Vynckier S. Impact of the number of discrete angles used during dose computation for TomoTherapy treatments. Med Phys 2012;39(11):6947–56.

[19] Laub WU, Crilly R. Clinical radiation therapy measurements with a new commercial synthetic single crystal diamond detector. J Appl Clin Med Phys 2014;15(6):4890.

[20] Worthley B. Equivalent squares of rectangular fields. Br J Radiol 1966;39:559.

[21] Nilsson G. Delta4-A new tMRT QA device. Med Phy 2007;34(6):2432.

[22] Geurts M, Gonzalez J, Serrano-Ojeda P. Longitudinal study using a diode phantom for helical tomotherapy IMRT QA. Med Phys 2009;36(11):4977–83.

[23] Sadagopan R, Bencomo JA, Martin RL, Nilsson G, Matzen T, Balter PA. Characterization and clinical evaluation of a novel IMRT quality assurance system. J Appl Clin Med Phys 2009;10(2):2928.

[24] Salz H, Howitz S, Brachwitz T, Wiezorek T. Patient-related QA for helical TomoTherapy with Delta4: analysis of the results. Curr Dir Biomed Eng 2017;3(2):635–8.

[25] Low DA, Harms WB, Mutic S, Purdy JA. A technique for the quantitative evaluation of dose distributions. Med Phys 1998;25(5):656–61.

[26] Nelms BE, Simon JA. A survey on planar IMRT QA analysis. J Appl Clin Med Phys 2007;8(3):76–90.

[27] Langen KM, Papanikolaou N, Balog J, Crilly R, Followill D, Goddu SM, et al. QA for helical tomotherapy: report of the AAPM Task Group 148. Med Phys 2010;37(9):4817–53.

[28] Chen M, Chen Y, Chen Q, Lu W. Theoretical analysis of the thread effect in helical TomoTherapy. Med Phys 2011;38(11):5945–60.

[29] Kissick MW, Fenwick J, James JA, Jeraj R, Kapatoes JM, Keller H, et al. The helical tomotherapy thread effect. Med Phys 2005;32(5):1414–23.

[30] Olivera GH, Shepard DM, Reckwerdt PJ, Ruchala K, Zachman J, Fitchard EE, et al. Maximum likelihood as a common computational framework in tomotherapy. Phys Med Biol 1998;43(11):3277–94.

[31] Shepard DM, Olivera GH, Reckwerdt PJ, Mackie TR. Iterative approaches to dose optimization in tomotherapy. Phys Med Biol 2000;45(1):69–90.

[32] Sterzing F, Uhl M, Hauswald H, Schubert K, Sroka-Perez G, Chen Y, et al. Dynamic jaws and dynamic couch in helical tomotherapy. Int J Radiat Oncol Biol Phys 2010;76(4):1266–73.

[33] ICRU. Prescribing, recording and reporting photon beam therapy (supplement to ICRU Report 50). Bethesda, MD: I.C.o.R.U.a. Measurements; 1999.

[34] Ezzell GA, Burmeister JW, Dogan N, LoSasso TJ, Mechalakos JG, Mihailidis D, et al. IMRT commissioning: multiple institution planning and dosimetry comparisons, a report from AAPM Task Group 119. Med Phys 2009;36(11):5359–73.

[35] Czarnecki D, Zink K. Monte Carlo calculated correction factors for diodes and ion chambers in small photon fields. Phys Med Biol 2013;58(8):2431–44.

[36] Alfonso R, Andreo P, Capote R, Huq MS, Kilby W, Kjall P, et al. A new formalism for reference dosimetry of small and nonstandard fields. Med Phys 2008;35(11):5179–86.

A. Weitere wissenschaftliche Beiträge

Kongressbeiträge

(a) **Howitz S**, Czarnecki D, Zink K; *Abhängigkeit des Verhältnisses der Stoßbremsvermögen Wasser zu Luft von der Feldgröße klinischer Elektronenfelder*. In: DGMP - Tagungsband; Jena; 2012. 508-5011

(b) **Howitz S**, Weibert K, Wiezorek T; *Deviations of DQA-results as a function of plan parameters with helical TomoTherapy*. In: DGMP – Tagungsband; Zürich; 2014.

(c) **Howitz S**, Schwedas M, Wiezorek T, Zink K; *Bestimmung des Korrektionsfaktors k'q unter Nichtreferenzbedingungen für TomoHD*. In: DGMP – Tagungsband; Marburg; 2015.

(d) **Howitz S**, Wiezorek T, Zink K; *Influence of TomoTherapy-specific planning parameters on technical treatment parameters and dose distribution* In: DGMP – Tagungsband; Dresden; 2017.

(e) Teichmann T, Salz H, Schwedas M, **Howitz S**, Wiezorek T; *A multi-institutional survey evaluating patient related QA – phase II*. Current Directions in Biomedical Engineering, 3(2), pp. 639-642. Retrieved 17 Oct. 2017, from doi:10.1515/cdbme-2017-0134

(f) Salz H, **Howitz S**, Brachwitz T, Wiezorek T; *Patient-related QA for helical TomoTherapy with Delta4: analysis of the results*. Current Directions in Biomedical Engineering, 3(2), pp. 635-638. Retrieved 17 Oct. 2017, from doi:10.1515/cdbme-2017-0133

weitere Vorträge

(g) 2014 Abhängigkeit der DQA-Ergebnisse von verschiedenen Tomo - Parametern, UserMeeting Accuray

(h) 2016 Evaluation der patientenbezogenen Qualitätssicherung mit Delta4, DGMP Regionalsektion Mitteldeutschland

(i) 2016 Planungsunsicherheiten pulmonaler Zielvolumina, verifiziert mit Planned Adaptive, DGMP Arbeitskreis TomoTherapy

(j) 2017 60 Monate TomoTherapy am Universitätsklinikum Jena, DGMP Arbeitskreis IMRT, invited Speaker von Accuray

(k) 2017 Fluenzmodulierte Feldgröße in der TomoTherapy, DGMP Arbeitskreis TomoTherapy

Betreuung universitärer Abschlussarbeiten

(l) Gebser F, *Implementierung der helikalen Tomotherapie in die Monte Carlo Simulation mittels EGSnrc*, in UKJ Strahlentherapie und Radioonkologie. 2016, University of Applied Science Mittweida.

(m) Buck C*, Implementierung des binären TomoTherapy MLC im Monte-Carlo EGSnrc User Code*, in UKJ Klinik für Strahlentherapie und Radioonkologie. 2017, TU Ilmenau.

B. Verzeichnis der akademischen Lehrer/-innen

Meine akademischen Lehrer/ -innen in Zwickau waren die Damen und Herren:

Busch, Clausius, Füssel, Flach, Heiland, Hartmann, Häber, Krautheim, Klose, Lenk, Neidhardt, Reinhold, Schnabel, Veit, Wöhrl

Meine akademischen Lehrer an der Technischen Hochschule Mittelhessen waren die Damen und Herren:

Breckow, Fiebich, Koch, Zink

C. DANKSAGUNG

In den folgenden Zeilen möchte ich mich besonders bei den Menschen bedanken, die es mir ermöglicht haben, die Dissertation durchzuführen und in diesem Rahmen abzuschließen.

Ich bedanke mich bei Prof. Vorwerk für die Möglichkeit der Promotion an der medizinischen Fakultät der Philips Universität Marburg.
Ein besonderer Dank geht an Prof. Zink für die fachlichen Diskussionen und Unterstützung, durch die diese Arbeit entstanden ist.

Ganz herzlich möchte ich mich bei PD Wiezorek bedanken, der mich stets ermutigt hat, weiter zu forschen und den Fokus stets im Auge zu behalten.

Zuletzt möchte ich meiner Frau und meiner Familie danken, die mich stets unterstützt, motiviert und mir Zeit gegeben hat, diese Arbeit fertig zu stellen.